:UMENTATION PAGE

Form Approved
OMB No 0704-0188

1. AGENCY USE ONLY (Leave blank)	2. REPORT DATE	3. REPORT TYPE AND DATES COVERED
	May 1992	THESIS/DISSERTATION

4. TITLE AND SUBTITLE
Temporal Variability of the Trade Wind Inversion: Measured with A Boundary Layer Vertical Profiler

5. FUNDING NUMBERS

6. AUTHOR(S)
Cecilia M. Grindinger, Captain

7. PERFORMING ORGANIZATION NAME(S) AND ADDRESS(ES)
AFIT Student Attending: Univeristy of Hawai'i

8. PERFORMING ORGANIZATION REPORT NUMBER
AFIT/CI/CIA- 92-098

9. SPONSORING / MONITORING AGENCY NAME(S) AND ADDRESS(ES)
AFIT/CI
Wright-Patterson AFB OH 45433-6583

10. SPONSORING / MONITORING AGENCY REPORT NUMBER

11. SUPPLEMENTARY NOTES

12a. DISTRIBUTION / AVAILABILITY STATEMENT
Approved for Public Release IAW 190-1
Distributed Unlimited
ERNEST A. HAYGOOD, Captain, USAF
Executive Officer

12b. DISTRIBUTION CODE

13. ABSTRACT *(Maximum 200 words)*

14. SUBJECT TERMS	15. NUMBER OF PAGES 93
	16. PRICE CODE

17. SECURITY CLASSIFICATION OF REPORT	18. SECURITY CLASSIFICATION OF THIS PAGE	19. SECURITY CLASSIFICATION OF ABSTRACT	20. LIMITATION OF ABSTRACT

TEMPORAL VARIABILITY OF THE TRADE WIND INVERSION:

MEASURED WITH A BOUNDARY LAYER VERTICAL PROFILER

A THESIS SUBMITTED TO THE GRADUATE DIVISION OF THE UNIVERSITY OF HAWAI'I IN PARTIAL FULFILLMENT OF THE REQUIREMENTS FOR THE DEGREE OF

MASTER OF SCIENCE

IN

METEOROLOGY

MAY 1992

BY

Cecilia M. Grindinger

Thesis Committee:

Thomas A. Schroeder, Chairperson
Gary M. Barnes
Yi-Leng Chen

We certify that we have read this thesis and that, in our opinion, it is satisfactory in scope and quality as a thesis for the degree of Master of Science in Meteorology.

THESIS COMMITTEE

Chairperson

ACKNOWLEDGEMENTS

I would like to express my appreciation for the many hours worth of helpful suggestions and comments given to me by Dr. Gary Barnes and Dr. Thomas Schroeder.

A special thanks goes to my husband Greg for his understanding and moral support during this study.

ABSTRACT

This study uses Hawaiian Rainband Project (HaRP) data, from the summer of 1991, to show a boundary layer wind profiler can be used to measure the trade wind inversion. An algorithm has been developed for the profiler that objectively measures the depth of the moist oceanic boundary layer. The Hilo inversion, measured by radiosonde, is highly correlated with the moist oceanic boundary layer measured by the profiler at Paradise Park. The inversion height on windward Hawaii is typically 2253 $\pm$ 514 m. The inversion height varies not only on a daily basis, but on less than an hourly basis. It has a diurnal, as well as a three to four day cycle. There appears to be no consistent relationship between inversion height and precipitation. Currently, this profiler is capable of making high frequency (12 minute) measurements of the inversion base variation, as well as other features.

TABLE OF CONTENTS

ACKNOWLEDGEMENTS iii

ABSTRACT iv

LIST OF TABLES vii

LIST OF FIGURES viii

LIST OF ABBREVIATIONS x

PREFACE xii

CHAPTER 1. INTRODUCTION 1

CHAPTER 2. DATA, INSTRUMENTS AND LOCALE 6

2.1 Data 6

2.2 Instrument Description and Limitations 9

2.3 Synoptic Weather Conditions and Locale 14

CHAPTER 3. SOUNDING ANALYSIS AND RESULTS 21

3.1 Sounding Analysis 21

3.2 Inversion Base Specification 27

3.3 Inversion Index 30

3.4 Inversion Results and Statistics 35

CHAPTER 4. PROFILER ANALYSIS AND RESULTS 41

4.1 Profiler Analysis 41

4.2 Inversion Base Specification 46

4.3 Subjective Filtering of Method Three 50

TABLE OF CONTENTS, cont'd

CHAPTER 5. PROFILER VERSUS SOUNDING 54

5.1 Raw Versus Averaged Data 54

5.2 Subjectively Corrected Results 61

CHAPTER 6. PRACTICAL USES OF THE PROFILER 65

6.1 Inversion Base Diurnal Cycle 65

6.2 Diurnal and Synoptic Scale Patterns 69

6.3 Strong Versus Weak Trade Wind Days 69

6.4 Inversion Base Versus Precipitation 72

CHAPTER 7. SUMMARY 75

7.1 Conclusions 75

7.2 Suggestions for Further Work 78

APPENDIX A: PARADISE PARK INVERSION AND PRECIPITATION 80

APPENDIX B: REGRESSION ANALYSIS, CORRELATION AND F-TEST . . 90

REFERENCES 91

LIST OF TABLES

Table		Page
1.	Functional Precision of Radiosonde Temperature	10
2.	Functional Precision of Radiosonde Pressure	10
3.	Functional Precision of Radiosonde Humidity	11
4.	HaRP Profiler Characteristics	11
5.	Hilo Weather during HaRP	16
6.	Relative Humidity and Temperature Categories	32
7.	Relative Humidity Versus Temperature	34
8.	Inversion Statistics (Sounding)	38
9.	Distribution Statistics (Sounding)	39
10.	Regression Analysis for all Four Methods	51
11.	Regression Analysis for Different Averaging Tests	55
12.	Regression Analysis for Raw Data before Filtering	56
13.	Cause of Large Residuals	58
14.	Regression Analysis for Raw "Continuous Data" (Subjectively Corrected Versus Uncorrected)	61
15.	Distribution Statistics (Profiler)	64
16.	Mean Inversion Height Statistics	65
17.	Regression Analysis for Diurnal Precipitation and Inversion Height (Profiler)	68
18.	Average Inversion Height for Strong and Weak Trade Wind Days	71
19.	Regression Analysis for Rain Versus Inversion Height	74

LIST OF FIGURES

Figure		Page
1.	Vertical Cross Section of Trade Wind Regime	2
2.	Equipment Location and Topography	7
3.	July Climatology: 200 mb and Surface Level	15
4.	Local Weather Patterns	18
5.	Precipitation Time Series and Correlation	20
6.	Trade Wind Soundings	22
7.	Superadiabatic Lapse Rate at Inversion Base	25
8.	Inversion Base Decision Tree (Sounding)	29
9.	Multiple Inversion Model	31
10.	Relative Humidity Classifications	33
11.	Inversion, Layers, Strength and Precipitation (Sounding)	36
12.	Inversion Base Distribution (Sounding)	40
13.	Clear Air Return	42
14.	Rain Return	44
15.	Mid-level Return	45
16.	Weak Gradients/Spikes	47
17.	Inversion Base Specification (Profiler): Method One and Two	48
18.	Inversion Base Specification (Profiler): Method Three and Four	48
19.	Removal of Mid-level Return and Spikes	52
20.	Regression Analysis for RH/TEMP 3-5/3-5 "Continuous Data"	57

LIST OF FIGURES, cont'd

Figure — Page

21. Regression Analysis for 5-5/5-5 "Continuous Data" 57

22. Regression Analysis for 1-5/1-5 "All Data" 59

23. Regression Analysis for Subjectively Corrected Data 59

24. Inversion Base Distribution (Profiler) 63

25. Diurnal Cycle: Inversion Height and Precipitation (Profiler) 66

26. Regression Analysis for Diurnal Cycle: Inversion Height and Precipitation (Profiler) 67

27. Spectral Density Function (Profiler) 70

28. Time Series and Correlation for Inversion Versus Precipitation 73

LIST OF ABBREVIATIONS

ATEX: Atlantic Trade-Wind Experiment

C: centigrade

DBz: decibel

E: east

HaRP: Hawaiian Rainband Project

HST: Hawaiian Standard Time

km: kilometer

m: meter

mb: millibar

MBz: millibel

MHz: megahertz

MLO: Mauna Loa Observatory

μs: micro-second

mm: millimeter

N: north

n: refractive index

N: refractivity

NWS: National Weather Service

NOAA: National Oceanic and Atmospheric Administration

PAM: portable automated mesonet

PC: personal computer

LIST OF ABBREVIATIONS, cont'd

RH/TEMP: relative humidity/temperature

s: second

S: south

SALR: superadiabatic lapse rate

SER: sub-equatorial ridge

TD: tropical depression

TUTT: tropical upper-tropospheric trough

UHF: ultrahigh frequency (300 to 3000 MHz)

UTC: coordinated universal time

V: vertical

VHF: very high frequency (30 to 300 MHz)

W: west

PREFACE

The purpose of this study is to answer two questions. First, and foremost, can a boundary layer wind profiler be used to measure the trade wind inversion? I will determine this by comparing results from the Hilo soundings to results from the profiler. Secondly, if the wind profiler does indeed measure the inversion, what are its characteristics? In particular, (a) Is there significant variability of inversion height and strength? (b) Is there any periodicity of the inversion height or depth of the trade wind moist layer? and (c) Is there any relationship between inversion height and precipitation?

CHAPTER 1

INTRODUCTION

The trade wind inversion is the transition layer between dry, upper level air subsiding in the oceanic subtropical anticyclones and low-level, moist marine air. The inversion is a persistent feature that occurs over a large portion of the global tropics. For example, the Pacific warm season trade wind inversion occurs almost 100% of the time off the California coast. Its frequency decreases slightly to around 90% over the Hawaiian Islands (Neiburger 1960).

Known to be an important regulatory valve in the global tropics (Riehl et al. 1951; Malkus 1958; Augstein et al. 1973; Albrecht 1984), the inversion has fascinated meteorologists over the years and has been the subject of many studies. The trade wind inversion inhibits vertical development of clouds, thus the trade wind flow transports sensible and latent heat equatorward. This process provides energy for the maintenance of the Hadley circulation (Riehl 1979).

C. Piazzi-Smyth discovered the trade wind inversion in 1858 (Riehl 1979). The first detailed analysis of the inversion was done over the Atlantic by the Meteor expedition (von Ficker 1936). Since then, many authors have discussed the cause and maintenance of the inversion (Malkus 1958; Riehl 1979; Ramage 1990).

Vertically, the trade wind regime consists of four layers (Figure 1 from Malkus 1958): (1) the subcloud layer, (2) the cloud layer, (3) the inversion, and (4) the dry stable layer (Riehl et al. 1951; Malkus 1958). The sub-inversion air is moist and consists of a subcloud layer and cloud layer. Turbulent eddies in the subcloud layer mix water

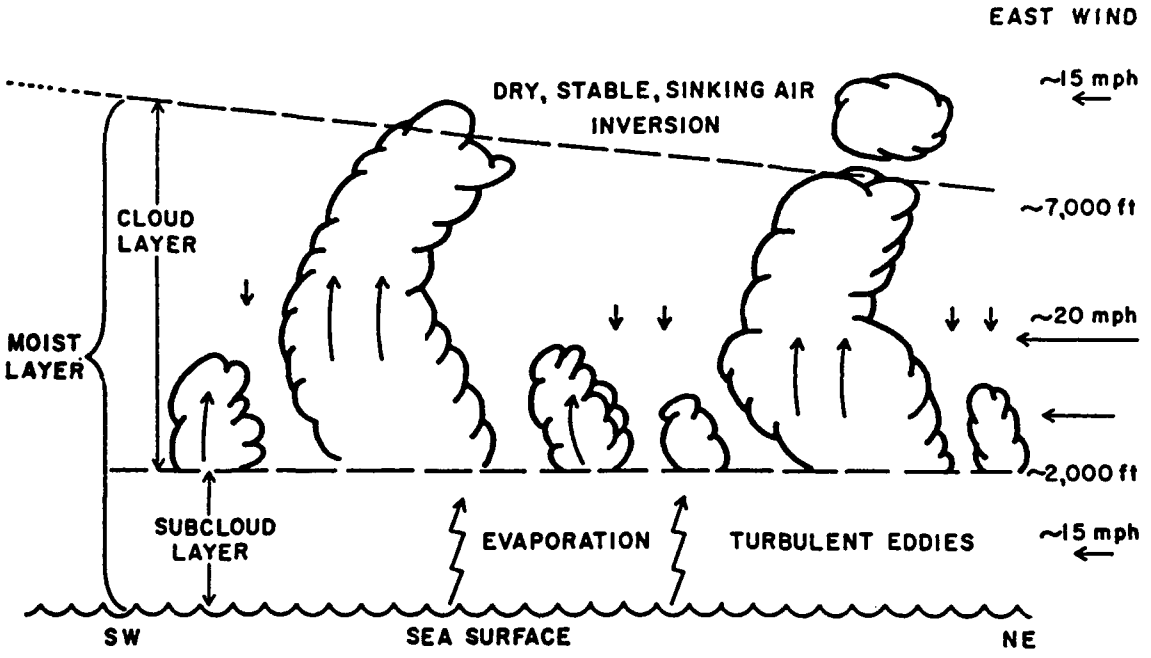

Figure 1. Vertical cross section of the trade wind regime. Arrows at the right show typical wind speeds. The moist layer deepens by about 305 m (1000 ft) in 806 km (500 miles) horizontal distance; clouds are thus drawn much larger than to actual scale. (from Malkus 1958)

vapor upward to form the mixed layer. The water vapor condenses around 650 meters (m) to form trade wind cumulus. The cumulus distribute water vapor throughout the cloud layer. However, only a few cumulus penetrate the inversion where they quickly evaporate. Above this moist layer, the inversion acts as a transition zone between the moist marine air and the dry air subsiding from above.

In spite of divergence and air columns sinking throughout the four layers, the inversion base rises downstream. The traditional explanation is that overshooting cumulus towers penetrate the inversion, and thus evaporate in the dry stable layer. This process causes the inversion to weaken and rise downstream (Riehl et al. 1951; Malkus 1958; Augstein et al. 1973). However, a more recent modeling study (Albrecht 1984) gives a more complex picture. Inversion height variation depends on a combination of (1) sea surface temperature, (2) divergence, (3) variation in temperature and moisture above the inversion, (4) surface wind speed, and (5) radiative cooling. Additionally, downstream inversion heights may depend more on upstream conditions than local conditions.

The trade wind inversion in the Pacific Basin has the following characteristics. The inversion base is lowest (around 400 m) and strongest (6° Centigrade (C) temperature difference between base and top) along the California coast. It slowly rises and weakens to the southwest along the average trade wind trajectory (Neiburger 1960; Riehl 1979). For example, the average summertime inversion base over Hawaii is slightly more than 2000 m with a strength of 2 °C. The relative humidity is almost constant (around 80%) throughout the moist layer. At the inversion base, there is a first order relative humidity

discontinuity. The relative humidity rapidly decreases above the inversion base by more than 50% off the California coast, to more than 40% over Hawaii. The air is dry (relative humidity < 30%) above the inversion.

Other studies, more focused on a particular station or smaller area, have made some interesting observations. Leopold (1948); Riehl et al. (1951); and Lavoie (1967b) speculate there is a diurnal cycle in the trade wind inversion. Larson (1978) noted the inversion base is lower during dry trades and higher during wet trades. Specifically, the mean Hilo inversion for dry days ($\leq$ 5.1 millimeters (mm) precipitation per day) is 1520 to 1740 m and for wet days ($\geq$ 12.7 mm) it is 2070 to 2320 m.

The inversion height is more variable over island barriers than over the open ocean (Ramage and Oshiro 1977; Fellbaum 1984). Over the open ocean, upwind of the Hawaiian islands, Bean et al. (1973) found the inversion level (measured by aircraft) to be stable between 1.3 and 1.5 kilometers (km). However, the inversion lifts near the islands, due to interaction between the trade wind flow and mountain barriers. A modeling study (Lavoie 1974) showed the inversion lifts 300 m due to mountains on Oahu that do not penetrate the inversion (highest peak more than 1200 m). Unfortunately, most of these studies used only two soundings per day for periods of up to two months. Some studies include other data types on a similar time scale. The Atlantic Trade-Wind Experiment (ATEX) had the most comprehensive spatial coverage. Augstein et al. (1973) used three weeks of three hourly soundings and radar from a triangular array of three ships. My study differs in that it sampled the inversion every 12 minutes with the profiler for slightly more than five weeks. The Bean et al. (1973)

study was similar to mine in that it used an FM-CW radar (10 cm wavelength) in concert with a U-21 aircraft to examine the inversion. However, their study showed examples from only three days to see if the FM-CW radar could measure the inversion height. They did not have a large enough sample size to fully prove this. In addition, they did not use an extensive data set to examine inversion characteristics.

In this study I will use a comprehensive data set to study the trade wind inversion. In particular, I will test if a boundary layer wind profiler can routinely measure the depth of the moist oceanic boundary layer that is capped by the trade wind inversion. Hilo sounding results will show if the profiler is measuring the inversion. If the wind profiler does indeed measure the inversion, what are its characteristics? In particular, is there significant variability of inversion height and strength and for what time scales? Finally, is the inversion height related to precipitation?

CHAPTER 2

DATA, INSTRUMENTS AND LOCALE

2.1 Data

The Hawaiian Rainband Project (HaRP) occurred on the island of Hawaii during July to August 1990 (HaRP Experimental Design and Operations Plan 1990; HaRP Scientific Overview 1989). The primary data used for this study include soundings, wind profiler reflectivity data and automated surface weather observations. I also used synoptic charts and satellite imagery to assess when typical trade wind conditions dominated the weather.

2.1.1 Hilo Rawinsondes

The National Weather Service (NWS) at Hilo Airport (Figure 2) routinely provides soundings at 0 and 1200 coordinated universal time (UTC). The HaRP data base includes supplemental soundings. A total of 124 soundings are available from 11 July to 24 August (2 or more each day). The soundings have about a 30 m vertical resolution (6 second interval). Hilo weather observations are available in the Old General Lyman Field Local Climatological Data (NOAA 1990).

2.1.2 Wind Profiler Doppler Radar

This study uses data from a boundary layer wind profiler. The location was Paradise Park (17.5 km southeast of Hilo, Figure 2), from 13 July to 19 August. Only the vertical beam signal strength is used, courtesy of W. Ecklund and T. Riddle at NOAA. The signal strength unit is millibels (MBz = 1000 x $\log_{10}$[signal]). After 20 July, an antenna program was implemented that cycled through a sequence of pointing directions (alternating with a vertical scan between each primary direction [N, S, E, W]). This

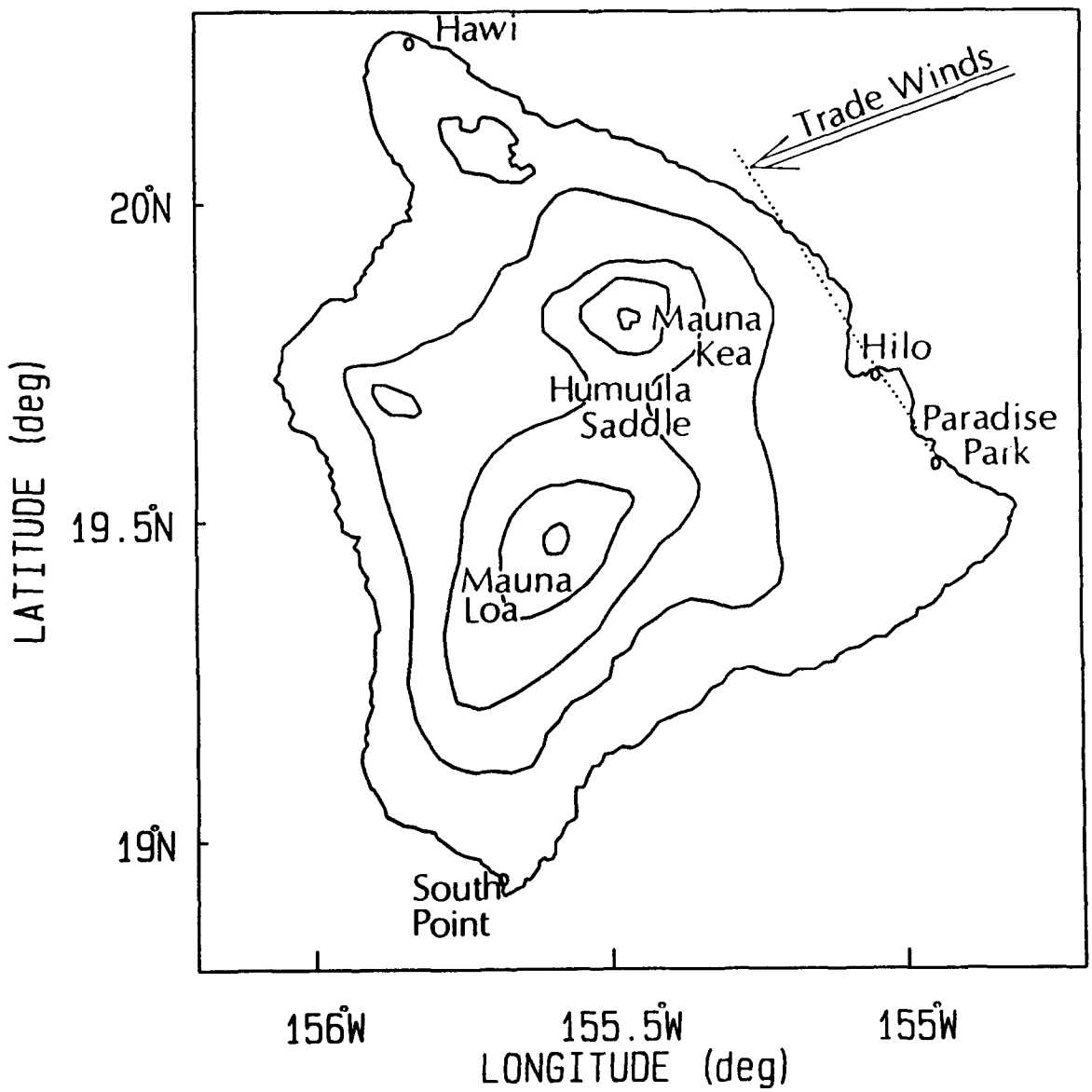

Figure 2. Map of equipment location and topography. Wind profiler is located at Paradise Park, and radiosonde is located at Hilo. Strong and weak trade winds are determined from Hawi and South Point surface wind observations.

allowed wind profiling as well as frequent observations in the vertical direction for monitoring shower evolution (Rogers et al. 1991). The dwell time for each direction is 30 seconds (s), with 5 s required for direction change. Consequently, the frequency of vertical observations is every 70 s and each measurement is a 30 s average. T. Riddle combined the raw data set to create the filtered (for interference) 12 minute median data set used for this study. Use of the median, rather than the mean, is a robust method to remove occasional erroneous values.

I divided the data set into two periods. The first period (called "all data") contains all the days. The second period (called "continuous data") contains 22 July, 10 UTC, to 19 August. I make this distinction because between 13 to 22 July, the radar suffered equipment problems which resulted in the loss of two entire days. Also, the radar operators tested two different antenna programs and then selected a third program on 20 July. The radar continued to undergo testing until around 10 UTC on 22 July. Finally, the "continuous data" set had only 13 missing 12 minute median observations out of a total of 3395 observations. To perform spectral analysis, I made the record continuous by interpolating the two closest times.

2.1.3 Mesonet (PAM II)

Part of the HaRP mesonet included a portable automated mesonet (PAM II) located at Paradise Park. Automated observations (wind, wet- and dry-bulb temperature, pressure, and rain) are available for every minute from 11 July to 24 August. From this, A. Nash (1992) computed a 15 minute average data set after eliminating suspect data. This study uses the 15 minute precipitation accumulation data.

2.2 Instrument Description and Limitations

2.2.1 Hilo Soundings

For many studies, the radiosonde is the standard used to compare new instruments. Radiosonde measurements differ from profiler measurements both spatially and temporally. A radiosonde, launched at least twice a day, takes measurements as the balloon ascends and drifts with the winds. The radiosonde reaches the inversion in about four to ten minutes, depending on atmospheric stability and inversion base height. It remains in the inversion layer for about one minute, depending on layer thickness. In contrast, the profiler takes a 30 s measurement.

Ahnert (1990) launched two sonde packages on the same balloon to measure functional precision. This method gives the reliability of the radiosonde, but does not measure the degree of conformity to a standard or true value. Reliability measures if the results are similar for repeated trials.

Tables 1, 2, and 3 list time comparisons from six-second data averaged for each minute (from Ahnert 1990). Temperature differences are between $\pm$ 0.5 °C more than 92% of the time for a temperature range from 34.9 °C to -5.0 °C. Between the 850 to 1009 millibar (mb) layer, 93.7% of the pressure differences are between $\pm$ 2 mb. Relative humidity differences (for the 40% to 100% range) are within $\pm$ 2.5% for more than 93% of the samples. At relative humidities between 20% to 39.9%, the sensor performs the worst (within $\pm$ 5% for more than 85% of the samples). However, any relative humidities this low would occur well above the inversion. Overall, the functional precision of the radiosonde in the lower levels of the atmosphere is good.

Table 1. Functional Precision of Radiosonde Temperature--
Frequency of Occurrence (from Ahnert 1990)

FROM ...TO (°C)	Sample Size/# Flights	0.0 to 0.5 °C	0.6 to -1.0 °C	1.1 to -1.5 °C	1.6 to 2.0 °C	2.1 to 2.5 °C	2.6 to 3.0 °C	≥ 3.1 °C
20... 34.9	55/15	92.7%	0%	0%	7.3%	0%	0%	0%
5... 19.9	206/28	94.7%	1%	1%	3.4%	0%	0%	0%
-5... 4.9	249/33	96.8%	.8%	.8%	1.6%	0%	0%	0%

Table 2. Functional Precision of Radiosonde Pressure--
Frequency of Occurrence (from Ahnert 1990)

FROM ...TO (mb)	Sample Size/# Flights	0.0 to 0.5 mb	0.6 to -1.0 mb	1.1 to -1.5 mb	1.6 to 2.0 mb	2.1 to 2.5 mb	2.6 to 3.0 mb	≥ 3.1 mb
850.. 1009	159/33	34%	26.4%	15%	8.2%	3%	5%	8.2%

2.2.2 Wind Profiler Doppler Radar

The wind profiler is a 915 megahertz (MHz) ultrahigh frequency (UHF; 300 to 3000 MHz) boundary layer radar. Table 4 lists profiler characteristics (from Rogers et al. 1991). The profiler usually detects clear air echoes up to about 4 km with a 104 m height resolution. Ecklund et al. (1988) describe basic system design and field test results from an initial prototype (1990). A personal computer (PC) based controller/processor controls the profiler.

Table 3. Functional Precision of Radiosonde Humidity--
Frequency of Occurrence (from Ahnert 1990)

FROM...TO (%)	Sample Size /# Flights	0.0 to 2.5%	2.6 to 5.0%	5.1 to 7.5%	7.6 to 10.0%
90 to 100	127/16	100%	0%	0%	0%
80 to 89.9	97/21	97.9%	2.1%	0%	0%
70 to 79.9	80/21	95%	5%	0%	0%
60 to 69.9	127/29	99.2%	.8%	0%	0%
50 to 59.9	108/29	98.1%	1.9%	0%	0%
40 to 49.9	74/26	93.2%	6.8%	0%	0%
30 to 39.9	87/24	86.2%	10.3%	2.3%	1.1%
20 to 29.9	97/24	56.7%	28.9%	12.4%	2.1%
10 to 19.9	277/23	90.6%	8.3%	1.1%	0%

Table 4. HaRP Profiler Characteristics
(from Rogers et al. 1991)

Frequency	915 MHz	Antenna aperture	1.8 m x 1.8 m
Wavelength	32.8 cm	Beamwidth	9 degrees
Bandwidth	5 MHz	Pulse repetition period	50 μs
Pulse Duration	0.7 μs	Antenna type	Microstrip array
Peak power	300 W	Number of range samples	49
Gate spacing	104 m	Maximum radial velocity	$\pm$ 10.9 ms^{-1}
		Number of spectral points	64

Wind profilers are sensitive to inhomogeneities in refractive index caused by turbulence. The detectable scale is equal to half the radar wavelength. The refractive index (n) for the troposphere and stratosphere is (Gage 1990):

$$n-1=\frac{3.73*10^{-1}e}{T^2}+\frac{77.6*10^{-6}p}{T}-\frac{N_e}{2N_c} \qquad (2.1)$$

where e (mb) is the vapor pressure, p (mb) is the atmospheric pressure, T (Kelvin) is the absolute temperature, N_e (m^{-3}) is the number density of electrons, and N_c (m^{-3}) is the critical plasma density for the radio frequency (f) ($N_e = 1.24 \times 10^{-2}$ f[MHz]^2). The first term (water vapor term) dominates in the lower troposphere. The second term (dry air term) dominates above 5 km. The third term is the contribution due to the presence of free electrons and it enhances the radio refractive index above 50 km.

The contribution due to electrons is negligible in the boundary layer, so this application can use a simpler form of equation 2.1 (Bean and Dutton 1966):

$$N=n-1*10^6=77.6\frac{p}{T}+3.73*10^5\frac{e}{T^2} \qquad (2.2)$$

where N is the refractivity. Bean et al. (1973) found one kilometer refractivity variations are primarily due to moisture (75 to 84%). Temperature (4 to 10%) and pressure (6 to 21%) account for the rest of the refractivity variations.

The radar equation relates the received signal strength to a particular radar system. The radar equation for partial reflection (Gage and Balsley 1980) is:

$$P_r=\frac{P_t A_e^2}{4\lambda_R^2 r^2}|\rho|^2 \qquad (2.3)$$

where P_r is the received power, P_t is the transmitted power, A_e is the effective area of the antenna, λ_R is the radar wavelength, r is the range, and ρ is the power reflection coefficient. The radar equation for isotropic scattering (Gage and Balsley 1980) is:

$$P_r = \frac{\pi}{64} \frac{P_t A_e \Delta r}{r^2} \eta_{turb} \qquad (2.4)$$

where η_{turb} is the volume reflectivity.

Use of a higher frequency (915 MHz) makes this system sensitive to precipitation as well as clear air scattering. However, lower frequency VHF (very high frequency; 30 to 300 MHz) profilers are unable to measure the boundary layer. Reflectivity of clear air (η_a) is given by (Rogers et al. 1991):

$$\eta_a = 0.38 C_n^2 \lambda^{-1/3} \qquad (2.5)$$

where c_n^2 is the refractive index structure constant and λ is the radar wavelength. Reflectivity for rain or clouds (η_d) is (Rogers et al. 1991):

$$\eta_d = 0.93 \pi^5 Z \lambda^{-4} \qquad (2.6)$$

where Z is the reflectivity factor. For ordinary weather radars, which operate in a lower centimeter wavelength range than a profiler, η_a is usually much less than η_d. Although both η_a and η_d decrease with increasing wavelength, η_d decreases at a faster rate. As a result, as wavelength increases, clear air scattering becomes dominant. Rogers et al. (1991) compute a scaling argument with equations 2.5 and 2.6 (λ = 33 cm and $c_n^2 = 10^{-13}$ $m^{-2/3}$). From this, the reflectivity factor of drops would have to be 4 decibels (DBz) to equal clear air reflectivity. Hence, the profiler is about as sensitive to moderately turbulent clear air as it is to drizzle.

Ecklund et al. (1990) address two situations that could cause a problem. First, it is possible to have ground clutter caused by nearby moving objects. Finally, interference from small birds is possible and will cause false echoes.

2.2.3 Mesonet (PAM II)

The HaRP Experimental Design and Operations Plan (1990) provides the accuracy and resolution of the PAM II instruments. The precipitation sensor is a tipping bucket. The accuracy is $\pm$ 15% and the resolution is 0.25 mm.

2.3 Synoptic Weather Conditions and Locale

2.3.1 Synoptic and Local Weather Conditions

Figure 3 (from Sadler 1975; Sadler et al. 1987) shows typical summertime surface and 200 mb flow patterns for the northeast Pacific Ocean. At 200 mb (Figure 3a), the tropical upper-tropospheric trough (TUTT) extends from the southwest through northeastern part of the North Pacific Ocean. Further south, the sub-equatorial ridge (SER) extends from 130°E, eastward to 50°W. The anticyclones, in the eastern (and western) Pacific part of the ridge, overlie tropical cyclone activity. At the surface (Figure 3b), the well established oceanic subtropical anticyclone causes northeasterly trade winds to its south. The trade winds are strongest between 15 to 20°N.

Weather conditions during the period of this study were similar to average conditions. At times, the surface subtropical anticyclone was split or shifted around. Surface winds, on windward Hawaii, were predominantly northeasterly. However, the winds sometimes shifted to a more easterly or north-northeasterly direction, between 2

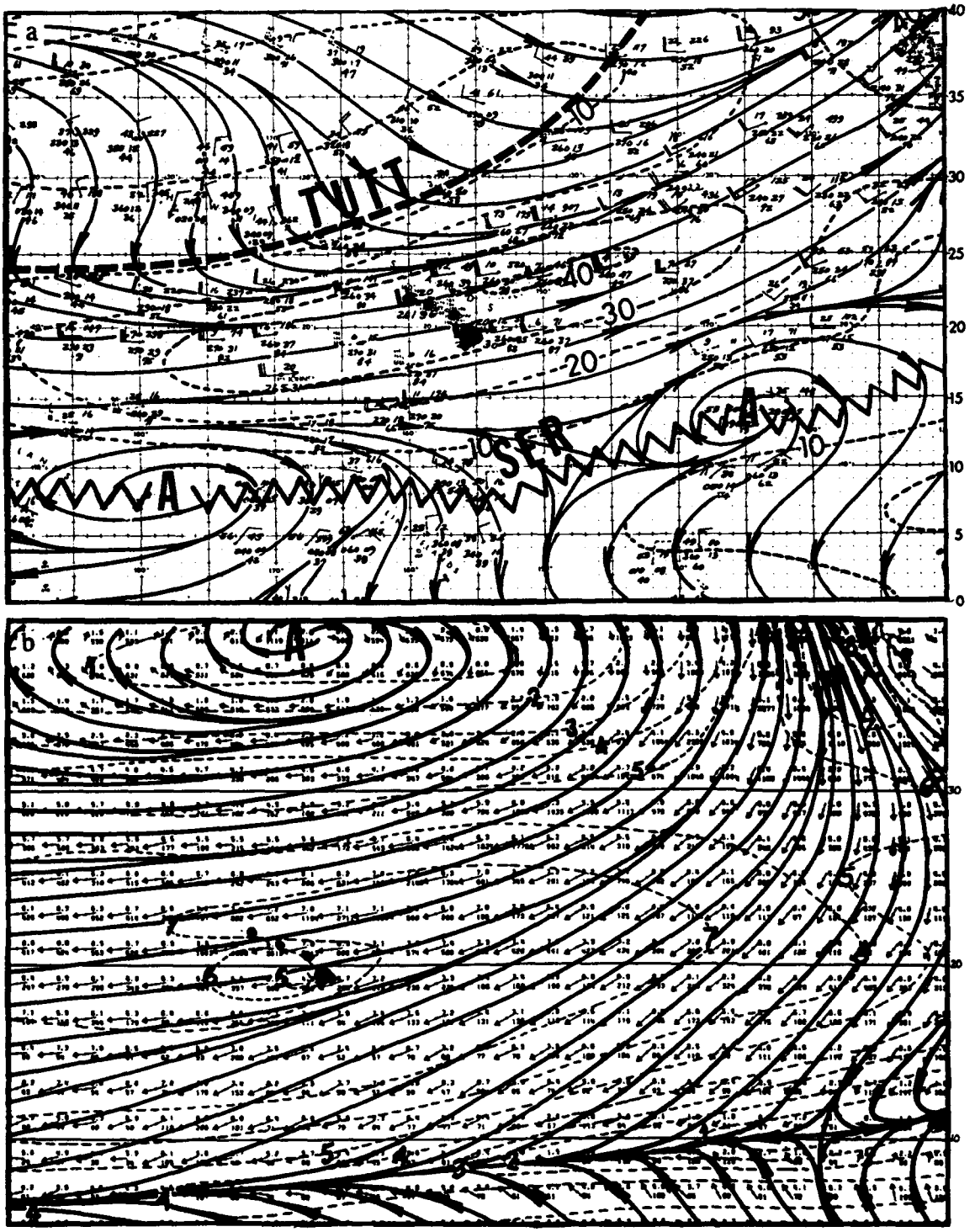

Figure 3. July climatology: (a) 200 mb level: wind speed (--) in knots and streamlines (__). (b) Surface level: wind speed (--) in ms^{-1} and streamlines (__). TUTT: tropical upper-tropospheric trough. SER: sub-equatorial ridge. (from Sadler 1975; Sadler et al. 1987)

to 9 ms^{-1}. Observed wind steadiness was high. Enhanced trade showers and local effects accounted for most of the island precipitation during HaRP.

Only one tropical depression affected Hawaiian weather. Tropical Depression (TD) 2C occurred south of the Hawaiian islands from 11 to 13 August. Associated with TD 2C, a large area of clouds passed over the islands on the 13th. Daily precipitation for Hilo and Paradise Park can be seen in Figure 11 and Appendix A, respectively.

Another check shows conditions during July and August 1990 were close to normal at Hilo. Table 5 contains averaged weather observations from the Local Climatological Data (NOAA 1990) from Old General Lyman Field in Hilo. Temperature departures from the mean were small, with temperatures 0.3 °C (July) and 0.6 °C (August) warmer than normal. Precipitation departures from the mean were 53.3 mm more than normal for July and 55.9 mm less than normal for August. Average resultant wind direction was from the north-northeast with a speed of more than 3 ms^{-1}. Although July (August) was slightly wetter (drier) than normal, conditions represent the average trade wind climatology for Hilo.

Table 5. Hilo Weather During HaRP, July to August 1990
(from NOAA 1990)

	Avg Max Temp (°C)	Avg Min Temp (°C)	Avg St Pres (mb)	Pcp > .254 mm (days)	Total Pcp (mm)	Wind Dir (deg)	Avg Speed (ms^{-1})
Jul	28.1	20.7	1015	29	273.8	040	3.3
Aug	28.9	21.1	1014	26	198.1	030	3.4

2.3.2 Local Topography Effects

A complication to this study is that local effects disturb the trades. Local effects include island topography, enhanced surface friction, thermally induced turbulence, and katabatic-anabatic flow (Fellbaum 1984). Two massive volcanoes, Mauna Loa and Mauna Kea, extend well above the inversion. Mauna Kea (Figure 2), to the north, is fairly circular and extends to 4.2 km above sea level. Further south, more elongated and more massive, Mauna Loa extends to 4.17 km above sea level. Between the two volcanoes is the Humuula Saddle (1.8 to 2 km above sea level).

The trade wind inversion forces the trade wind flow to diverge around the volcanoes and converge through the Humuula Saddle (Leopold 1949; Lavoie 1967a). Windward Hawaii experiences a daytime sea breeze that is orographically lifted up the eastern volcano slopes to produce a daytime precipitation maximum on the slopes at elevations above one km and below the inversion (Schroeder et al. 1977). This flow reverses at night as the land breeze dominates, causing a nocturnal coastal (Hilo and Paradise Park) precipitation maximum. Diagrams of these local patterns are in Figure 4 (from Garrett 1980).

2.3.3. Sensor Location

The Paradise Park profiler was not collocated with the Hilo radiosonde. Consequently, both instruments might not be sampling air with the same characteristics. In Figure 2, the sites form a line roughly perpendicular to the average trade wind flow. It is possible that a convective system could affect one site at a different time than the other site. In addition, if the convective scale is small, it might only affect one site.

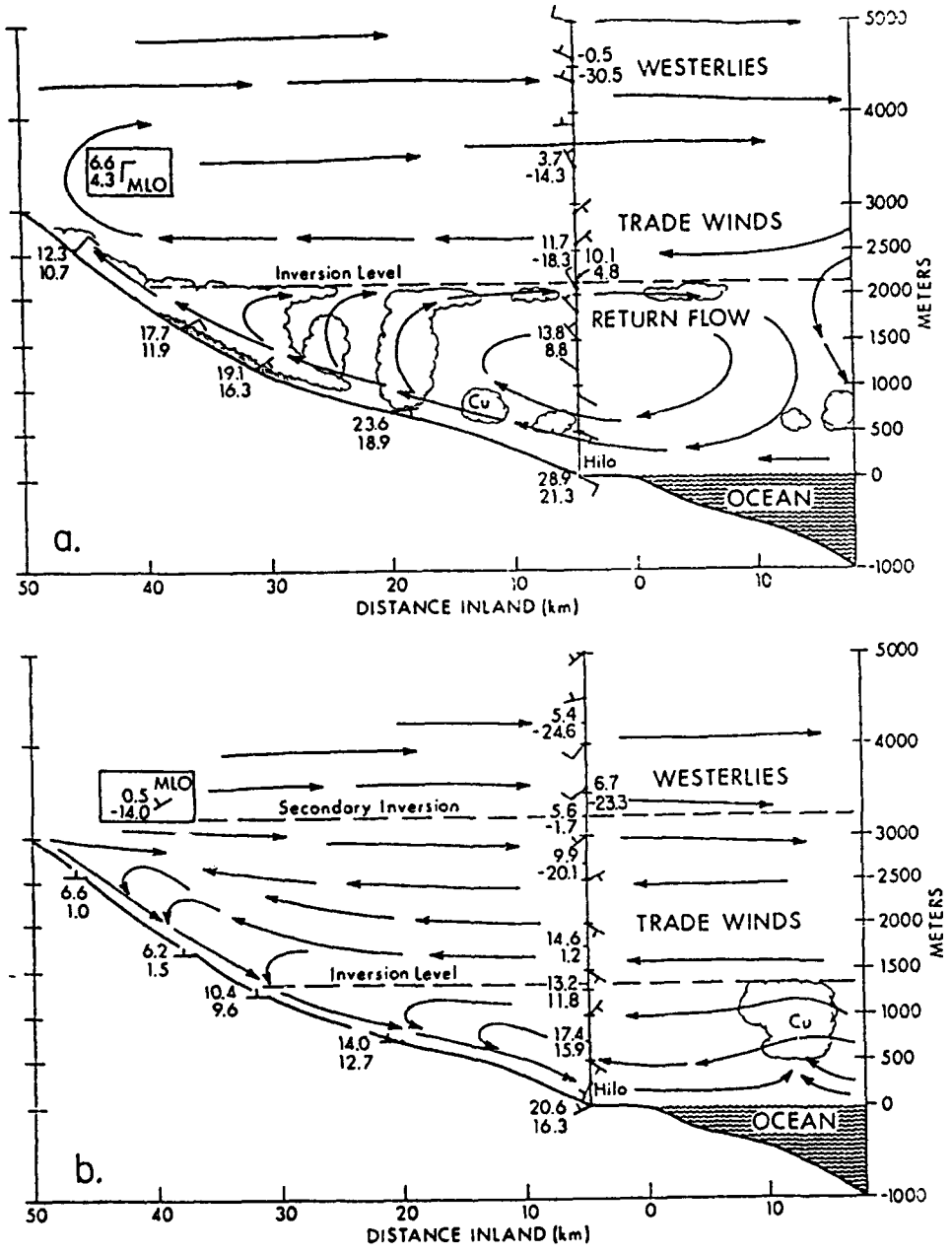

Figure 4. Local weather patterns (from Garrett 1980). East-west cross section depicts conceptual model of land and mountain sea breeze circulations. (a) Daytime upslope/sea breeze, 3 June, 1400 Hawaiian Standard Time (HST). (b) Nighttime drainage/land breeze, 5 June, 0600 HST. Horizontal wind arrows: half barb = 2.5 ms^{-1}, full barb = 5.0 ms^{-1}. Drybulb temperatures (°C) are plotted above dewpoints and accompany wind arrows at each surface station. The same plotting convention is used for the Hilo sounding. Mauna Loa observatory (MLO) is included only as an insert because terrain slopes north-south there.

To investigate these concerns, I plotted average Hilo daily precipitation (from NOAA 1990) and Paradise Park (Figure 5a). Hilo averages 9 $mmday^{-1}$ and Paradise Park averages 7 $mmday^{-1}$. Although Hilo receives more precipitation, the trends agree. Regression analysis (Appendix B) yields a correlation of 0.74, a slope of 0.52, a y-intercept of 2.3 m, and an F-Value of 44 (Figure 5b). The 99th percentile value for this F-Distribution (F[.99,1,36]) is 7.41, so it is statistically significant. As a result, there is reasonable agreement between sites. Even though the sensors are separated by 17.5 km, these results show they are usually affected by the same mesoscale gamma phenomena within a one hour period.

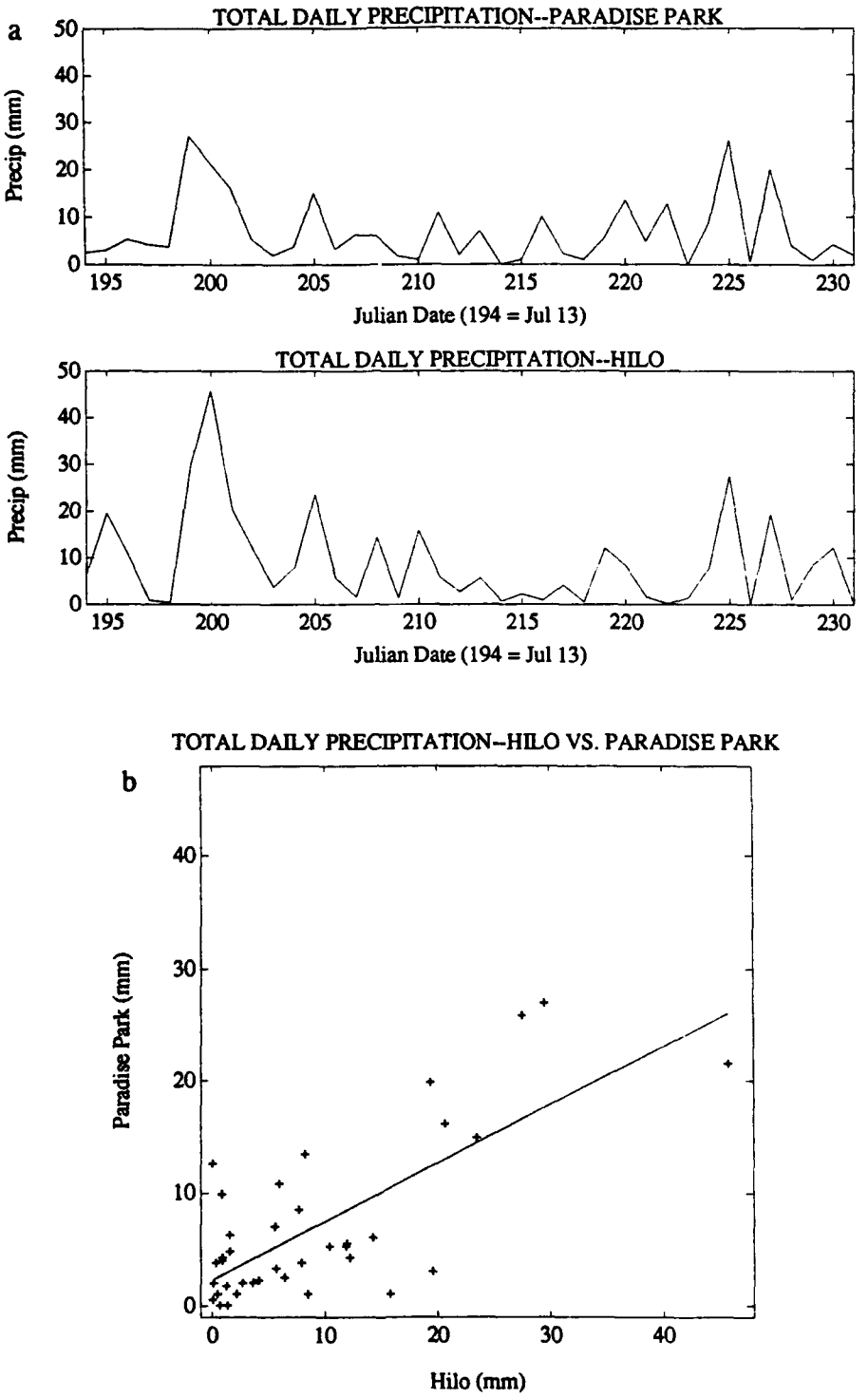

Figure 5. Precipitation time series and correlation. (a) Total daily precipitation time series for Paradise Park profiler and Hilo sounding. (b) Regression analysis for Hilo and Paradise Park total daily precipitation.

CHAPTER 3

SOUNDING ANALYSIS AND RESULTS

3.1 Sounding Analysis

A "typical trade wind sounding" is shown in Figure 6a. The inversion base is the point where the temperature starts to increase with height (2239 m). An alternate method to determine the inversion base is to use the relative humidity curve. The inversion base is collocated with the point where the relative humidity starts to drop rapidly.

Careful analysis shows that several of the Hilo soundings do not look like the "typical trade wind sounding." Some of the soundings (Figure 6b) have multiple inversions, and it is often difficult to select a particular level as the inversion. In several cases, the temperature signal (Figure 6c) does not show an inversion. However, the relative humidity plot shows a well defined moist and dry layer. Therefore, I will define a subjective method to measure the inversion base using both moisture and temperature.

Another issue is the occurrence of superadiabatic lapse rates at the top of the moist layer (Figure 7a). This phenomenon occurs in 52% of the soundings. Superadiabatic lapse rates can occur near the ground when associated with strong surface heating, and for short periods in the atmosphere. This would indicate a very unstable condition, with rapid overturning of the air, and could not exist for an extended time. Since so many soundings have this feature, I suspect it is due to an equipment problem.

The temperature sensor is a rod thermistor coated with white lead carbonate paint (Ahnert 1990). A plausible explanation is that the temperature sensor is getting wet while passing through cloud or in rain. The radiosonde then emerges from the cloud into

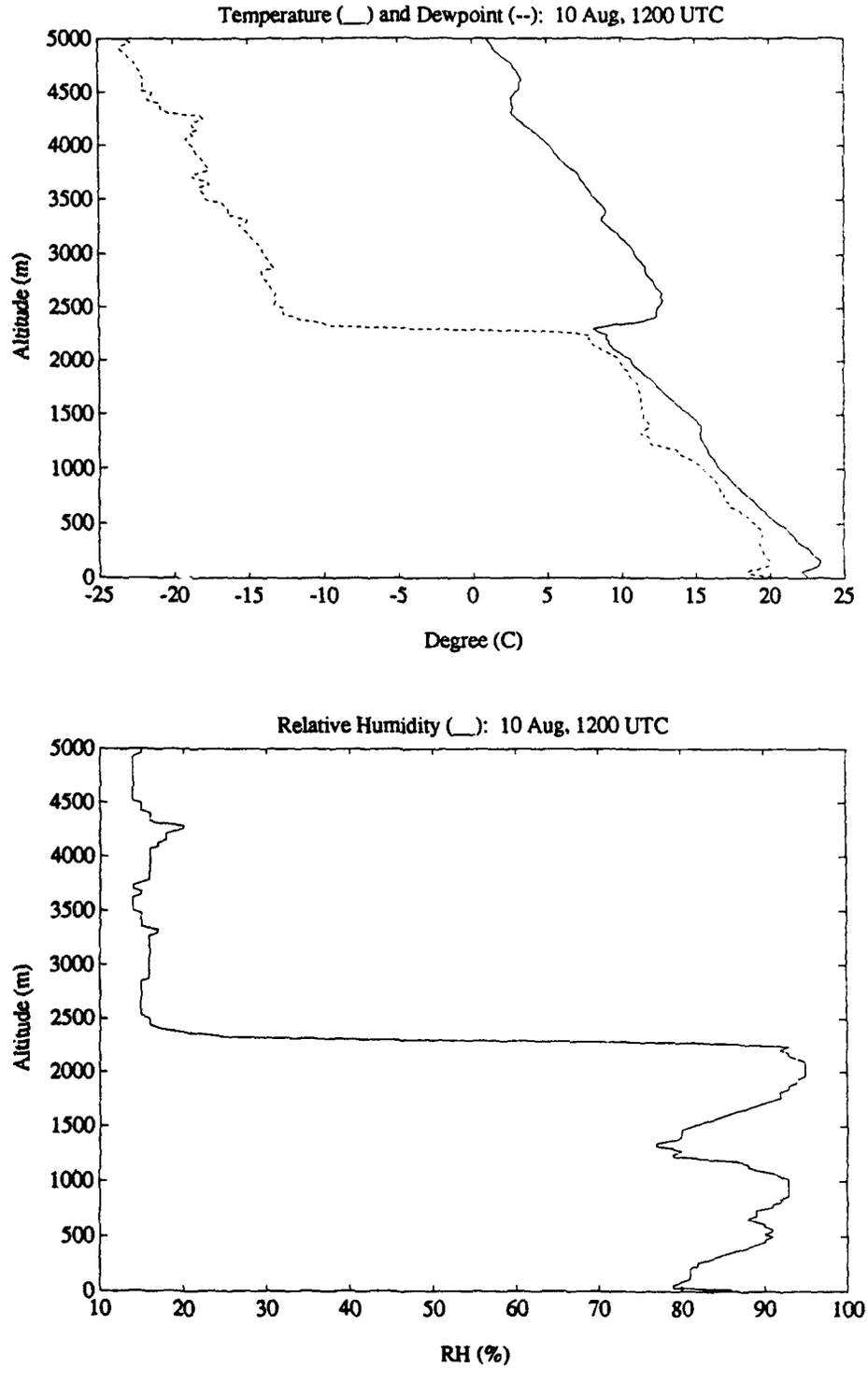

Figure 6a. "Typical trade wind sounding."

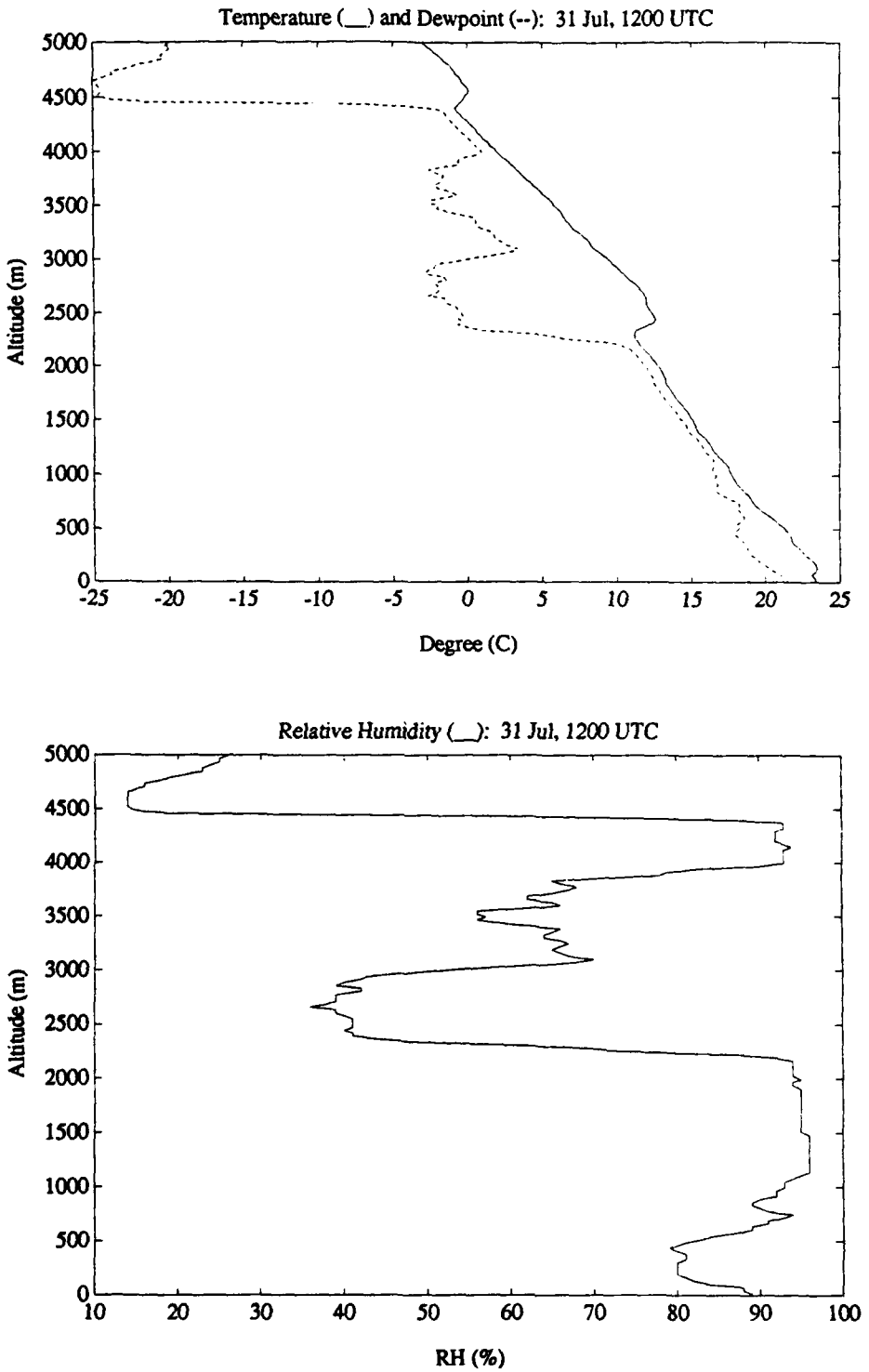

Figure 6b. Trade wind sounding with multiple inversions.

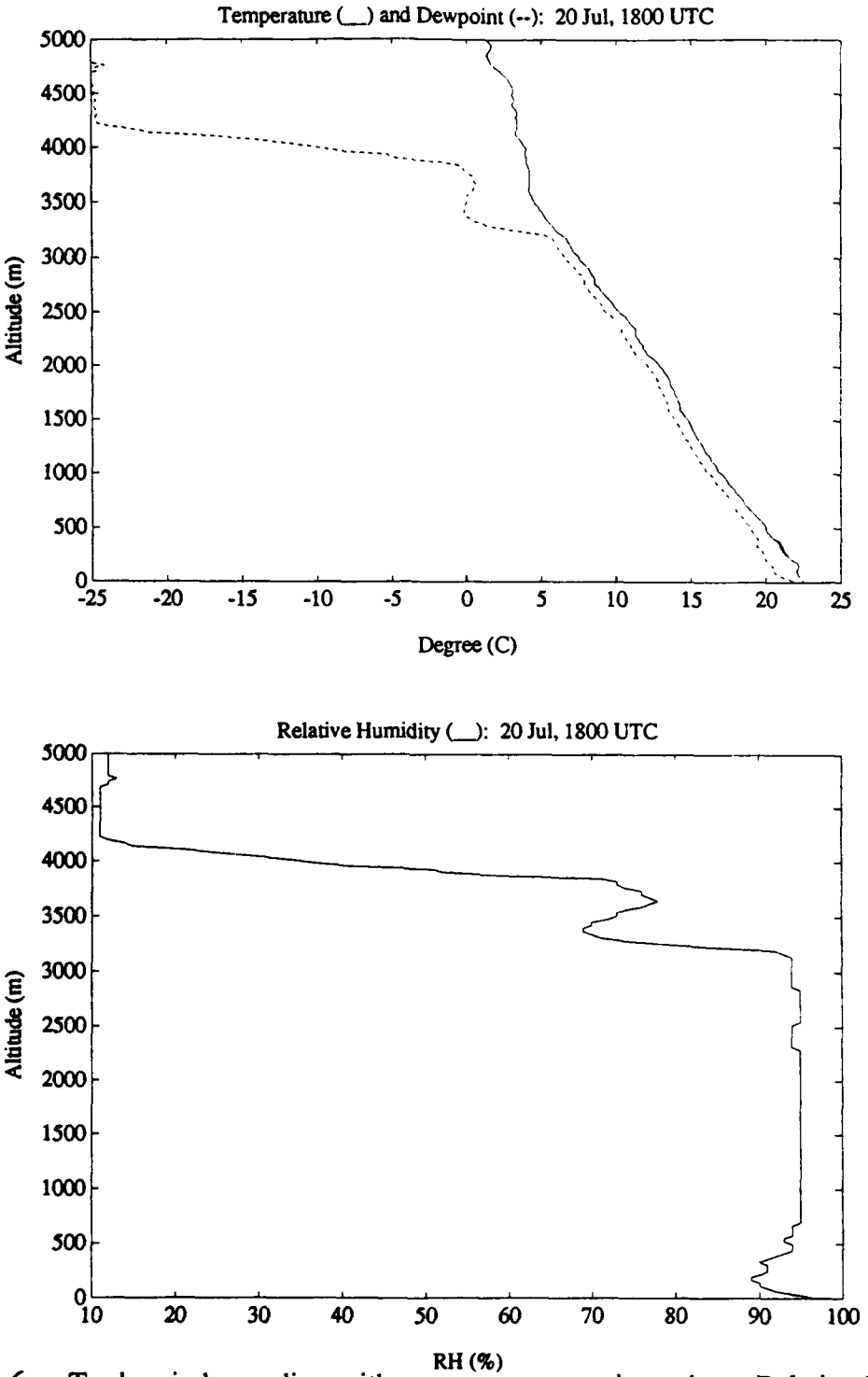

Figure 6c. Trade wind sounding without a temperature inversion. Relative humidity plot shows a well defined moist and dry layer.

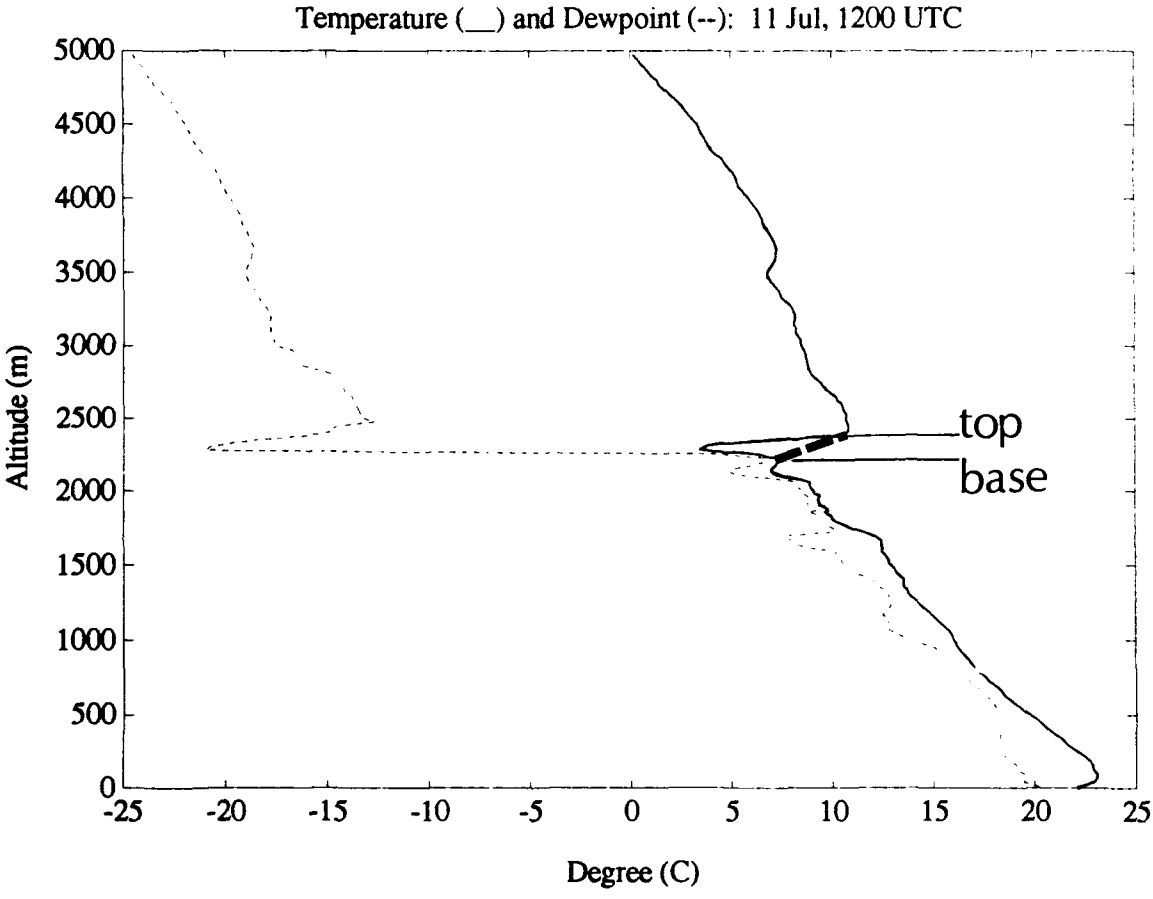

Figure 7a. Correction technique for a superadiabatic lapse rate at the inversion base. The corrected temperature at the inversion base is the last level before the lapse rate changes to superadiabatic. There is no change to the temperature at the inversion top.

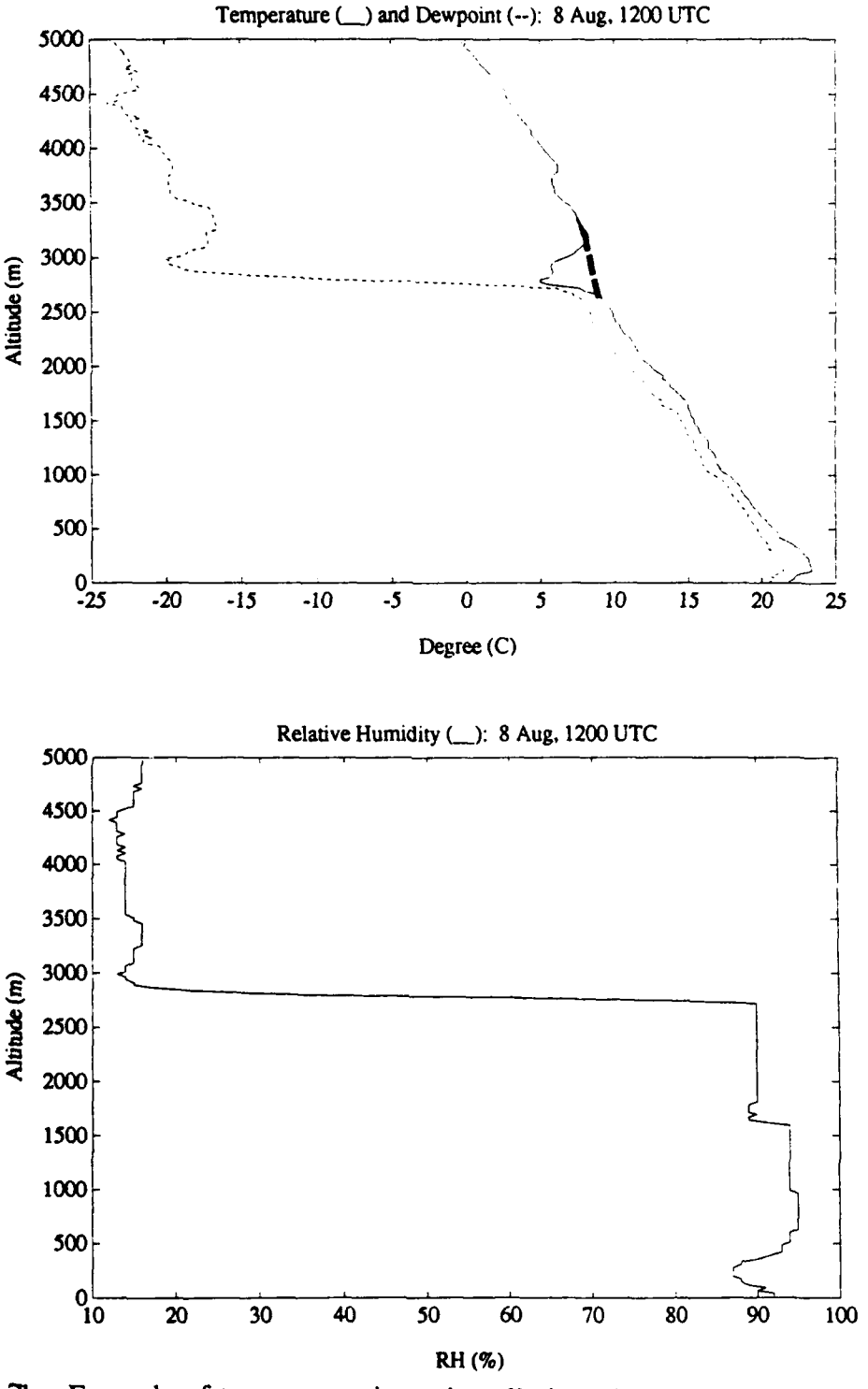

Figure 7b. Example of temperature inversion eliminated due to superadiabatic lapse rate correction. The relative humidity curve shows a well defined moist and dry layer.

the dry, warmer air above. This causes the wetted sensor to experience evaporative cooling which results in a superadiabatic lapse rate above the moist layer. The superadiabatic lapse rate usually occurs for less than a minute. The temperature sensor then quickly recovers and reports temperatures that increase with height.

Careful examination of soundings without superadiabatic lapse rates (Figure 6a) shows that the temperature starts to increase at about the same level that the relative humidity starts to decrease rapidly. The temperature increases at a fairly constant rate until the inversion top. With this in mind, when a superadiabatic lapse rate occurs at the inversion base, I correct it with the following technique (Figure 7a): (1) The corrected temperature at the inversion base is the last level before the lapse rate changes to superadiabatic, (2) There is no change to temperature at the inversion top, and (3) A line connecting the corrected inversion base to the inversion top depicts the corrected inversion lapse rate. This method corrects the inversion strength (defined as the temperature difference between the base and top of inversion). In 15% of the soundings, this correction eliminates the temperature inversion (Figure 7b). However, the relative humidity curve shows a well defined moist and dry layer.

3.2 Inversion Base Specification

After many aborted attempts to identify the inversion, I devised a method using both temperature and relative humidity. By using the traditional approach (temperature increasing with height) to measure the inversion, 76.6% of the soundings contain an inversion. However, a major part of this study is to compare the sounding to the profiler. As stated before, the profiler responds to changes in the index of refraction.

In addition, the index of refraction is primarily a function of moisture (75 to 84%) with temperature contributing only 4 to 10%. Therefore, it makes sense to define the inversion based on both temperature and relative humidity.

Accordingly, I select the inversion base as follows (Figure 8):

(1) Use the traditional approach when the relative humidity decreases rapidly (immediately above moist cloud layer) at about the same level as the temperature increases.

(2) Use the relative humidity approach when discrepancies exist:

(a) Temperature and relative humidity signal do not occur at about the same level (decoupled in only 3, or 2.4% of the cases).

(b) No temperature signal occurs (8.9%) or the temperature signal is erased due to correction for superadiabatic lapse rate (14.6%).

This definition is not the traditional method of using temperature only to define the inversion. For 74.6% of the soundings, the traditional method is followed since the temperature increase occurs at the same level as the relative humidity decrease. For the remaining 25.4% of the soundings, I use the relative humidity curve to define the inversion since there is not a temperature signal (23%) or it is decoupled (2.4%). Accordingly, this definition really identifies the top of the moist layer and not necessarily the temperature inversion. However, since the profiler is most sensitive to moisture, this definition is appropriate. In addition, the moisture and temperature signals almost always occur near the same level. Therefore, I define the top of the moist layer as the inversion base in this study.

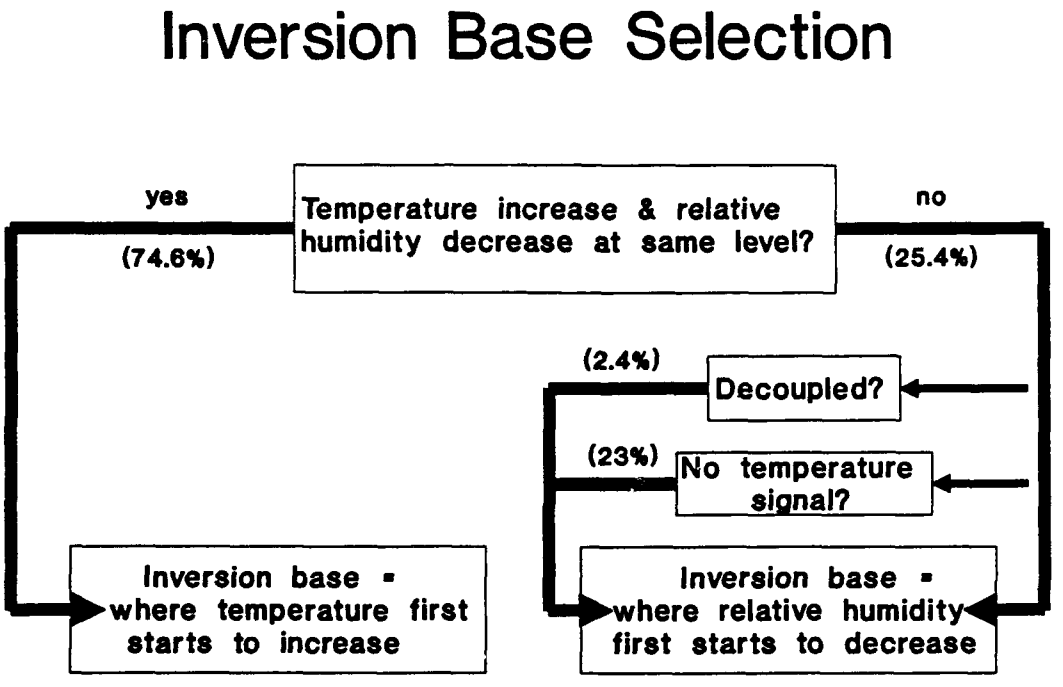

Figure 8. Inversion base decision tree (sounding).

For multiple inversions the atmosphere is more complex than shown in Figure 1. Under these conditions, a new model is necessary (Figure 9). As before, there is a subcloud layer and a cloud layer below the lower inversion. The subcloud layer can be further subdivided into a surface layer, a mixed layer and a transition layer, although only the subcloud layer is shown in the figure. The lower inversion is the transition zone between the lower cloud layer and middle layer. The middle layer is a secondary transition zone between the moister marine air below and the dry air above in the free atmosphere. Above the middle layer is another inversion and finally, the dry free atmosphere. The profiler responds primarily to moisture inhomogeneities (75 to 84%). Therefore, I selected the lower inversion for comparison since it occurs with the first significant relative humidity decrease. However, I show upper inversions and all significant inversions and layers for the reader.

3.3 Inversion Index

An important point is that this inversion base definition always gives an inversion level. For this reason, it is useful to determine the quality and strength of the inversion with an index. I have classified each inversion by the characteristics of the relative humidity curve and strength of the inversion. Defined in Table 6, the classification is a number from one to five for both relative humidity and temperature.

The relative humidity is usually high below the inversion and low above the inversion. Consequently, there is a large relative humidity gradient between the layers. Sometimes the signal is rather constant ($< 25\%$ variability in layer) and sometimes the signal is more variable ($\geq 25\%$ variability in layer). Examples of the relative humidity

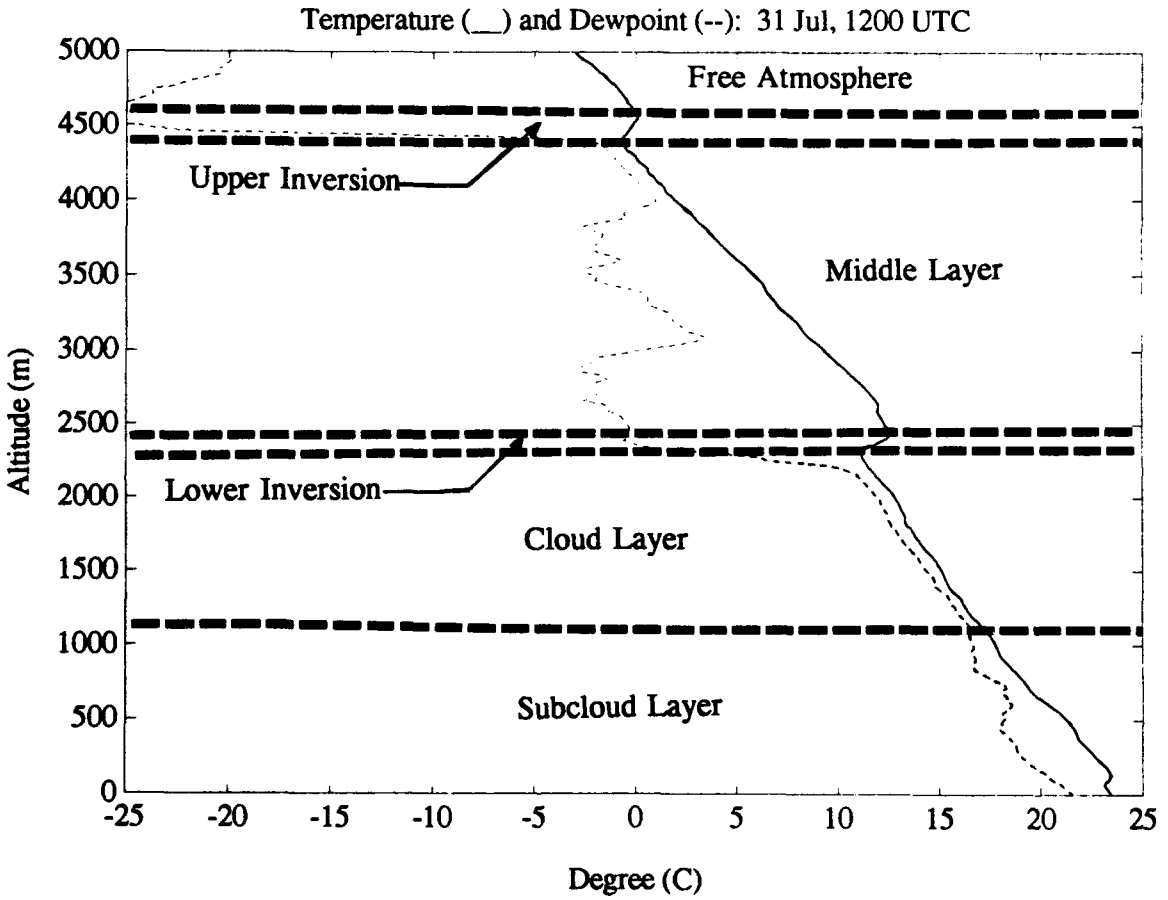

Figure 9. Multiple inversion model.

classifications appear in Figure 10. In contrast, the temperature typically decreases with height, except in the inversion. I define the inversion strength as the temperature difference between inversion base and top.

Table 6. Relative Humidity and Temperature Categories

	RELATIVE HUMIDITY			TEMPERATURE	
	Dry Layer	Moist Layer	Transition Layer Gradient	Strength	Signal Description
5	C[a]	C	large	≥ 1.0°C	good
4	C	V[b]	large	0.5 to < 1.0°C	fair
3	V	C	large	0.0 to < 0.5°C	weak
2	V	V	large	none	erased due to SALR[c] correction
1	V	V	small/none	none	no inv based on temperature

NOTES:
(a) C = Constant (< 25% variability in layer).
(b) V = Variable (≥ 25% variability in layer).
(c) SALR = superadiabatic lapse rate.

The classification results are shown in Table 7. Both relative humidity and temperature are in categories 3 or higher for 69% of the data. For relative humidity alone, 91% of the data are categories 3 through 5. In comparison, temperature categories 3 through 5 occur for 77% of the data.

I use this classification scheme to compare the inversion seen on the profiler to the sounding. I divide the soundings into three different groups: (1) RH/TEMP 5/5:

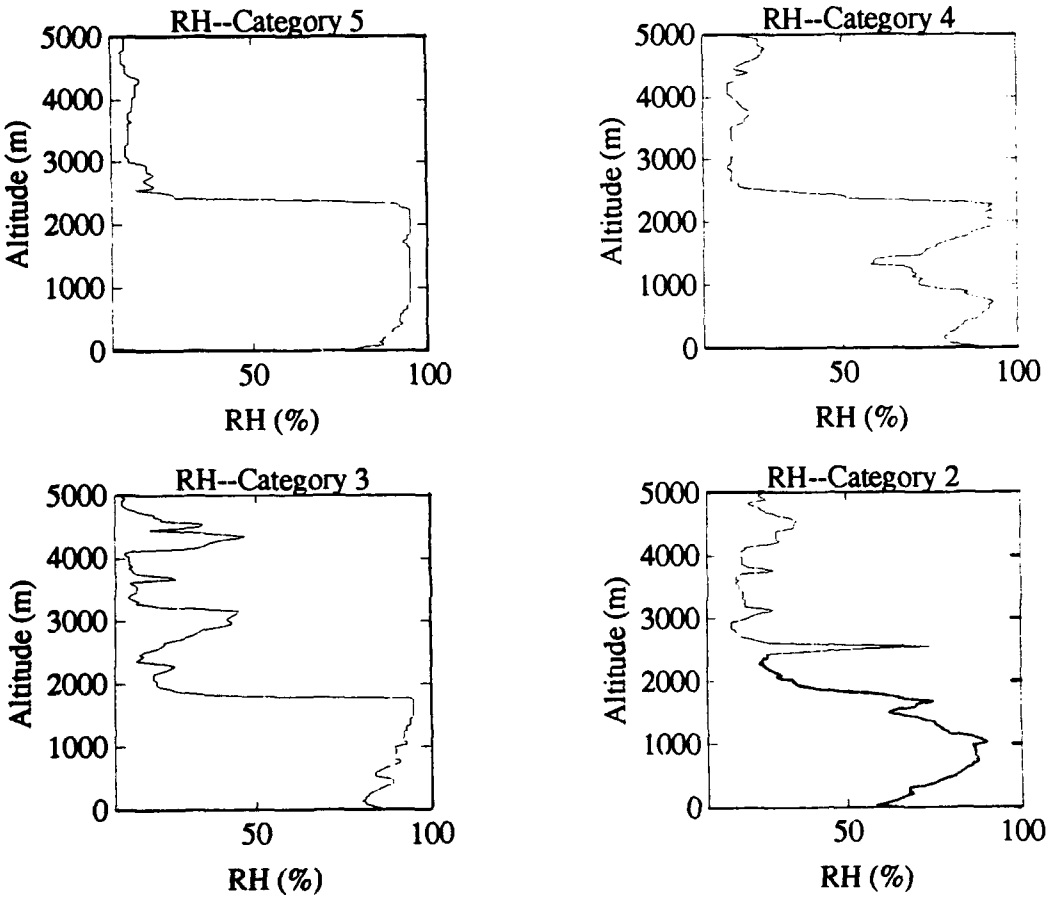

Figure 10. Relative humidity classification examples for categories 2 through 5. Relative humidity category 5 is constant in the moist and dry layer. Relative humidity category 4 has > 25% variability in the moist layer and is constant in the dry layer. Relative humidity category 3 is constant in the moist layer and has > 25% variability in the dry layer. Relative humidity category 2 has > 25% variability in the moist and dry layer.

Relative humidity and temperature category 5; occurs for 23% of the soundings, (2) RH/TEMP 3-5/3-5: Relative humidity and temperature category 3 through 5 combined; occurs for 69% of the soundings, and (3) RH/TEMP 1-5/1-5: Relative humidity and temperature category 1 through 5 combined; occurs for 100% of the soundings.

Table 7. Relative Humidity (RH) Versus Temperature

		TEMPERATURE CATEGORY					
RH CATEGORY		5	4	3	2	1	TOTAL
	5	29(23%)	2(2%)	10(8%)	12(10%)	2(2%)	55(44%)
	4	13(11%)	1(1%)	1(1%)	0(0%)	2(2%)	17(14%)
	3	17(14%)	5(4%)	7(6%)	6(5%)	6(5%)	41(33%)
	2	3(3%)	2(2%)	2(2%)	0(0%)	1(1%)	8(6%)
	1	1(1%)	1(1%)	1(1%)	0(0%)	0(0%)	3(2%)
	TOT	63 (51%)	11 (9%)	21 (17%)	18 (15%)	11 (9%)	124 (100%)

Since the profiler is more sensitive to moisture, I expect the highest correlation for a well defined relative humidity signal with little contribution from the temperature signal. Therefore, I expect the highest correlation for RH/TEMP category 5/5, but results might not be statistically significant with this small sample size. The second highest correlation should be for RH/TEMP category 3-5/3-5. I have a high level of confidence in the inversions in this group. Also, the group is large enough to be

statistically significant. The RH/TEMP category 1-5/1-5 contains some questionable soundings and will probably give the lowest correlations.

3.4 Inversion Results and Statistics

A time series for the inversion base results, other layers, and precipitation at Hilo is shown in Figure 11a. The precipitation is the accumulation since the previous sounding (from the Hilo Local Climatological Data, NOAA 1990). The height of the inversion base is quite variable, with frequent changes of over 1000 m in 12 hours. Between 13 to 14 August, the inversion dropped over 2500 m in 12 hours. Three disturbed periods are evident between 18 to 22 July, 12 to 14 August, and after 23 August. There sometimes is a relationship between higher inversion height and increased precipitation (18 to 22 July), but not always (7 to 9 August).

Figure 11b is a time series of inversion base, strength and top (when it exists by the temperature method). When the inversion strength is zero, the inversion base (or moist layer top) was identified from relative humidity since there was no temperature signal. As mentioned before, 15% of the soundings lose their temperature inversion from superadiabatic lapse rate correction. An additional 9% of the soundings do not have a temperature inversion. As a result, there is not an inversion top when the strength is zero.

Table 8 lists some inversion statistics. A diurnal variation is visible in the inversion base. The inversion is lower and stronger during the day (00 UTC, or 1400 HST), and higher and thicker during the night (1200 UTC, or 0200 HST). The mean strength is 1.75 °C for inversions corrected for a superadiabatic lapse rate, and 1.5 °C for

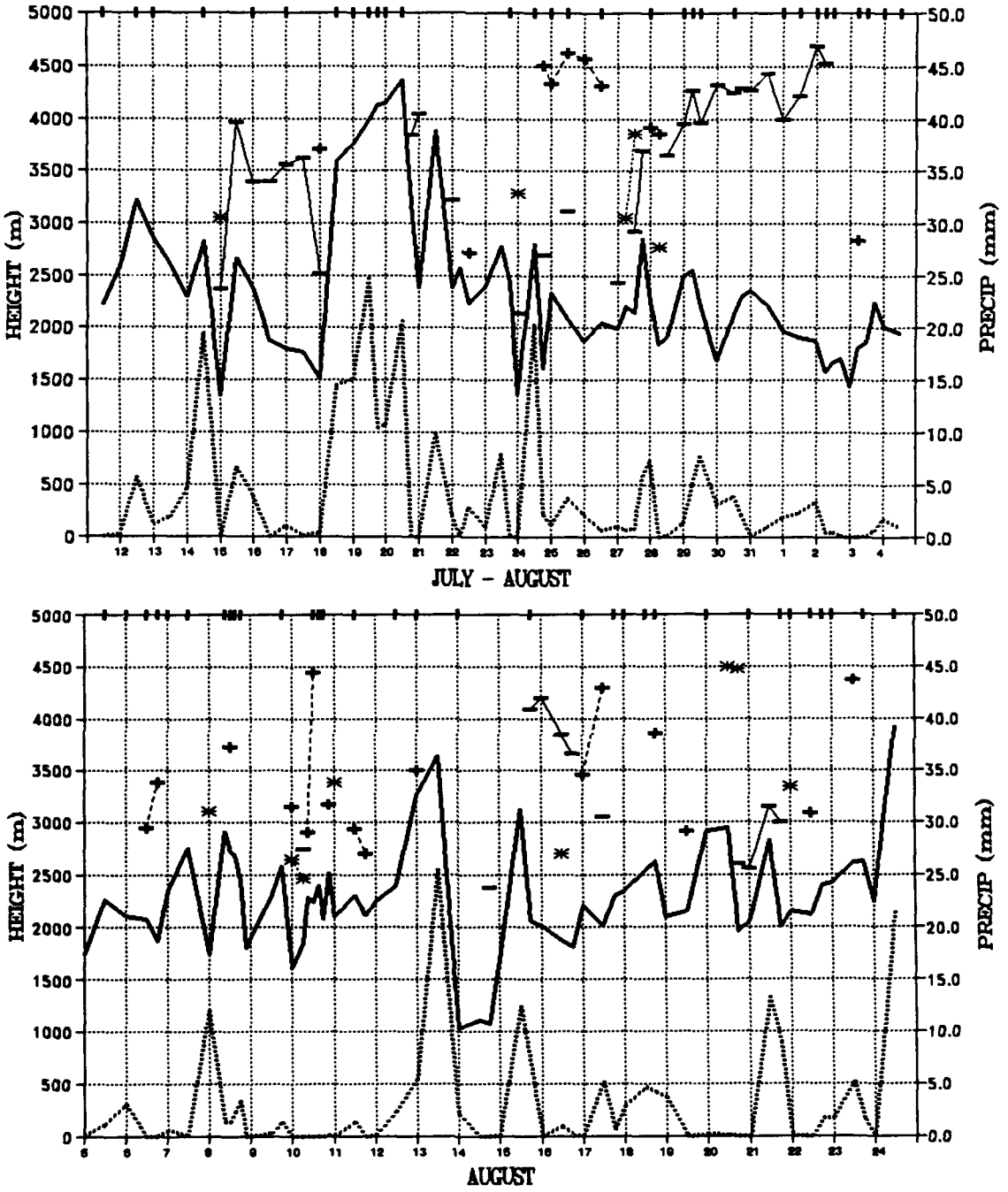

Figure 11a. Inversion base results, other layers, and precipitation (sounding). Key to symbols: ▬ = inversion base; — = upper layer inversion base (multiple inversion); + = secondary inversion base with temperature signal; * = secondary inversion base with temperature and relative humidity signal; ▮ = soundings with superadiabatic lapse rate (top of graph); ····· = precipitation accumulated since previous sounding.

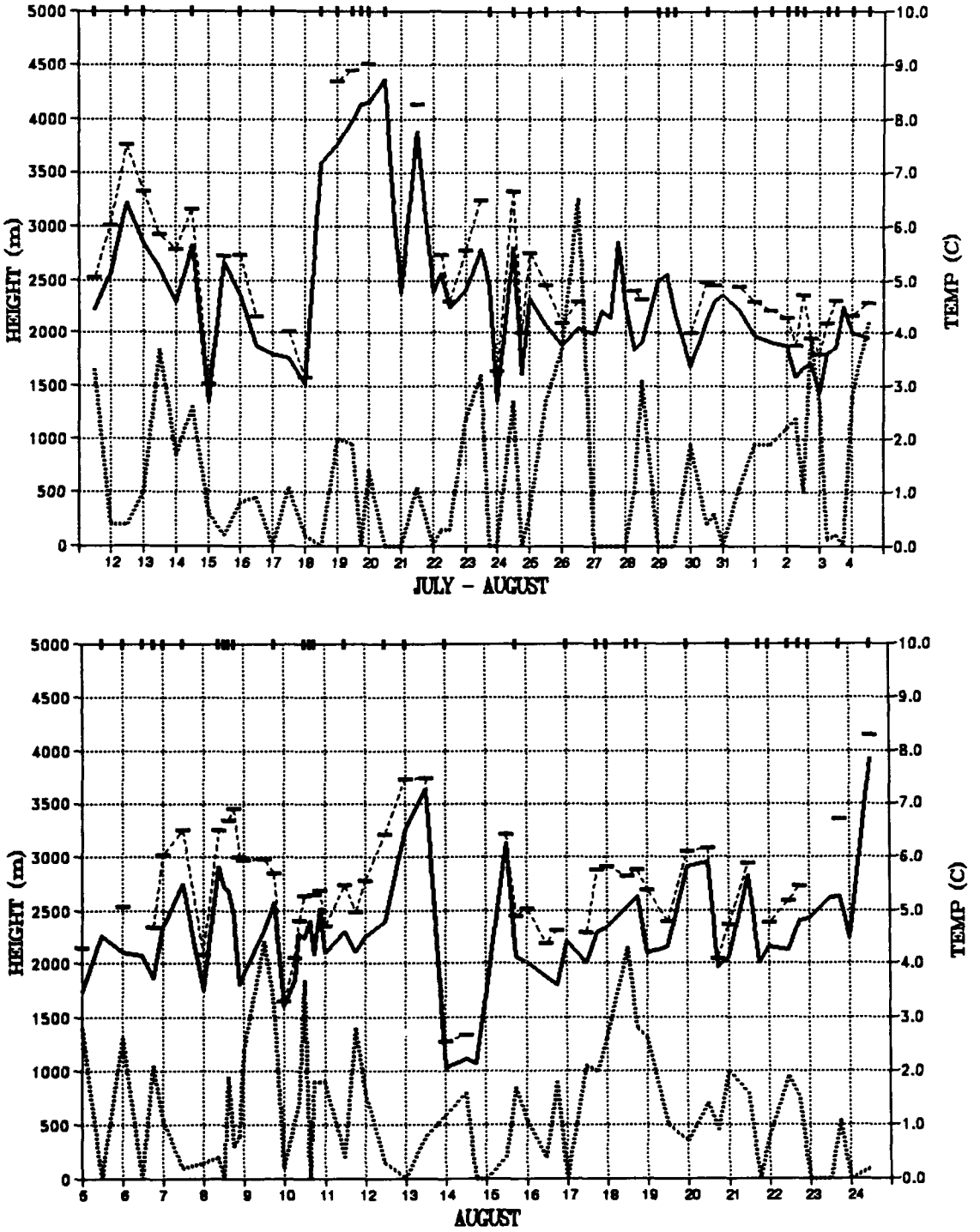

Figure 11b. Inversion base, top and strength (sounding). Key to symbols: ▬ = inversion base; ▬ = inversion top (when it exists); ····· = inversion strength; ▮ = soundings with superadiabatic lapse rate (top of graph).

inversions that do not require a correction. As a result, the inversion strengths obtained from this correction are reasonable.

Table 8. Inversion Statistics (Sounding)

	Overall	00Z	12Z
Mean Base	2322 m	2174 m	2508 m
Standard Deviation	624 m	576 m	683 m
Mean Strength	1.6 °C	1.5 °C	1.8 °C
Mean Thickness	373 m	379 m	340 m

Since many statistics assume a normal distribution, I tested the distribution of the inversion base. A Chi-squared (χ^2) test shows if the data is a good fit to the normal curve (Spiegel 1991):

$$\chi^2=\sum\frac{o^2_j}{e_j}-N \qquad (3.1)$$

where o_j is the observed frequency, e_j is the expected frequency based on the normal distribution, and N is the total number of observations. If $\chi^2 = 0$, the observed and theoretical frequencies agree exactly. The larger the value of χ^2, the greater the discrepancy between the observed and expected value.

Table 9 lists the distribution statistics. The raw data (Figure 12a) have a larger peak around the mean than does the normal distribution. A Chi-squared (χ^2) test shows it is not a good fit to the normal curve. I performed the same method for the natural log of inversion base (Figure 12b). The logarithmic data still has a larger peak around the mean than does the normal distribution, but is smaller than the raw data. A Chi-squared

(χ^2) test shows the logarithmic distribution is a better fit to the normal curve than the raw data. Although the distributions are not strictly "normal," I have accepted the assumption of normality in the subsequent analysis.

Table 9. Distribution Statistics (Sounding)

Dist[a]	± 1 STD[b]	± 2 STD	± 3 STD	χ^2	DF[c]	$\chi^2_{.995}$
Raw	78%	91%	99%	95	33	58
Log	77%	93%	99%	47	27	50
Normal	68.3%	95.5%	99.7%			

NOTES:
(a) Dist = Distribution.
(b) STD = Standard deviation.
(c) DF = Degrees of freedom.

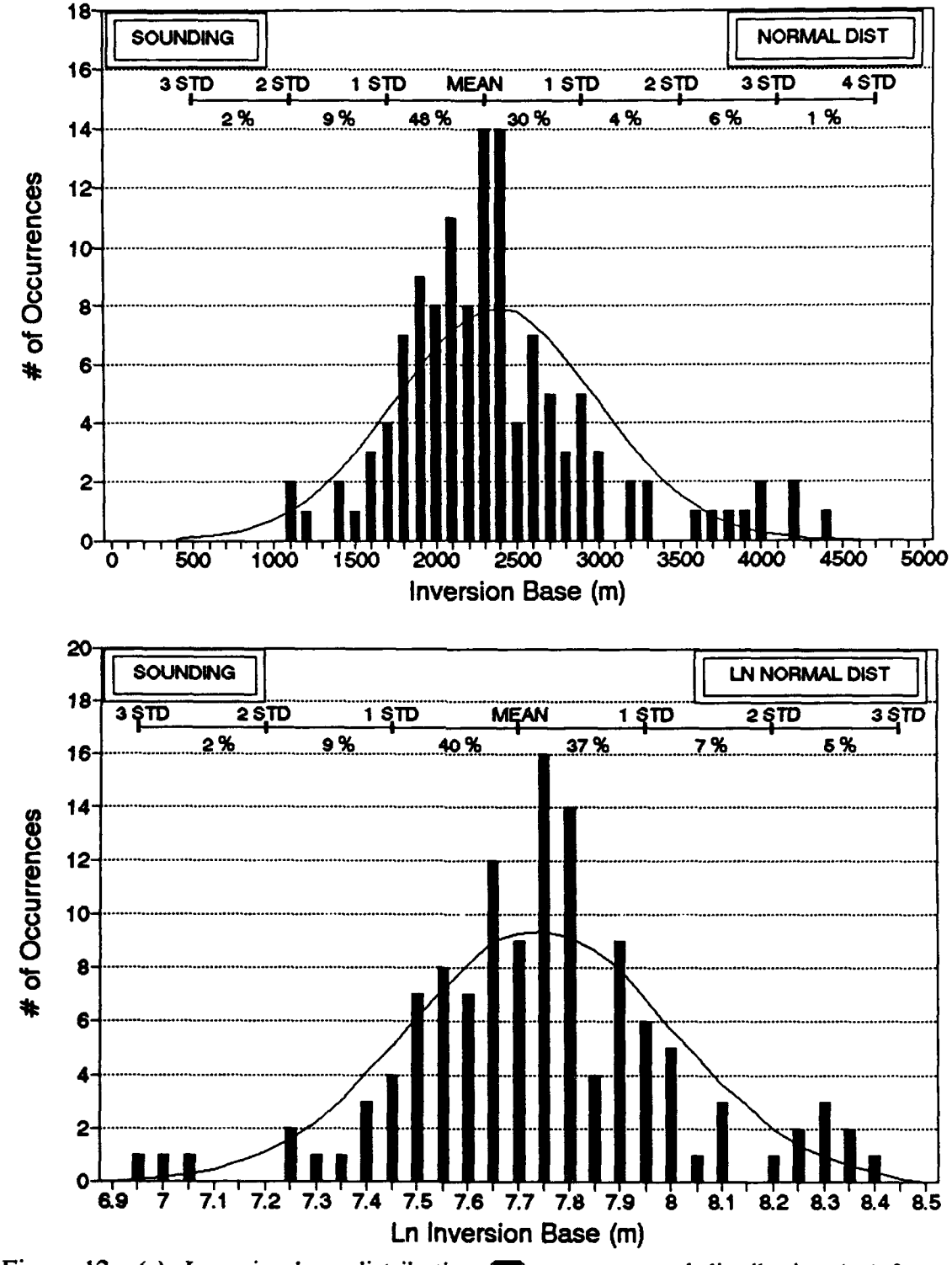

Figure 12. (a) Inversion base distribution (▮) versus normal distribution (⎯) for sounding. (b) Natural log of inversion base distribution (▮) versus normal distribution (⎯) for sounding. STD = Standard deviation.

CHAPTER 4

PROFILER ANALYSIS AND RESULTS

4.1 Profiler Analysis

Examination of the profiler vertical signal strength (reflectivity) reveals four characteristic signals: clear air return, rain return, mid-level return, and weak gradient/spikes.

Since the profiler is more sensitive to moisture than temperature, it is really sensing the top of the moist layer. As pointed out in Chapter 3.2, the moisture and temperature signals almost always occur near the same level. Accordingly, I defined the top of the moist layer as the inversion base.

The clear air return (Figure 13) is probably the most frequent signal, with signal strength decreasing gradually to the inversion. At the inversion, the signal strength can vary, but is usually greater than 900 MBz. A strong clear air return (signal strength 2300 MBz at inversion) is shown in Figure 13a. A typical inversion strength of 1380 MBz is shown in Figure 13b. Above the inversion, the signal strength rapidly drops to a small value in the dry air. Figure 13c is a contour plot of the clear air return examples. An interesting feature is observed between 1100 to 1300 HST (2100 to 2300 UTC), between 800 to 1500 m. This feature has low reflectivity values in the center, surrounded by higher values, and is often seen in clear air returns (although not usually this dramatic). As expected with clear air returns, there is no precipitation at Paradise Park for this day (2 August, Appendix A).

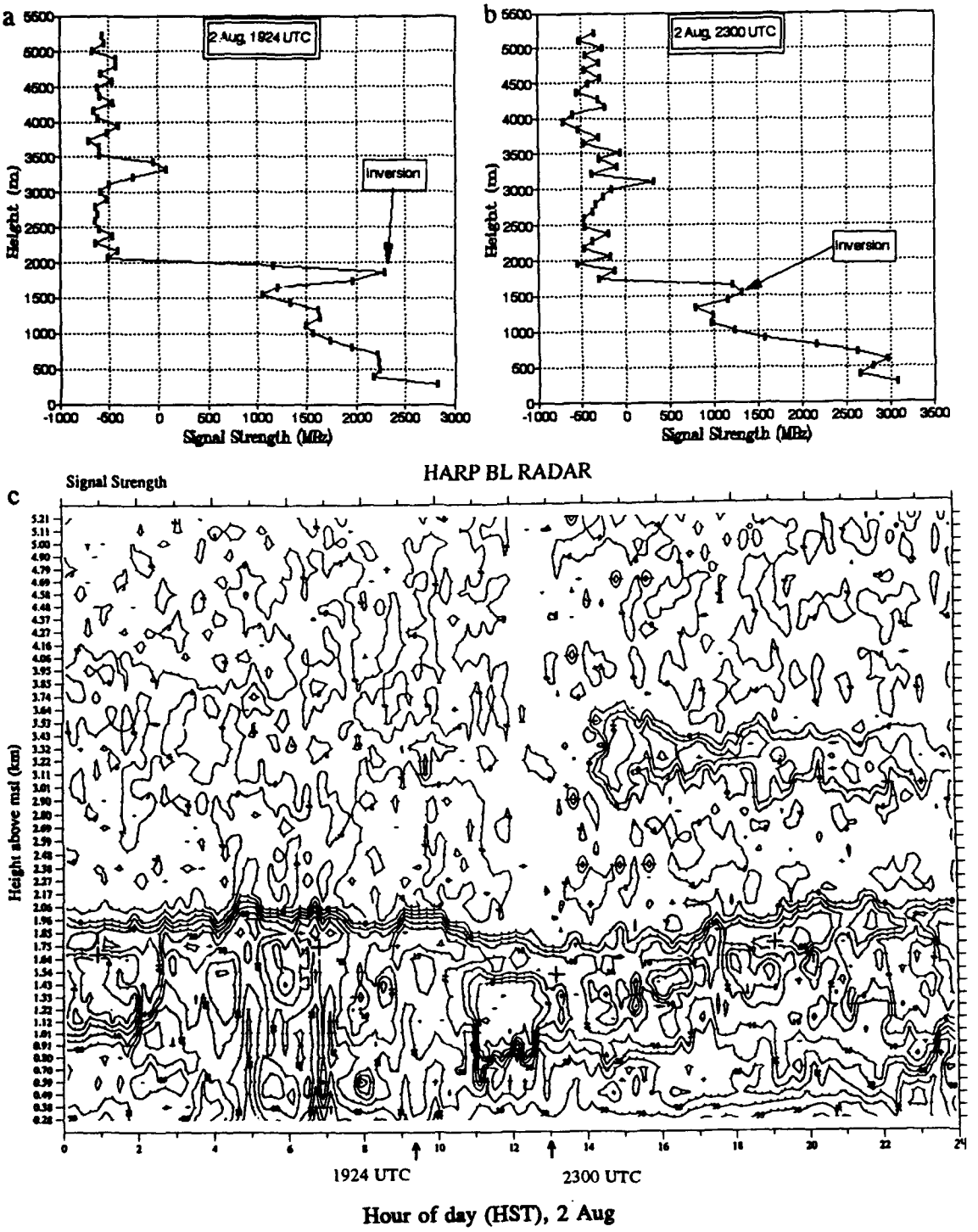

Figure 13. Clear air return. (a) Strong clear air return. (b) "Typical clear air return." (c) Signal strength contours (these plots courtesy of T. Riddle at NOAA). Contour increments: 5 DBz, or 500 MBz. A '+' symbol shows Hilo inversion base. A '↑' symbol indicates time of clear air returns.

The profiler is also sensitive to rain. Hence, another common signal is the rain return (Figure 14a and 14b). The sub-inversion air has a higher moisture content than the clear air return; consequently, the signal strength is often higher for the rain return. The signal strength decreases gradually to the inversion. At the inversion, the signal strength is usually, though not always, greater than the typical clear air return. Above the inversion, the signal strength rapidly drops off to a small value in the dry air aloft. Figure 14c is a contour plot of the entire day of the rain return examples (Figures 14a and 14b). The profiler gives a detailed analysis of the shower evolution. In contrast, the sounding (though only six hours apart) completely misses the event. Rain returns can be identified by tightly contoured areas of high reflectivity surrounded by lower values. Detailed evolution of individual rain events can be seen between 0100 to 0500 HST and 1000 to 1400 HST. The rain events often, but not always, appear to temporarily raise the inversion as seen between 1000 to 1400 HST. A dramatic example of a shower possibly penetrating the inversion is seen between 0100 to 0500 HST. Appendix A shows a significant amount of precipitation at Paradise Park for this convective activity (30 July).

The mid-level return occurs infrequently and is associated with mid-level moisture or clouds. Figure 15c, a contour plot of the mid-level return examples (Figures 15a and 15b), shows a persistent mid-level feature from 1500 to 2400 HST, at about 3 km. The mid-level return differs from the weak gradient/spikes (Figure 16) in that it occurs for a relatively long period. The vertical profile of the signal strength is similar to the clear air return except above the inversion. As before, the signal strength rapidly drops above

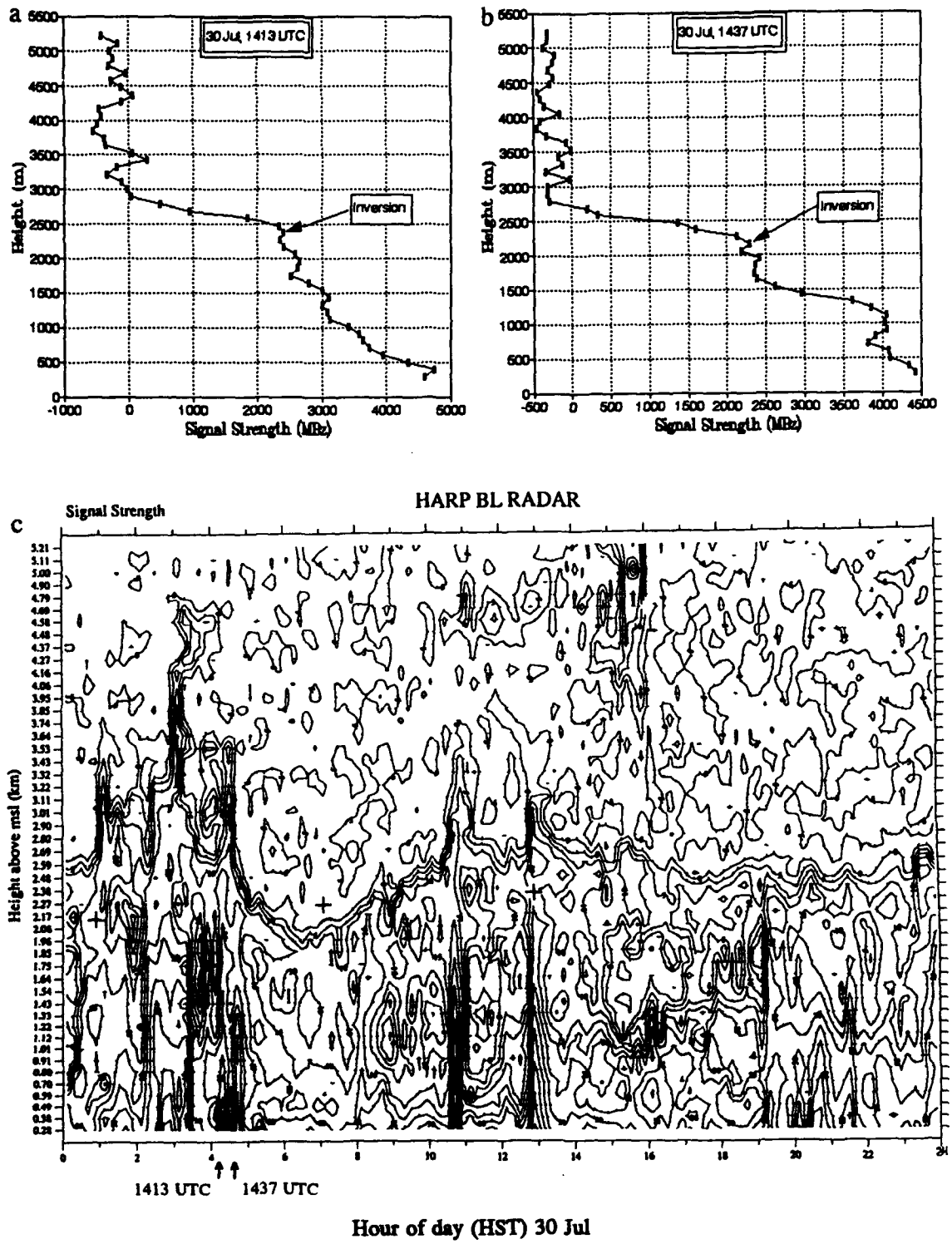

Figure 14. (a) Rain return. (b) Rain return. (c) Signal strength contours (increments: 5 DBz, or 500 MBz). Symbols as is Figure 13.

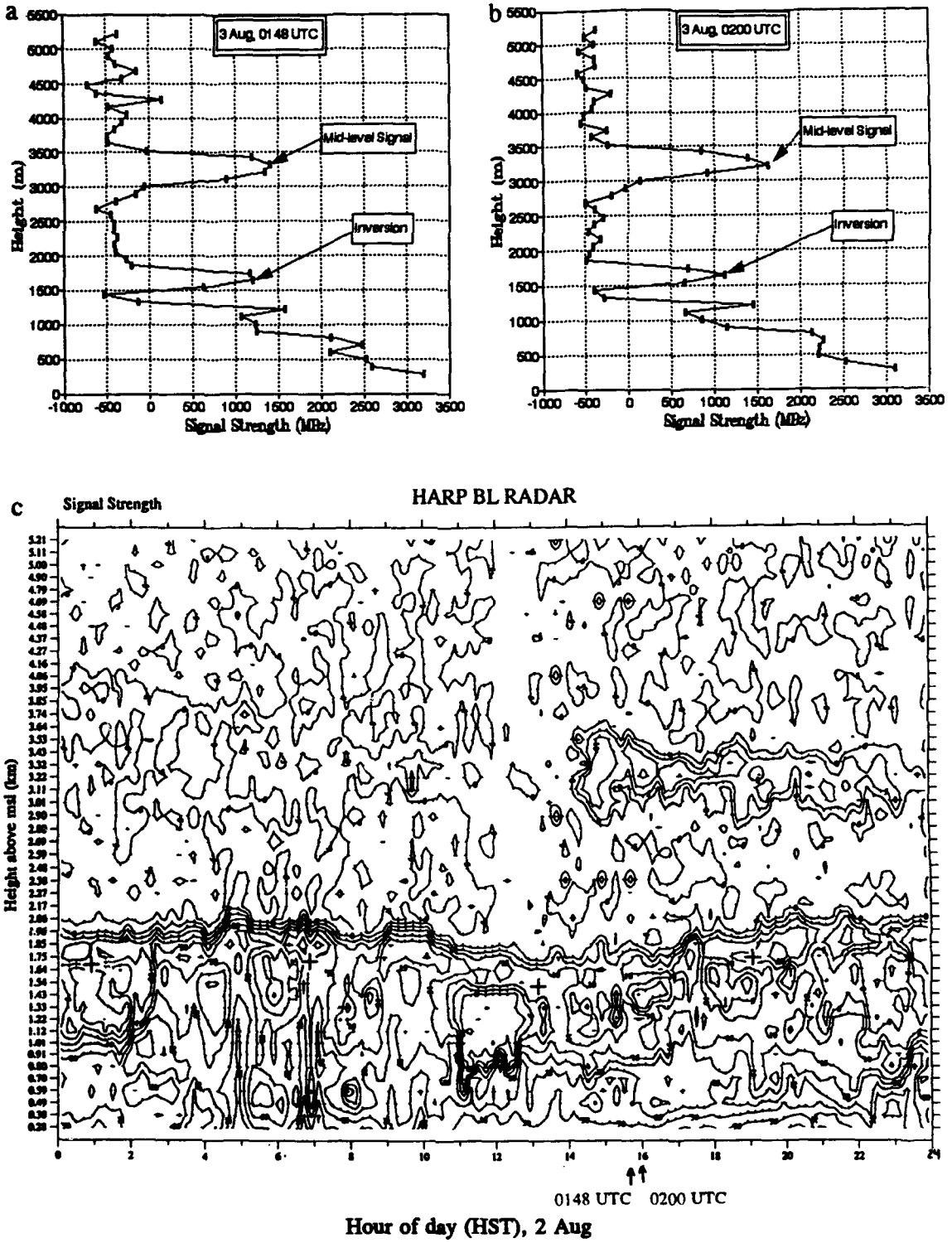

Figure 15. (a) Mid-level return. (b) Mid-level return. (c) Signal strength contour plot (increments: 5 DBz, or 500 MBz). Symbols as is Figure 13.

the inversion. However, mid-level clouds/moisture (noted in R. Rogers' profiler log) cause the signal strength to increase (Figure 15a and 15b). Above the mid-level clouds the signal strength again rapidly decreases.

The weak gradient/spikes (Figures 16a and 16b) are not a persistent feature. A lower spike (Figure 16a) is an increase of reflectivity below the inversion that has a higher signal strength than the inversion. Lower spikes often occur after a convective shower, seen in Figure 16c, or when the signal strength gradient at the top of the moist layer is weak. An upper spike (Figure 16b) is similar to a lower one save that it is above the inversion where the signal strength (usually negative, or small) is significant ($\geq$ 900 MBz). An upper spike is thought to be a false return well above the moist layer. Figure 16c, a contour plot of the day, shows the inversion oscillating between 2 to 2.5 km.

4.2 Inversion Base Specification

I designed and tested four different algorithms to determine the inversion base.

4.2.1 Method One

Method One searches for the maximized level of the sum of the square of the natural log of the signal strength:

$$\frac{\Sigma(\ln(signal.above))^2}{N} - \frac{\Sigma(\ln(signal.below))^2}{N} \qquad (4.1)$$

where signal is the signal strength, and N is the number of levels above or below, respectively. The program starts at the bottom (Figure 17) and works upward one level

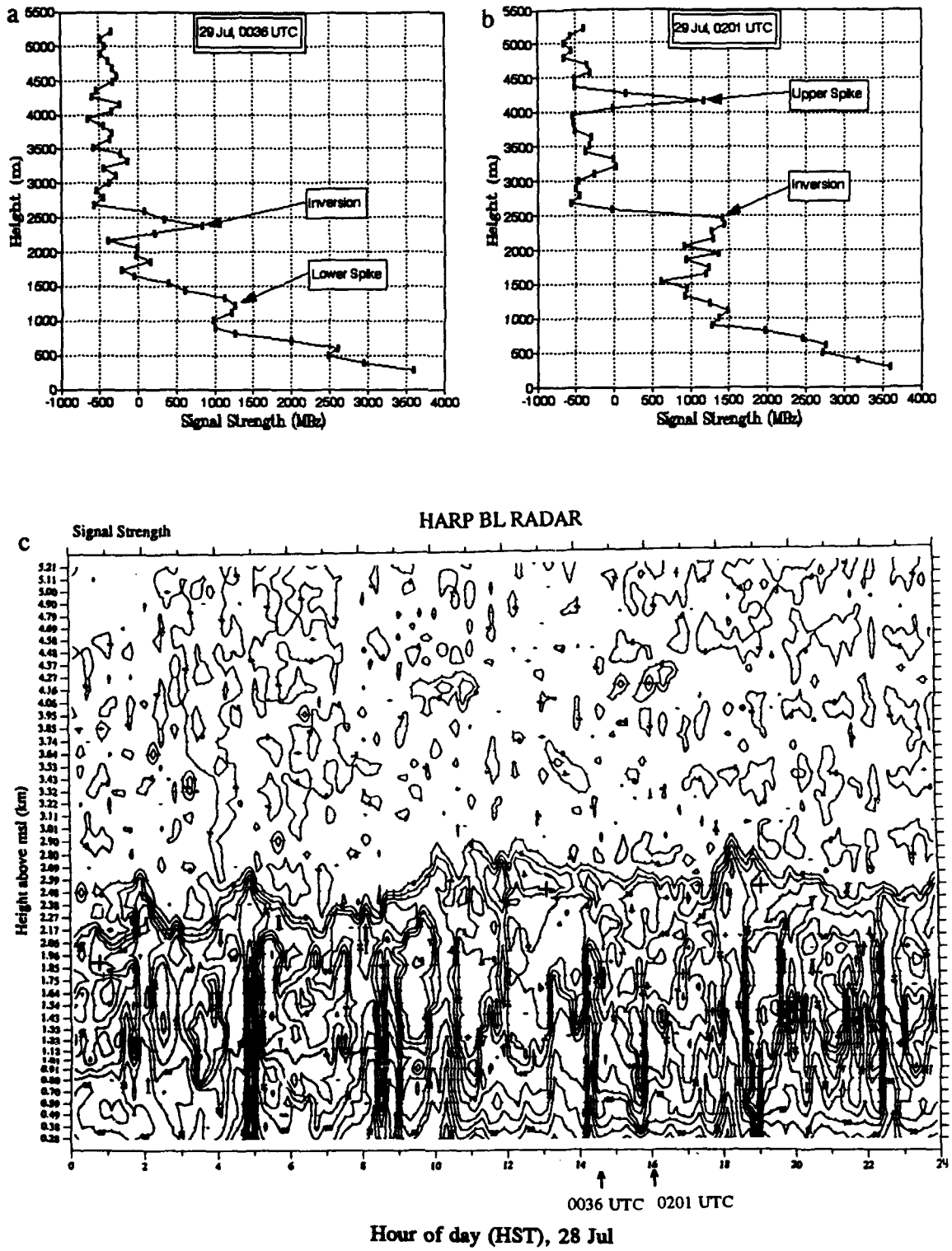

Figure 16. Weak gradients/spikes. (a) Lower spike. (b) Upper spike. (c) Signal strength contour plot (increments: 5 DBz or 500 MBz). Symbols as is Figure 13.

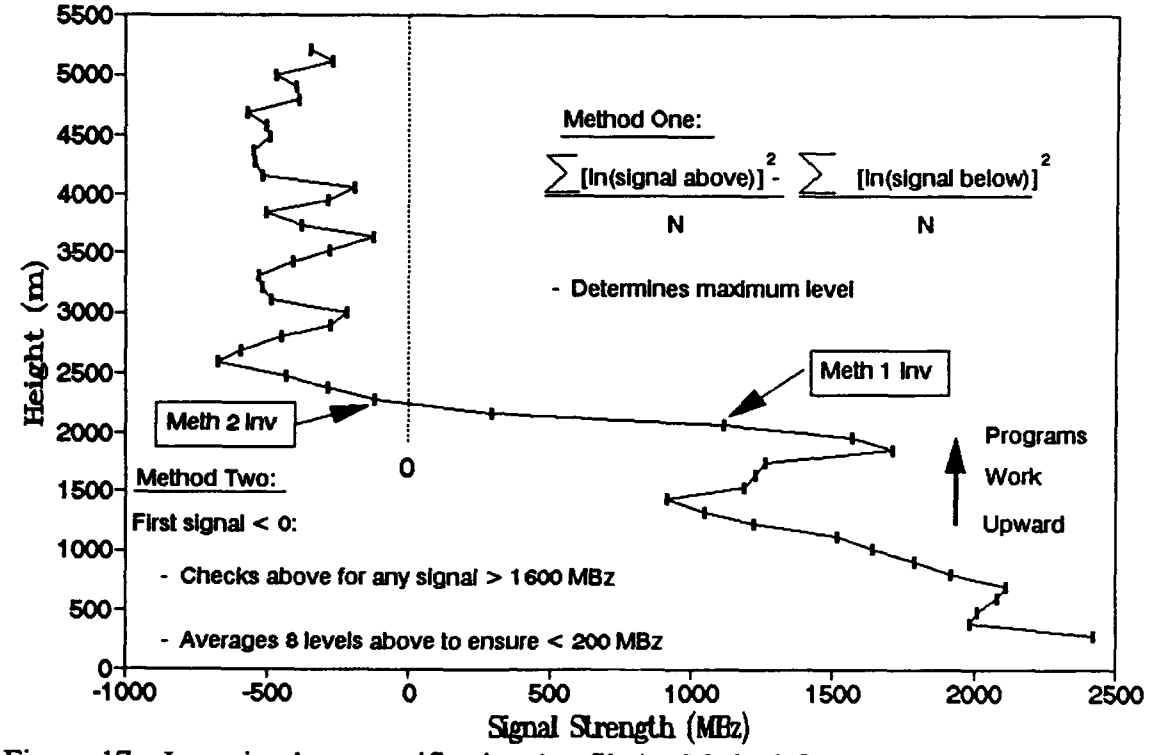

Figure 17. Inversion base specification (profiler): Method One and Two.

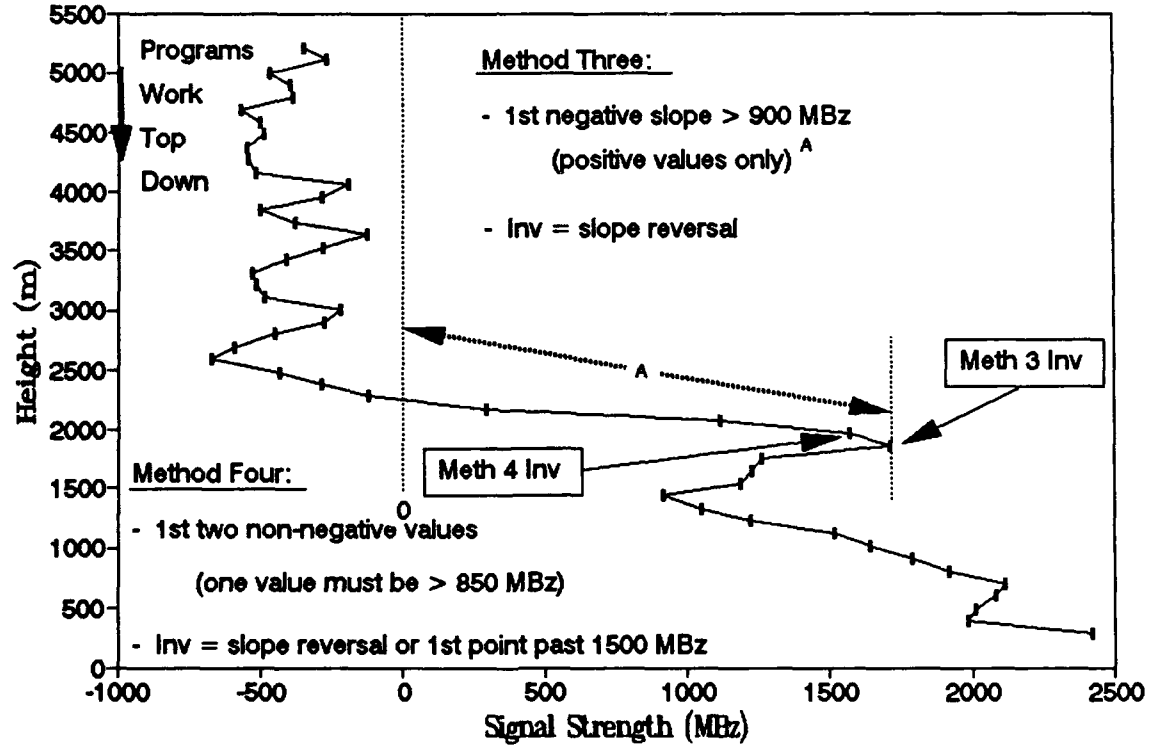

Figure 18. Inversion base specification (profiler): Method Three and Four.

at a time. It determines equation 4.1 at each level. The inversion is the level with the largest difference. This method often identifies levels below the inversion.

4.2.2 Method Two

Method Two looks for first level of "continuous zero value." The program starts at the bottom (Figure 17) and works upward to find a zero crossing of the signal strength. At the first level less than zero, it checks the levels above for a signal strength greater than 1600 MBz. In addition, it adds the eight levels above the zero crossing to see if their average is less than 200 MBz. These tests attempt to ensure the values above the zero crossing remain small as seen in Figures 13 through 16. The inversion is the first level above the zero crossing (if it passes the two tests). This method also often identifies levels below the inversion. In retrospect, a possible improvement to this method might be to reduce the significant signal strength (800 to 1000 MBz).

4.2.3 Method Three

Method Three looks for the first significant negative slope (Figure 18). This program works from the top down and looks for negative slopes. For each negative slope, it computes the magnitude from the highest positive signal strength to zero (excludes negative values). If the magnitude is greater than 900 MBz, the highest signal level (where the slope reverses to positive) is the inversion base. I found the best significant negative slope magnitude to be less than 900 MBz. The algorithm flags the first significant negative slope, but can be revised to flag all significant negative slopes. This method suffers when there is mid-level return (Figure 15) and weak gradient/spikes (Figure 16).

The lower (upper) spikes occur because the slope magnitude selected in the algorithm is too large (small). As a result, for lower spikes the method looks downward for the next significant negative slope. However, using a smaller significant negative slope in the method only identifies even more upper spikes.

4.2.4 Method Four

Method Four looks for the first two positive values (one of which must be greater than 850 MBz), measured from the top down (Figure 18). Like Method Three, the inversion is the highest signal level (where the slope reverses). However, there is a filter to see if the signal strength is larger than 1500 MBz. If it is, the program flags the inversion at the first level (working from the top down) after 1500 MBz. This test was an early attempt to despike the data. When strong downward spikes occur, this method stops the inversion from going all the way to the surface. However, the despiking solution in Chapter 4.3 is better. This method usually (but not always) gets the same level, or slightly higher, than Method Three. In addition, it has similar problems with mid-level return (Figure 15) and weak gradient/spikes (Figure 16).

4.3 Subjective Filtering of Method Three

Using regression analysis (Draper and Smith 1966; Appendix B) Methods One and Two have the lowest correlation for RH/TEMP 3-5/3-5 inversions determined by the radiosonde (Table 10). Method Three always performs better than Methods One and Two and performs somewhat better than Method Four. However, I can improve this method by subjectively removing mid-level return/interference, and then filtering the spikes in the data.

Table 10. Regression Analysis for all Four Methods, RH/TEMP 3-5/3-5, "All Data," Closest Time (Before Filtering for Mid-Level Return and Spikes)

	Method 1	Method 2	Method 3	Method 4
Correlation	.386	.389	.661	.611
Y-intercept (m)	542	1173	697	961
F-Value	11.7	11.9	52	40
F-Distribution	7.06	7.06	7.06	7.06
Total	69	69	69	69

I removed the mid-level return/interference using a modified version of Method Three. The program looks for all significant levels down to the surface, rather than only the first. By comparing a plot of the layers (Figure 19a) to the contour plots (Figure 19b), I can determine the proper level for the inversion. There are 700 hours of data in the "continuous data" set, of which only about 30 hours (4.3% of the data) required correction for mid-level return. Therefore, Method Three accurately determines the inversion almost 96% of the time. However, human interpretation can improve this method.

An example of the inversion before and after removing the spikes is shown in Figure 19c and 19d. I despiked the data based on physical reasoning. It is not likely the inversion would be constant at a particular level and then suddenly drop more than 450 m in 12 minutes. Nor is it likely it would quickly recover 12 or 24 minutes later to the original level. This example would give a downward vertical velocity of 62.5 cms^{-1} that reverses 12 to 24 minutes later to an upward vertical velocity of the same magnitude. In contrast, a typical synoptic scale vertical velocity in the tropics is .3 cms^{-1} (Holton

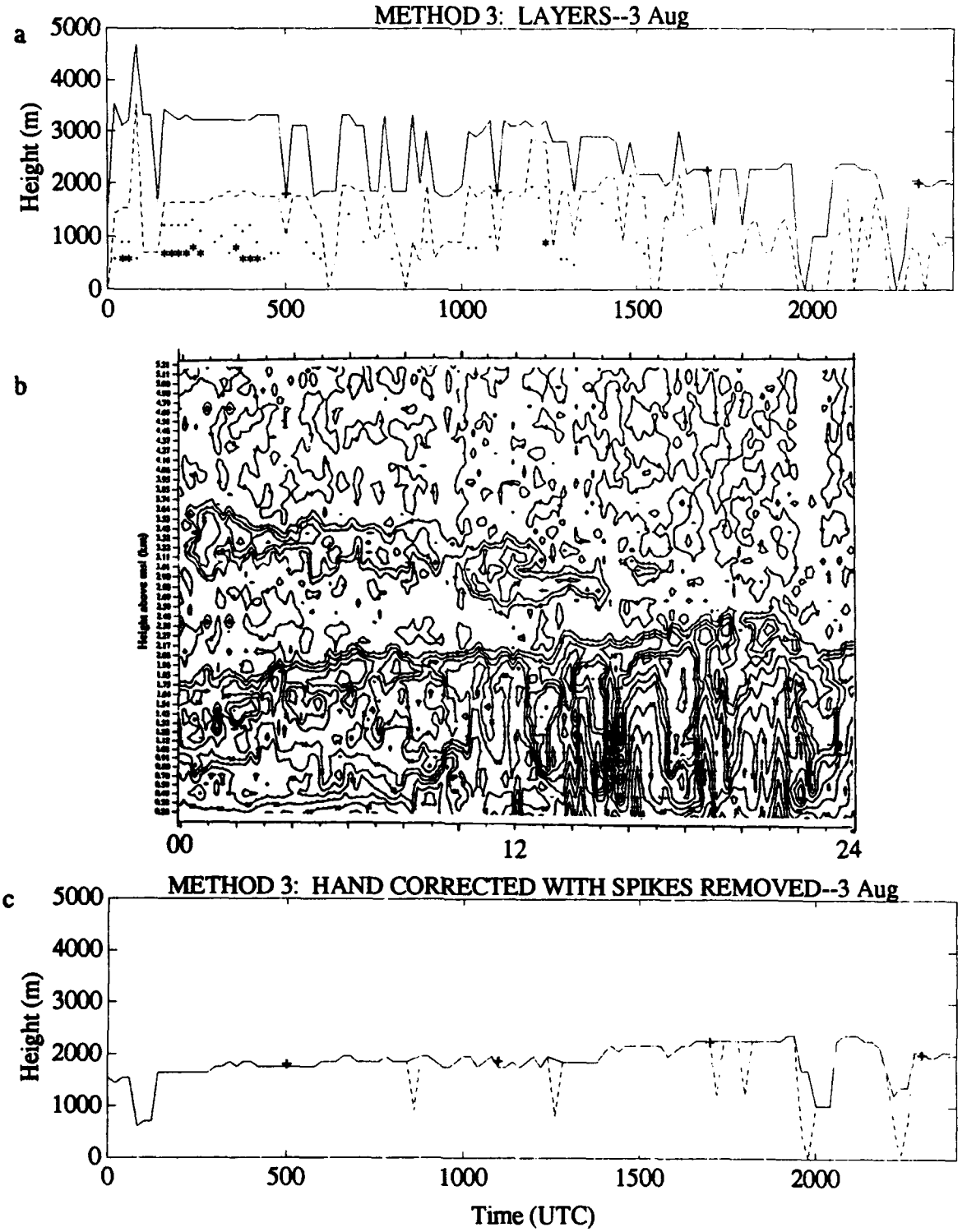

Figure 19. Removal of mid-level return and spikes. (a) Significant layers. (b) Contour plot. (c) Method 3 subjectively filtered for mid-level return with downward spikes (--), and corrected for downward spikes (__).

1979). Although there might be atmospheric phenomena that occur with vertical velocities of this magnitude, they are not considered in this study. Therefore, the despiking algorithm is: (1) Remove low inversion point if the inversion falls more than 450 m in 12 minutes and recovers more than 450 m in 12 or 24 minutes, and (2) Compute new inversion levels by averaging the two closest good inversion levels.

The reader might think that hand analysis of the contour plots (Figure 19b) would provide an accurate inversion base. However, the eye is fooled by these plots and can easily make errors in excess of 500 m. An automated algorithm for Method Three quickly determines the inversion and has problems only 4.3% of the time with mid-level returns. The despiking algorithm can also be automated and it improves the inversion results for Method Three. Like all automated algorithms, it can be fine-tuned by human interpretation, especially in an operational environment. Appendix A contains the subjective filtering results of Method Three inversion heights and precipitation for Paradise Park.

CHAPTER 5

PROFILER VERSUS SOUNDING

5.1 Raw Versus Averaged Data

I computed regression analysis, F-test for regression significance, and the correlation between the sounding and profiler following Draper and Smith (1966). A description of the equations are in Appendix B.

I tested a variety of averaging techniques to try to find the best fit and highest correlation between the soundings and the profiler. I used the inversion results before subjective filtering for mid-level returns and spikes. Reassuringly, the highest results are usually for the raw data (Table 11). The different averaging methods tested were (1) a running average of the inversion heights before correlation, and (2) an average of the inversion heights for the two closest profiler times to the sounding. I tested the soundings grouped in the RH/TEMP category 3-5/3-5, with the "all data" group (Table 11) and with the "continuous data" group. It is interesting that the correlation for Method Three is always lower for the averaging methods than for the raw data. In contrast, the correlation for Method Four is slightly higher for the averaging methods. The highest correlation for Method Three is .661 for the raw data. The highest correlation for Method Four is slightly lower (.643 for the 24 minute average). Although the correlations for the "continuous data" group are not shown, the averaging techniques affected the results even more than for the "all data" group. Since the results are not significantly better for any of the averaging techniques, the raw data is used in this study.

The results for the raw data (no averaging), before subjective filtering of Method

Three, for the various data groupings are shown in Table 12. The correlations for RH/TEMP category 1-5/1-5 are the lowest (.583 and .606) for the "continuous data." The RH/TEMP 3-5/3-5 grouping gave the highest correlations (.787 and .800) for the "continuous data." Figure 20 is a plot of the regression analysis for the RH/TEMP 3-5/3-5 "continuous data," Method Three. The RH/TEMP category 5/5, although expected to give the highest results, gave the second highest correlations. This is due to the effect of two outliers on a small sample size for Method Three (see Figure 21). However, the line of best fit is closest to zero (y-intercept of -44 m and 48 m) with this grouping.

Table 11. Regression Analysis for Different Averaging Tests, "All Data" (Prior to filtering for Mid-level Return and Spikes)

		METHOD 3			METHOD 4			F-Dist 99%	T O T
RH/ TEMP	Avg Meth (min)	Corr	Y-int (m)	F-Val	Corr	Y-int (m)	F-Val		
3-5/3-5	none	.661	697	52	.612	959	40	7.06	69
	24[a]	.590	991	36	.643	997	47	7.06	69
	36[b]	.616	1085	41	.637	1043	46	7.06	69
	60[c]	.611	1189	40	.623	1165	44	7.06	69

NOTES:
(a) Inversion averaged from 2 closest profiler values.
(b) Inversion averaged by 3 value running mean, closest profiler time selected.
(c) Inversion averaged by 5 value running mean, closest profiler time selected.

Method Three correlates higher for the "all data" grouping (Table 12). In contrast, Method Four correlates higher for the "continuous data" grouping. The reason Method Four does slightly better is due to the 1500 MBz filter described in Paragraph 4.2.4. When a downward spike occurs, this filter often decreases the size of the spike (but does

not remove it). However, this filter sometimes selects the inversion at a slightly higher level than shown in Figures 13 through 16. I recomputed the correlations for Method Three, including the 1500 MBz filter, for the "continuous data," and got similar results to Method Four, (1) RH/TEMP 1-5/1-5 correlation: .605, (2) RH/TEMP 3-5/3-5 correlation: .800, and (3) RH/TEMP 5-5/5-5 correlation: .700. Since the correlations for Method Three are almost always equal or higher than Method Four, it is the method of choice. However, I omit the 1500 MBz filter since Chapter 5.3 gives a much better method to despil · the data.

Table 12. Regression Analysis for Raw Data, Closest Time
(Before Filtering for Mid-Level Return and Spikes)

		METHOD 3			METHOD 4			F-Dist 99%	Tot
RH/ TEMP	Type	Corr	Y-int (m)	F-Val	Corr	Y-int (m)	F-Val		
1-5/ 1-5	all	.530	911	38	.517	1124	35	6.94	98
	cont	.583	809	43	.606	841	48	6.99	85
3-5/ 3-5	all	.661	697	52	.611	961	40	7.06	69
	cont	.787	256	94	.800	252	103	7.11	60
5-5/ 5-5	all	.462	1150	6	.246	1854	1	8.10	23
	cont	.626	48	11	.716	-44	18	8.53	19

NOTES:
(a) all = "all data" and cont = "continuous data"

Table 13 is an analysis of the residuals (difference between the profiler estimate and regression line) more than 400 m for the RH/TEMP 1-5/1-5 "all data." Of the 30 large residuals listed in Table 13, 4 would improve by subjectively correcting for mid-level clouds and 7 would improve by removal of the spikes. The causes of the skewed curve

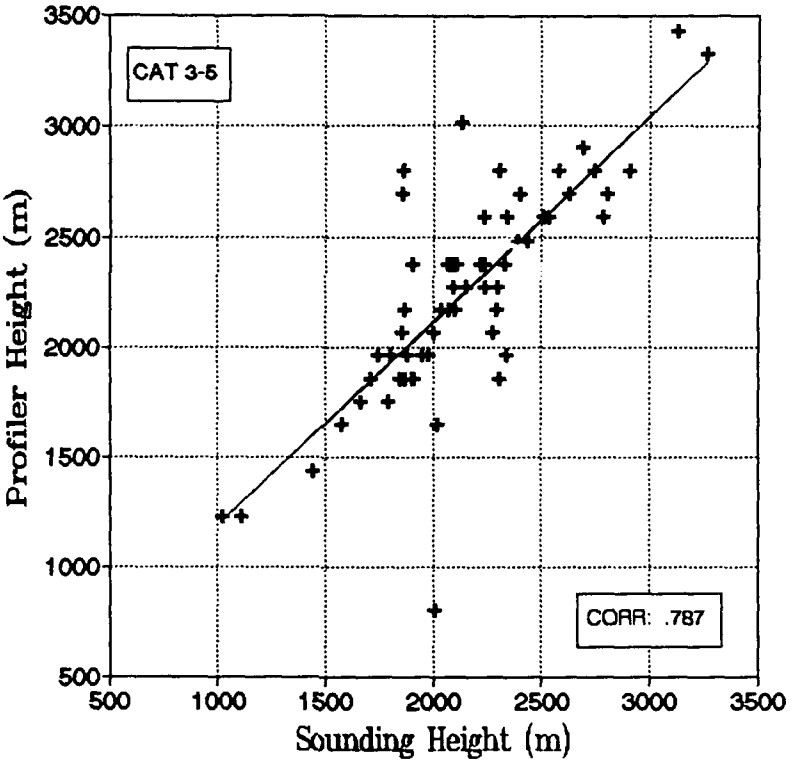

Figure 20. Regression analysis for RH/TEMP 3-5/3-5 "continuous data."

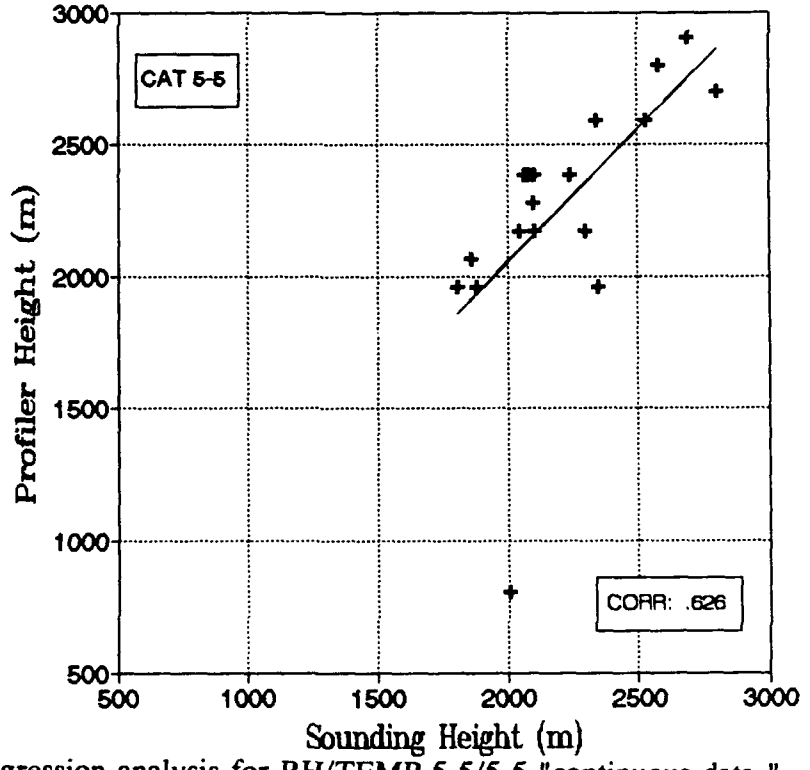

Figure 21. Regression analysis for RH/TEMP 5-5/5-5 "continuous data."

are high or low values that strongly affect the regression curve (see Figure 22). The correction of these 11 points should improve the 5 skewed curve points that have large residuals.

Table 13. Cause of Large Residuals (> 400 m).
(Prior to Filtering for Mid-Level Return and Spikes)

PROBLEM	#	COMMENTS
Rain/Virga	11	Cloud breaking through inversion?
Mid-level clouds	4	Improve by subjective correction
Interference	4	Instrument problem
Skewed curve	5	Not really bad
Layered sounding	5	Different inversion would improve
Unknown	1	

I tried to design a precipitation filter to improve the correlations, since 11 of the large residuals (Table 13) are due to precipitation. I compared the Method Three inversion level, at the 98 sounding times, to precipitation at Paradise Park (Appendix A). Unfortunately, my efforts proved fruitless. Of the 98 cases examined, precipitation occurred within a few hours for 27 cases. Of the 27 rain cases, only 10 give large residuals and the remaining 17 gave small residuals. In addition, there is no obvious reason why some rain events have small residuals and others do not. Consequently, removal of the sounding times that occur with rain would probably lower the correlation. However, an important conclusion can be drawn from this. Although rain can affect the inversion measured by the profiler, it more frequently does not. In fact, for 63% of the rain cases examined, the inversion measured by the profiler and sounding was very close.

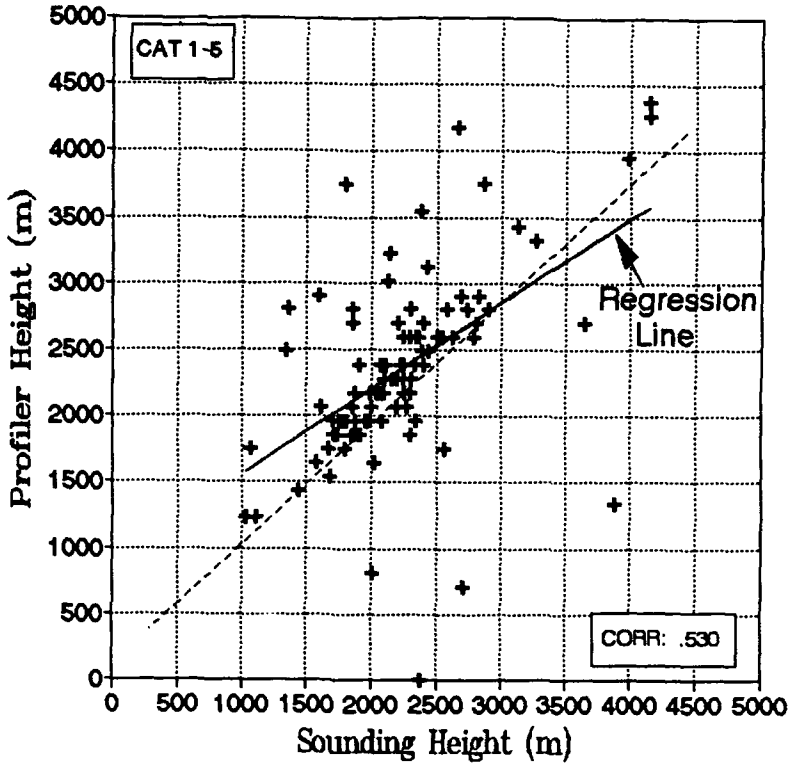

Figure 22. Regression analysis for RH/TEMP 1-5/1-5 "all data".

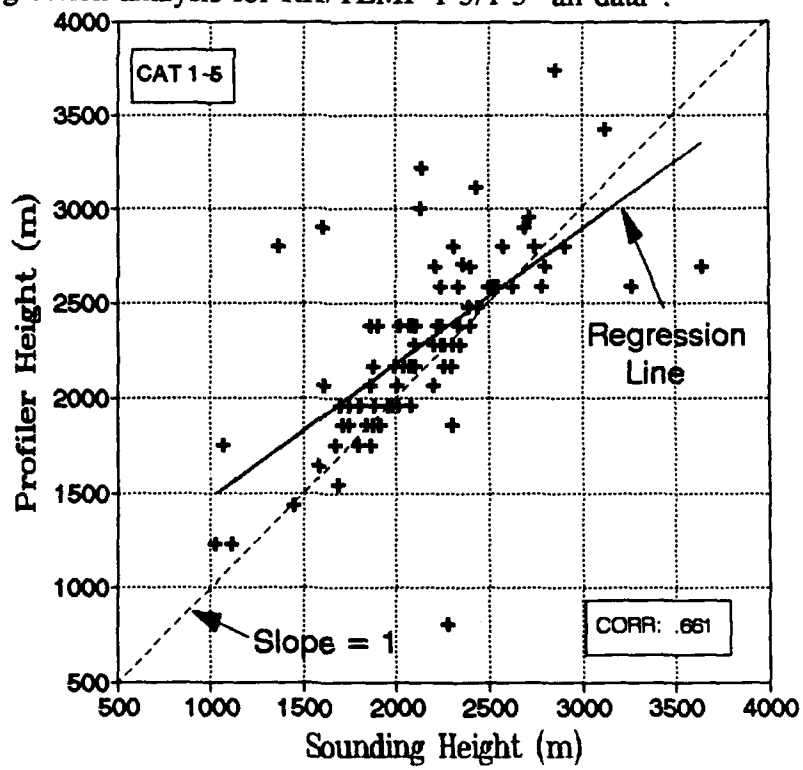

Figure 23a. Regression analysis: subjectively corrected RH/TEMP 1-5/1-5 "continuous data."

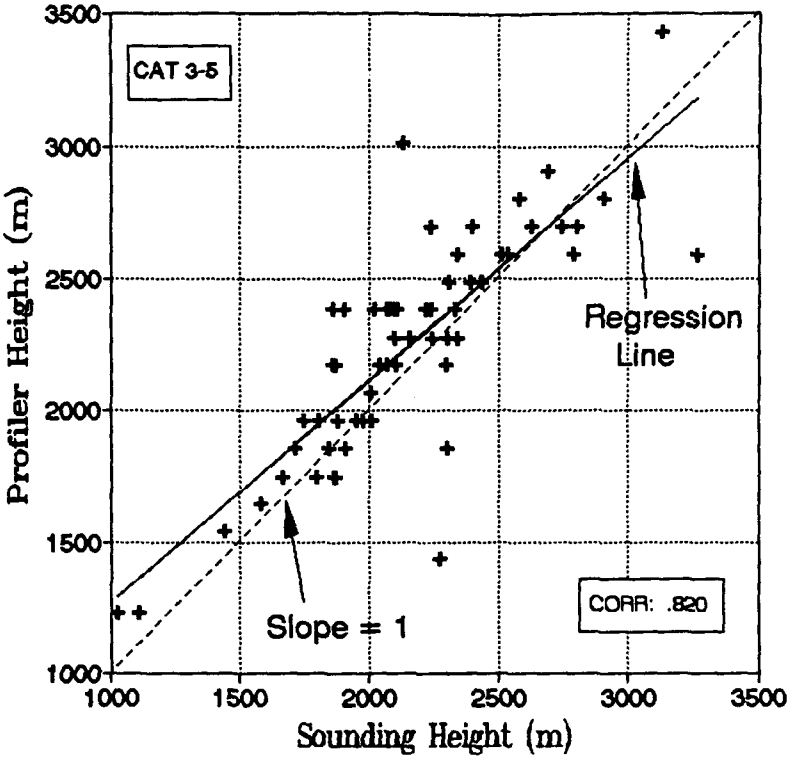

Figure 23b. Regression analysis: subjectively corrected RH/TEMP 3-5/3-5 "continuous data."

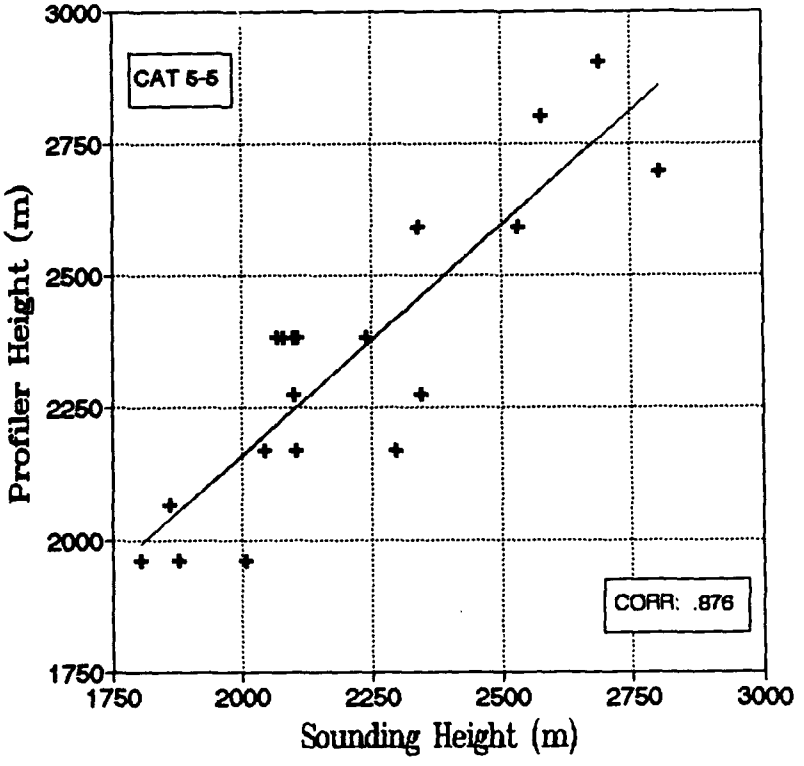

Figure 23c. Regression analysis: subjectively corrected RH/TEMP 5/5 "continuous data."

5.2 Subjectively Corrected Results

Chapter 4.3 describes the subjective correction of Method Three ("continuous data"). Table 14 is a summary of the regression analysis results of the subjectively corrected data versus the uncorrected "continuous data." The correlations are significantly higher than for the uncorrected data. The RH/TEMP 5/5 category now has the highest correlation (.876) since the correction of the outlier (Figure 21). Although the RH/TEMP 1-5/1-5 category has the lowest correlation (.661), the results are good. Figure 23 contains plots of the regression analysis for the subjectively corrected data.

Table 14. Regression Analysis for Raw "Continuous Data," Closest Time (Subjectively Corrected Versus Uncorrected)

RH/ TEMP	Corrected			Uncorrected			F-Dist (99%)	Tot
	Corr	Y-Int (m)	F-Val	Corr	Y-Int (m)	F-Val		
1-5/1-5	.661	758	63	.583	809	43	6.99	85
3-5/3-5	.820	428	119	.787	256	94	7.11	60
5/5	.876	421	56	.626	48	11	8.53	19

From these results, I conclude the profiler is measuring almost the same inversion level as the sounding with a small bias. The profiler identifies a higher (lower) inversion base/moist layer top for inversion heights less (greater) than 2500 m for the RH/TEMP 1-5/1-5 and 3-5/3-5 "continuous data." The profiler identifies a higher inversion base/moist layer top for all inversion heights for the RH/TEMP 5/5 "continuous data." The RH/TEMP 3-5/3-5 "continuous data" contain a significant sample size of soundings that I have a high level of confidence in. This data set provides very small differences

(less than 150 m) between the regression line and a line that passes through zero with a slope of one, for a majority of the points (heights between about 1800 to 3000 m). Even the RH/TEMP 1-5/1-5 "continuous data," which includes some questionable soundings, provide small differences (less than 300 m) for a majority of the points (heights between about 1800 to 3000 m). The small differences are probably due to the 17.5 km separation between the profiler and radiosonde.

I also tested the profiler inversion base distribution of the subjectively corrected "continuous data" to see if it fits a normal curve. Since many statistics assume a normal distribution, I tested the distribution of the inversion base determined by the profiler. Figure 24a depicts the inversion base distribution and its normal curve for the profiler. Table 15 summarizes the distribution statistics. The data has a larger peak around the mean than a normal distribution. Further, a Chi-squared (χ^2) test demonstrates it is not a good fit to the normal curve. Following the same procedure for the natural log of inversion base (Figure 24b), I obtained slightly better results for the χ^2 test. Unfortunately, the χ^2 test still does not meet the significance test ($\chi^2_{.995}$). However, Figure 24b shows the logarithmic data does resemble the normal curve. From this I conclude the distribution is close enough to normal to compute statistics that require a normal distribution.

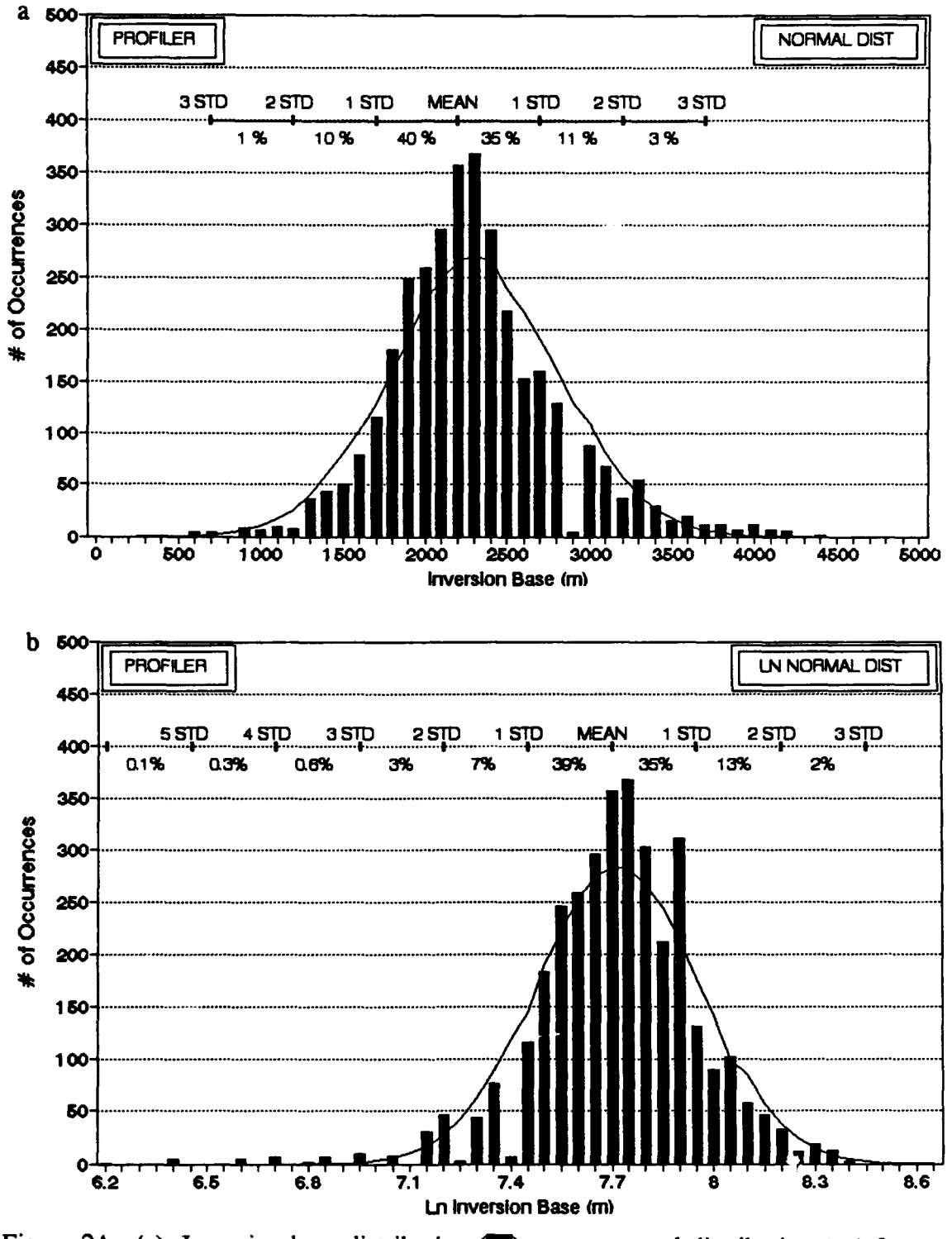

Figure 24. (a) Inversion base distribution (▇) versus normal distribution (_) for profiler. (b) Natural log of inversion base distribution (▇) versus normal distribution (_) for profiler. STD = Standard deviation.

Table 15. Distribution Statistics (Profiler)

Dist	± 1 STD	± 2 STD	± 3 STD	χ^2	DF	$\chi^2_{.995}$
Raw	75%	95%	99%	669	38	64
Log	75%	95%	99%	515	35	60
Normal	68.3%	95.5%	99.7%			

CHAPTER 6

PRACTICAL USES OF THE PROFILER

6.1 Inversion Base Diurnal Cycle

Table 16 lists some profiler inversion statistics for the subjectively corrected, "continuous data." Similar to the sounding, the profiler also shows a diurnal variation of inversion base. As expected, the profiler gives more detail about the diurnal variation than the typical radiosonde (12 hour frequency). I added the inversion bases for each hour (5 per hour for 34 days, thus each hourly average contains 170 inversion heights) and computed the corresponding hourly average. A plot of the average hourly inversion height measured by the profiler is more revealing. Figure 25b shows the inversion is lowest (2050 m) at 1600 to 1700 HST (0300 UTC), and highest (about 2350 m) during the night.

Table 16. Mean Inversion Height Statistics

	Overall	Standard Deviation	00Z	12Z
Profiler	2253 m	514 m	2228 m	2364 m
Sounding	2322 m	624 m	2174 m	2508 m

Figure 25c shows the corresponding diurnal cycle of precipitation accumulation. I added the precipitation for each hour (4 per hour for 34 days, thus each hour contains 136 precipitation records). Precipitation is higher during the night (around 15 mm) and lower during the afternoon (around 5 mm). The correlation (.697) between diurnal precipitation and inversion base is fairly high (Figure 26 and Table 17).

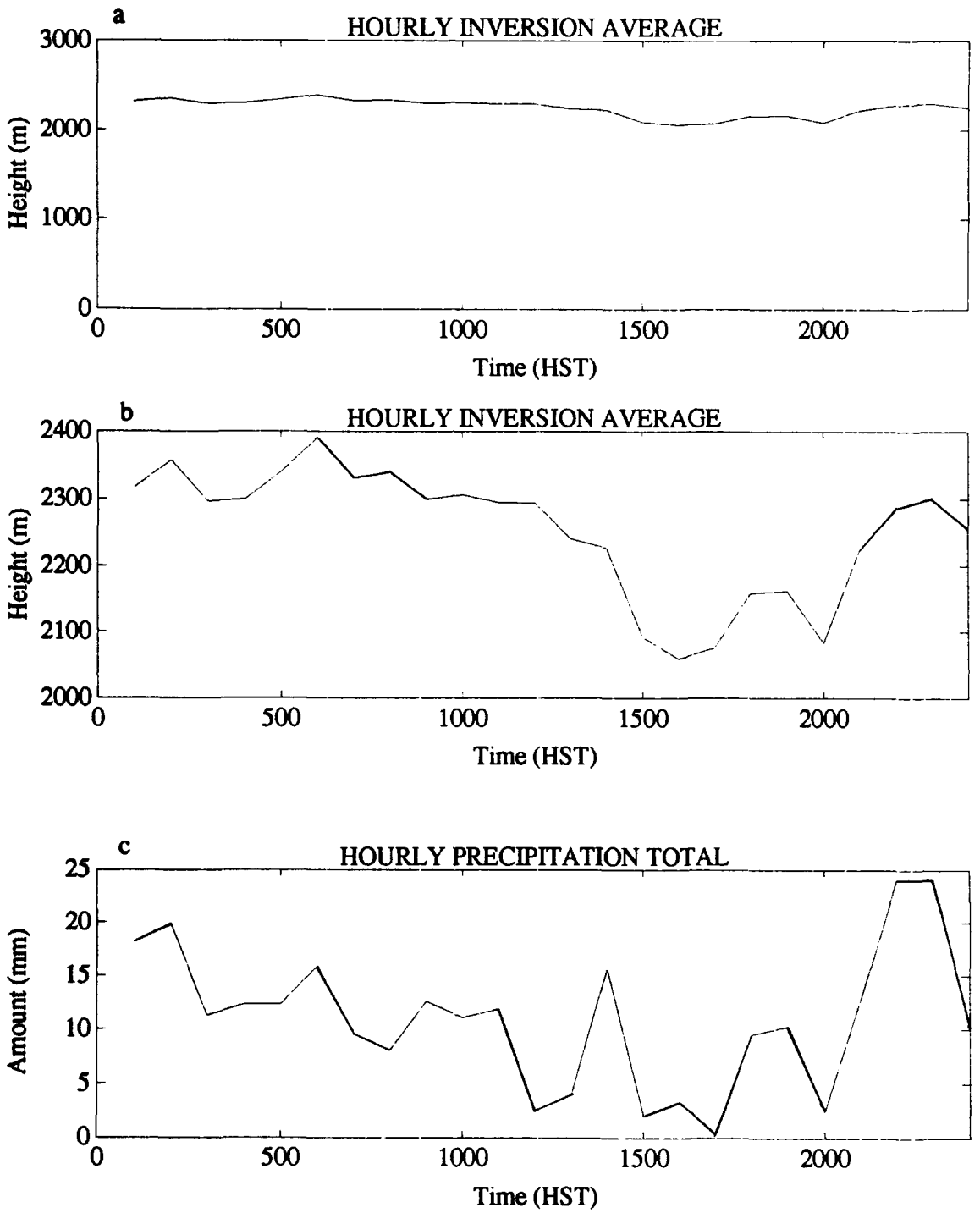

Figure 25. Diurnal cycle of inversion height and precipitation (profiler). (a) and (b) Diurnal cycle of inversion height. (c) Diurnal precipitation cycle.

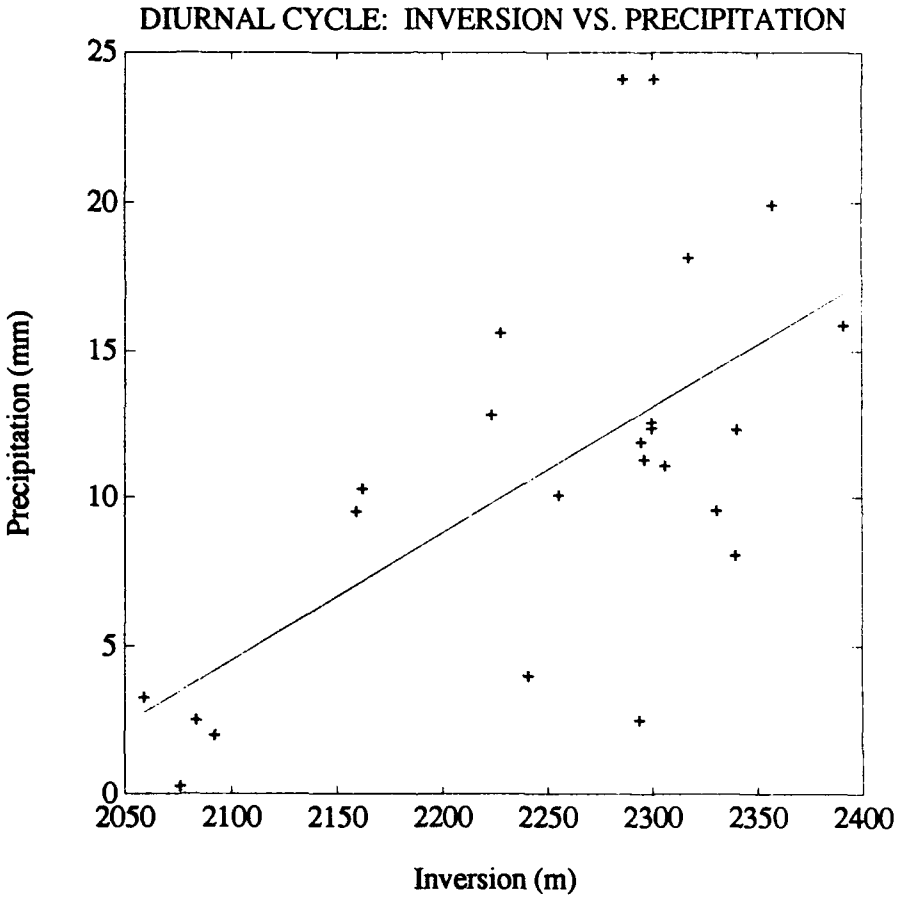

Figure 26. Regression analysis for diurnal cycle of inversion height and precipitation (profiler).

Table 17. Regression Analysis for Diurnal Precipitation and Inversion Height (Profiler)

Corr	Y-Int (m)	F-Val	F-Dist	Total
.697	-91	20.8	7.95	24

These results are surprising since I expected the inversion to be higher during the day. As the land heats, increased convective overturning in the moist layer should cause the inversion to be higher during the day. Leopold (1948) found the Honolulu (leeward Oahu) minimum inversion base height at 2200 HST and maximum height at 1100 HST. However, both the Hilo soundings and Paradise Park profiler show this is not the case. There must be some other causative mechanism perhaps due to local topography.

A modification to Garrett's (1980) daytime upslope sea-breeze model (Figure 4) for weak trades can explain this phenomenon. Apparently, the upper level return flow of the daytime sea breeze, on the average, is closer to the coast than depicted. This would account for convergence and sinking motion closer to the coastline. This sinking motion strengthens the already diverging air, and causes the inversion to lower during the daytime. At night, the downslope drainage flow does not appear to lift the inversion height. This is probably due to the smaller depth of the drainage flow as compared to the daytime sea breeze flow (Figure 4). Consequently, we see a "1/2 cycle effect" on the inversion base due to daytime upslope mid-level return flow converging and sinking close to the coast, with no effect at night.

6.2 Diurnal and Synoptic Scale Patterns

I conducted a spectral analysis to see if there are any cyclical variations in the trade wind inversion. The spectral density function (g{f}) is (Chatfield 1975, Box and Jenkins 1976):

$$g(f) = 2\{1 + 2\sum_{k=1}^{N} \rho_k \cos 2\pi fk\} \qquad (6.1)$$

where N is the number of observations, ρ_k is the autocorrelation and f is the frequency. The frequencies (f_i = i/N) are harmonics of the fundamental frequency (1/N). They range between 0 to 0.5 cycles. Figure 27 is a plot of the spectral density function for the subjectively corrected "continuous data."

The convective scale (few hours) is noisy, with no significant power (Figure 27). However, consistent with the observed diurnal cycle (Figure 24) there is a small peak around 24 hours. A larger peak emerges around 1 1/2 to 2 days and at the synoptic scale (3 to 4 days). This implies day to day and synoptic scale variations are larger than the diurnal cycle. A rule of thumb for spectral analysis is that it is significant to one-tenth the analysis time. Since this application considers 700 hours of data, I do no have much confidence in return power beyond three days.

6.3 Strong Versus Weak Trade Wind Days

I compare strong versus weak trade wind days for the HaRP experiment to examine if there is any relationship of wind strength to the inversion base. A. Nash (1992) selected the PAM site farthest south (South Point) to represent the most exposed PAM site (Figure 2). He then identified Hawi as the northern station with the highest wind speed correlation to South Point. From these two stations, he determined the 12

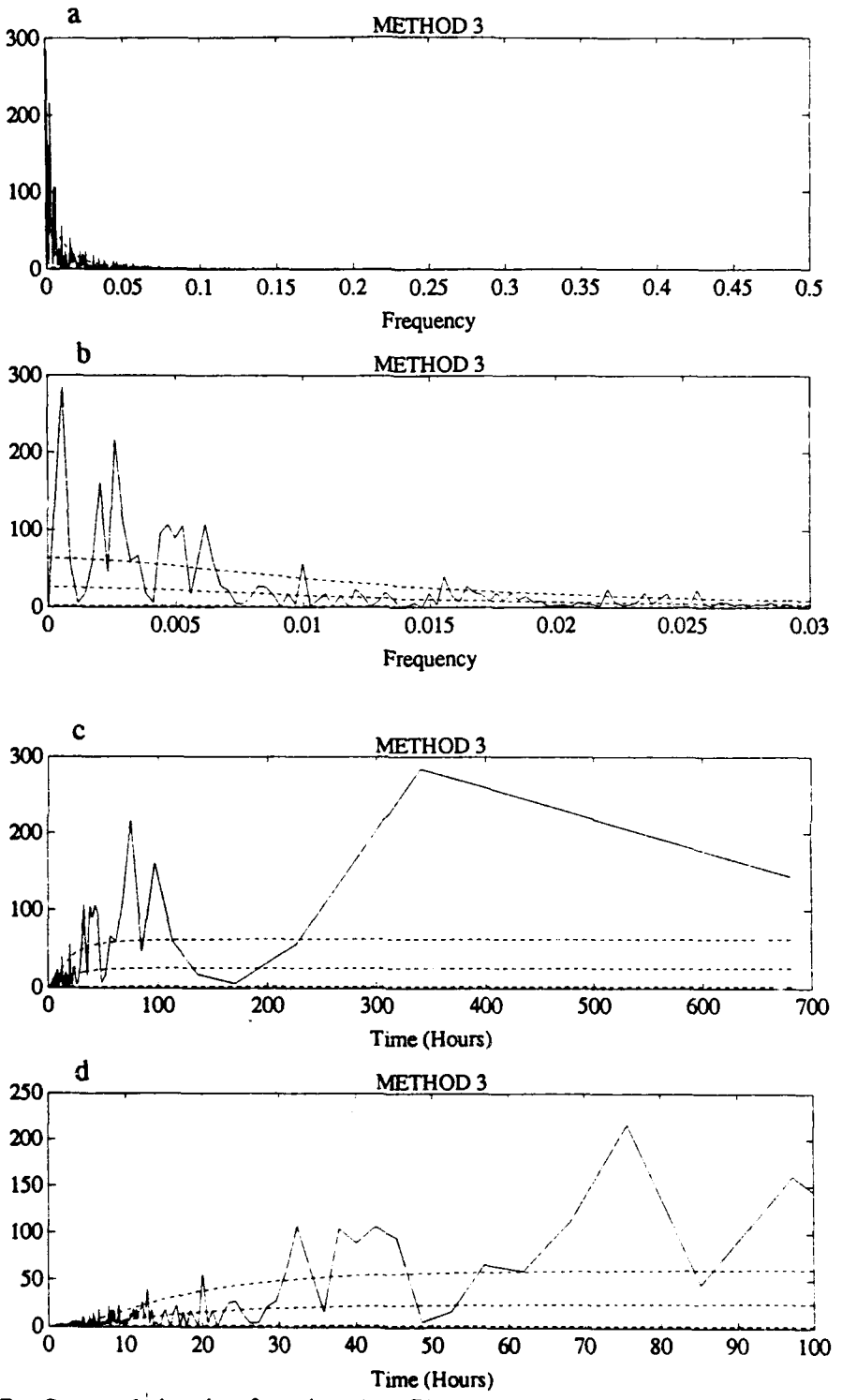

Figure 27. Spectral density function (profiler). (a) Spectral density function, frequency domain. (b) Magnified plot of Figure 27a. (c) Spectral density function, time domain. (d) Magnified plot of Figure 27c. (-- = red noise, 90%, and 10% confidence limit)

strongest and 12 weakest wind days. From this set, I used ten days from each subset since the profiler period is not as long as the PAM period.

Table 18 shows the average inversion height and precipitation for both strong and weak days. The average inversion base height is slightly higher for strong trades than for weak trades. Average precipitation is also higher for strong trades. These results conflict with Lavoie's (1974) theoretical model. Lavoie (1974) states that a lower inversion should have stronger winds. In general, he expects less precipitation, excluding precipitation associated with an enhanced land-sea breeze. However, Lavoie's (1974) model is for Oahu, with mountains that do not penetrate the trade wind.

Table 18. Average Inversion Height for Strong and Weak Trade Wind Days

Trade Winds	Average Inversion (m)	Average Precipitation (mm)
Strong	2355	7.14
Weak	2318	5.52

My results can be explained using local topography and the Smolarkiewicz et al. (1988) model. Smolarkiewicz et al. (1988) used a numerical prediction model to simulate interactions of the trade winds with the island of Hawaii. They categorized their results by the Froude Number (Fr): ($Fr = U/Nh$) where U is the mean upstream wind speed, N is the Brunt-Väisälä frequency, and h is the characteristic height of the mountains. They found that for lower Froude Numbers (0.1), and hence lower winds, the low-level convergence zone moves offshore of Hawaii and associated band clouds are weak or absent. For a higher Froude Number (0.2), and therefore higher winds, a stronger low-level convergence zone forms close to the shore. The results indicate

differing vertical velocity fields near the coast. It is plausible that enhanced low-level convergence and rising motion, just offshore and thus close to Hilo and Paradise Park, would cause the trade inversion to rise slightly.

6.4 Inversion Base Versus Precipitation

Is the inversion base correlated with more precipitation? A higher inversion base would allow for deeper convection, which is believed to enhance trade showers. Larson (1978) found a range of inversion heights for dry days ($\leq$ 5.08 mm precipitation per day) of 1520 to 1740 m, and for wet days ($\geq$ 12.7 mm) of 2070 to 2320 m. I used similar criteria, adjusted for less precipitation at Paradise Park (daily average 6.9 mm) than Hilo (daily average 9 mm) and found a weaker relationship. The mean inversion for dry days ($\leq$ 4.0 mm precipitation per day) at Paradise Park is 2232 m, versus 2394 m for wet days ($\geq$ 10 mm).

A closer look at precipitation and inversion height shows there is no clear cut relationship. Figure 28a is a time series of the average daily inversion height at Paradise Park versus the total daily precipitation. Figure 28b is the regression analysis for this time series. The correlation between the precipitation and average daily inversion height (Table 19) is 0.320. It explains only about 10% of the variance. The calculated F-Value shows this correlation is not statistically significant. Although there are days when the inversion is high and more precipitation falls, this is not always the rule. There are apparently other factors that influence trade wind precipitation, of which inversion height is only one ingredient.

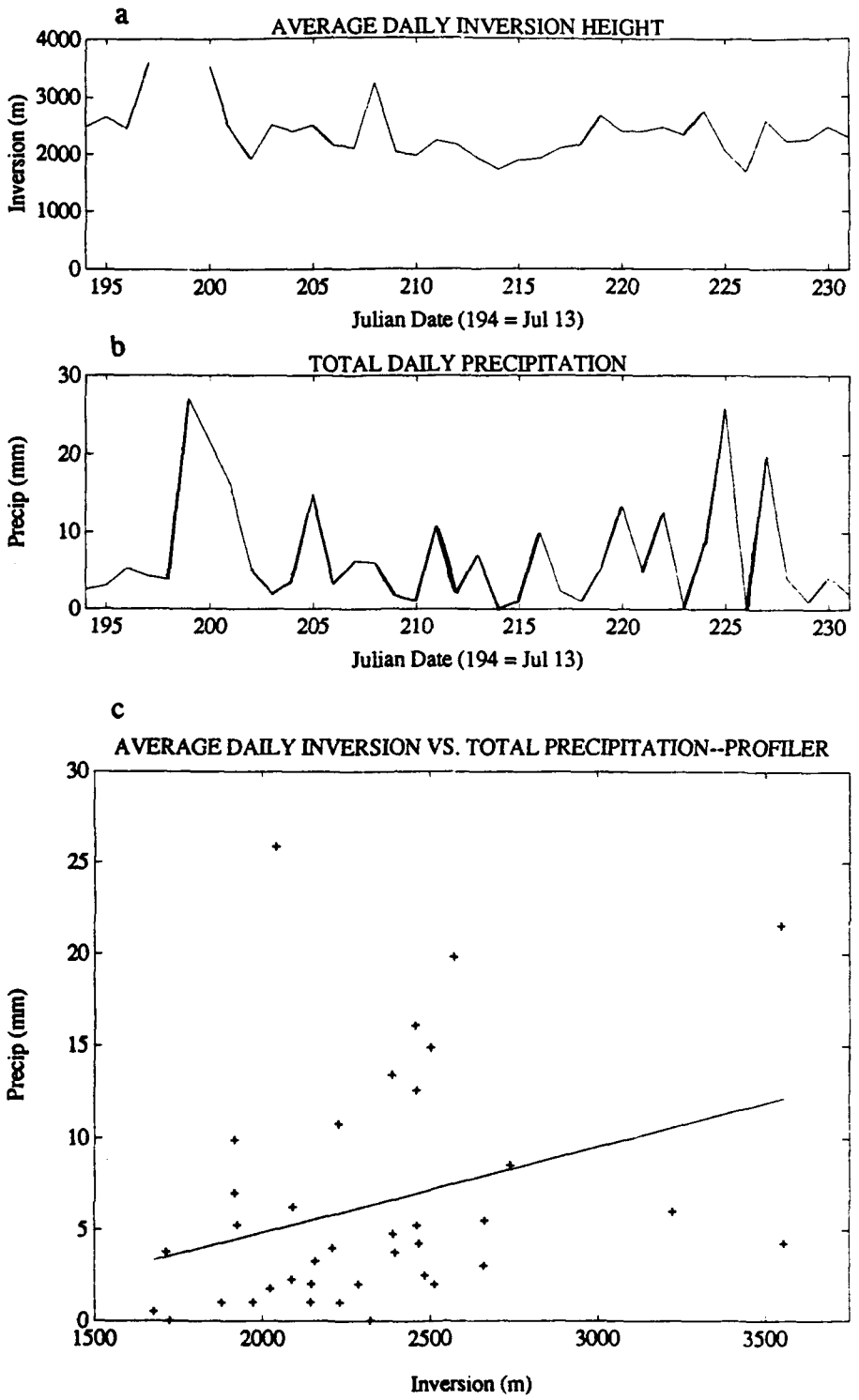

Figure 28. Time series and regression analysis for average daily inversion height versus total daily precipitation (profiler). (a) Average daily inversion height. (b) Total daily precipitation. (c) Regression analysis.

Table 19. Regression Analysis for Rain Versus Inversion Height

Corr	Y-int	F-Val	F-Dist (99%)	Total
.320	-4.6	4	7.4	37

CHAPTER 7

SUMMARY

7.1 Conclusions

Using 124 Hilo soundings, I determined the inversion base for comparison purposes to the profiler. I quickly discovered that real data is not always easy to interpret and requires careful analysis. 52% of the data had to be corrected for an erroneous superadiabatic lapse rate at the inversion base. My inversion base definition is based on both temperature and relative humidity. Although my inversion base specification is identifying the top of the moist layer, it almost always agrees with the inversion base. Since this definition always provides an inversion base, I devised a scheme to classify the quality of the soundings. I have the most confidence in the RH/TEMP category 3-5/3-5 since none of the soundings are questionable and the sample size (69) is large enough to be statistically significant. The soundings show the height of the inversion base to be rather variable, with frequent changes of over 1000 m in 12 hours. Consequently, many of the details of inversion base variability are not available with the sounding, and only the large scale changes are routinely available.

The profiler has four characteristic signals: clear air return, rain return, mid-level signal, and weak gradients/spikes. The clear air and rain return are the most frequently observed. The profiler provides a detailed evolution of convective activity. In some cases, the sounding completely missed the evolution of a shower period (Figure 14) and its effect on the inversion base and moist layer. In contrast, the profiler shows a detailed

record of the shower activity. The rain events often, but not always, appear to temporarily raise the inversion, and in some cases appear to penetrate the inversion.

I developed an algorithm for the profiler to determine the inversion base. It quickly determines the inversion and has problems only 4.3% of the time with mid-level returns. The inversion base results can be further improved by removing the spikes associated with vertical velocities greater than 62.5 cms^{-1}. Although there might be atmospheric phenomena that occur with vertical velocities of this magnitude, they are not considered in this study. In an operational environment, it can be fine-tuned by human interpretation (of mid-level return).

Regression analysis of the inversions from the soundings to the profiler yields promising results. I obtain a correlation of .82 for the RH/TEMP category 3-5/3-5 "continuous data." This data set provides very small differences (less than 150 m) between the regression line and a line that passes through zero with a slope of one, for a majority of the points (heights between about 1800 to 3000 m). These small differences can probably be attributed to the 17.5 km separation between the sounding and profiler. Therefore, I conclude the profiler is a valuable tool which provides an accurate and detailed record of the inversion base and other features. The profiler provides fine scale variability not fully seen with, or completely missed by the soundings.

The profiler provides detailed information about the diurnal cycle at Paradise Park. Although the diurnal cycle does appear in the Hilo sounding; twice daily soundings (0 and 1200 UTC) cannot adequately capture the cycle. The inversion is lowest (2050 m) at 1600 to 1700 HST (0300 UTC), and highest (about 2350 m) during the night. We see

a "1/2 cycle effect" on the inversion base due to daytime upslope mid-level return flow converging and sinking close to the coast, with no effect at night. There is a corresponding diurnal variation in precipitation with a correlation of .697 to the inversion base. On the average, precipitation is higher during the night (around 15 mm) and lower during the afternoon (around 5 mm).

The profiler also provides details on scales larger than the diurnal cycle. Two day and synoptic scale variability are greater than diurnal cycle variations. In addition, there is not a persistent cycle for the convective scales.

There is a slightly higher inversion base (2355 m) and more precipitation (7.14 mm) for strong trades for Paradise Park than for weak trades (2318 m and 5.52 mm). This is probably due to local topography and can be explained with the Smolarkiewicz et al. (1988) model. For a higher Froude Number (0.2), and thus higher winds, a stronger low-level convergence zone forms closer to the shore. Enhanced low-level convergence and rising motion, just offshore (close to Hilo and Paradise Park), could cause the trade inversion to rise slightly during strong trades.

There is no consistent relationship (correlation .320) between average daily inversion height and daily total precipitation. However, there are some interesting disturbed periods when a higher inversion height appears to be related to more precipitation. Apparently, other factors influence trade wind precipitation and inversion height is only one of the ingredients.

7.2 Suggestions for Further Work

Many other ideas can be pursued from this study. Hopefully, modeling studies and other studies can use these inversion base results. This study used only the vertical signal strength, and did not consider the profiler winds. The profiler winds undoubtedly contain a wealth of information on the airflow over Paradise Park.

A possible follow-up study to this work is to use analyzed HaRP observations in a detailed mesoscale model. The observations used in this model should include these inversion base results, profiler winds, PAM observations, aircraft soundings, and dual Doppler radar observations. Previous modeling studies of the tropics have not had the wealth of weather observations that are available with the HaRP data set. Potential features to model include wind flow, precipitation and vertical motion, and their relationship to inversion height. This proposed study could serve to test the validity of the ideas presented in this study for diurnal variation and strong versus weak trades.

Another potential study is to try to identify the various layers often seen with the profiler. In particular, can the profiler measure cloud base or any other features? Also, other features (in particular, convective activity and virga) can be seen in the profiler data. It would be useful to quantify these features.

It would be intriguing, both to the research and operational weather community, to have a boundary layer wind profiler located in the Hawaiian Islands. Then this study could be repeated for an even a longer record. This would provide a better climatology of the trade wind inversion variation. If the profiler were fixed in the vertical pointing direction only, with a shorter data averaging time (this study uses a 12 minute median),

it might be possible to study gravity waves and other fine scale phenomena. In addition, interaction between the inversion and convective towers could be explored in great detail.

More studies need to be done on the effect of mountain barriers on the inversion and how they effect the open ocean inversion. Ideally, one would use a transect of profilers (on the ocean to the slopes of Hawaii). This would provide a detailed analysis of inversion modification by mountain barriers. The experiment design might be a profiler, mounted on a research vessel, as well as several profilers located up the Hawaiian volcanoes slopes (in a transect parallel to the trade wind flow).

APPENDIX A

PARADISE PARK INVERSION AND PRECIPITATION

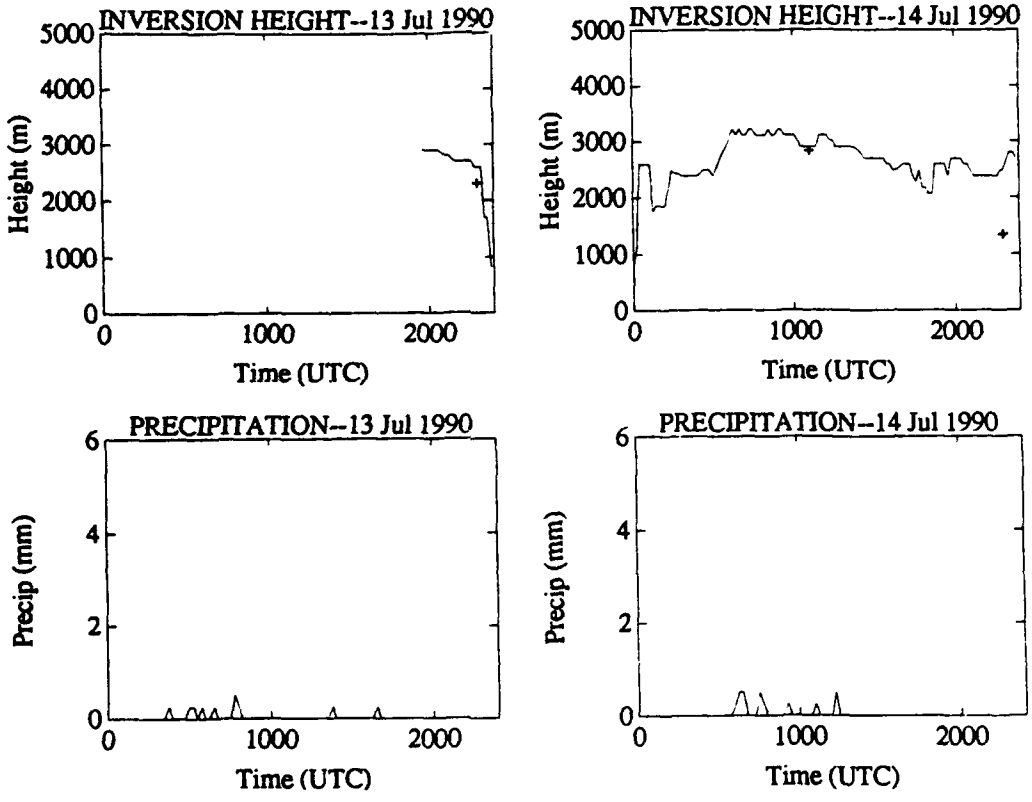

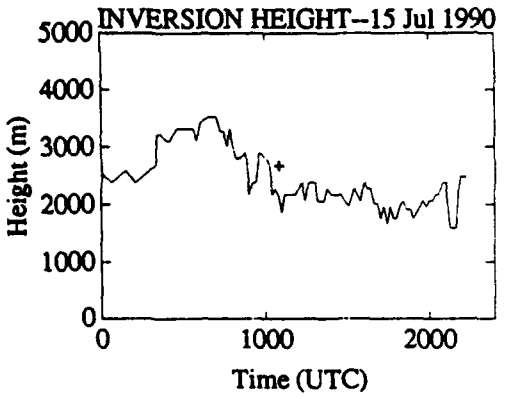
INVERSION HEIGHT--15 Jul 1990
Height (m)
5000
4000
3000
2000
1000
0
0
1000
2000
Time (UTC)

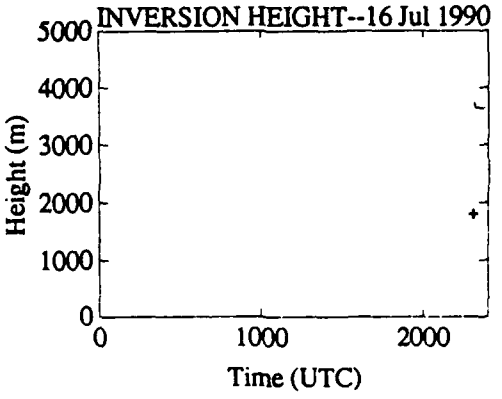
INVERSION HEIGHT--16 Jul 1990
Height (m)
5000
4000
3000
2000
1000
0
0
1000
2000
Time (UTC)

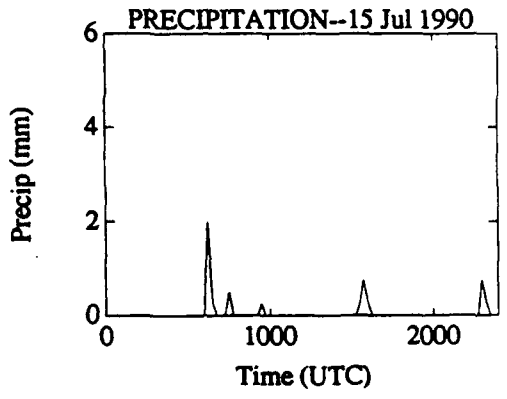
PRECIPITATION--15 Jul 1990
Precip (mm)
6
4
2
0
0
1000
2000
Time (UTC)

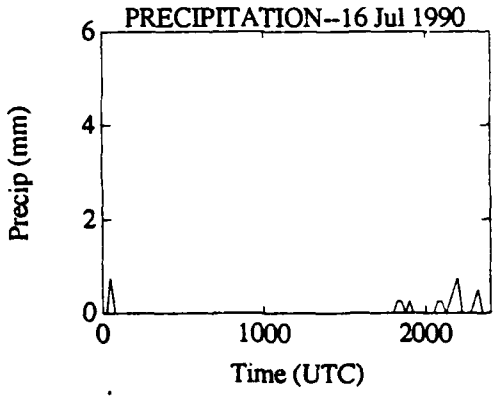
PRECIPITATION--16 Jul 1990
Precip (mm)
6
4
2
0
0
1000
2000
Time (UTC)

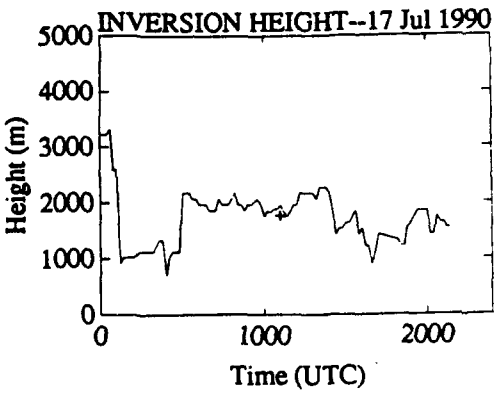
INVERSION HEIGHT--17 Jul 1990
Height (m)
5000
4000
3000
2000
1000
0
0
1000
2000
Time (UTC)

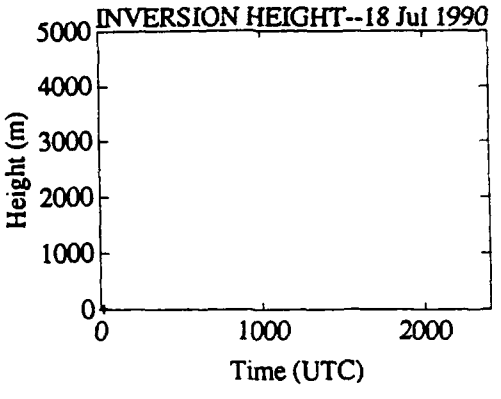
INVERSION HEIGHT--18 Jul 1990
Height (m)
5000
4000
3000
2000
1000
0
0
1000
2000
Time (UTC)

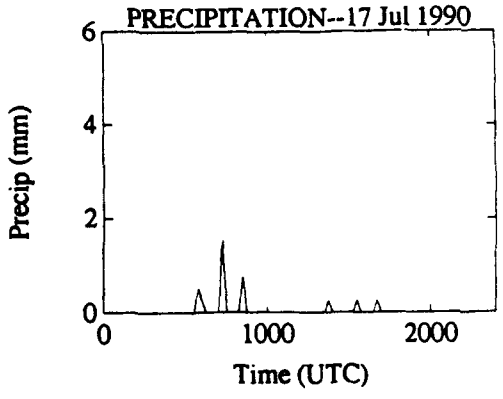
PRECIPITATION--17 Jul 1990
Precip (mm)
6
4
2
0
0
1000
2000
Time (UTC)

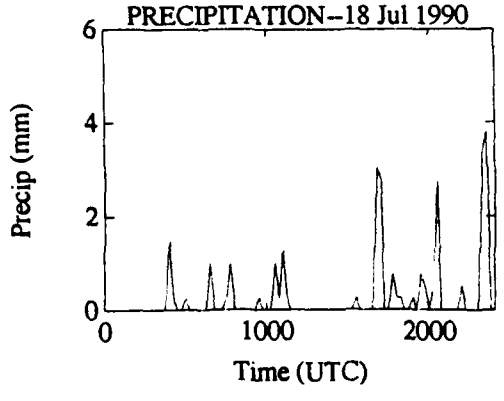
PRECIPITATION--18 Jul 1990
Precip (mm)
6
4
2
0
0
1000
2000
Time (UTC)

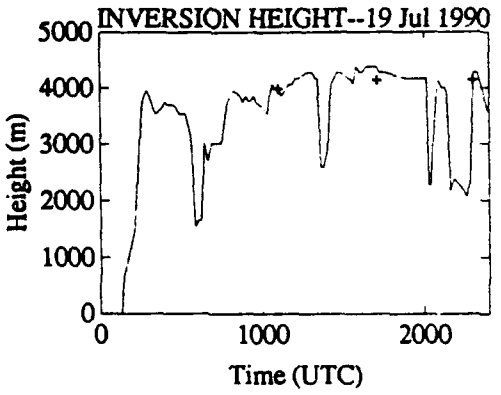
INVERSION HEIGHT--19 Jul 1990
Height (m)
Time (UTC)

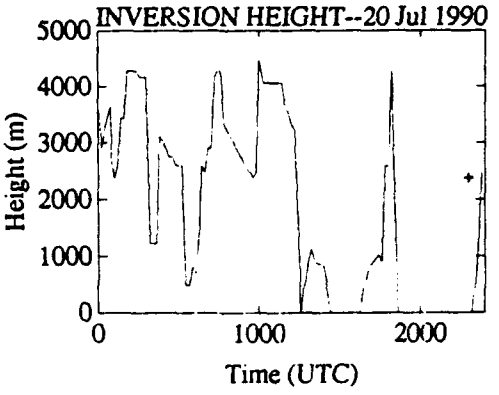
INVERSION HEIGHT--20 Jul 1990
Height (m)
Time (UTC)

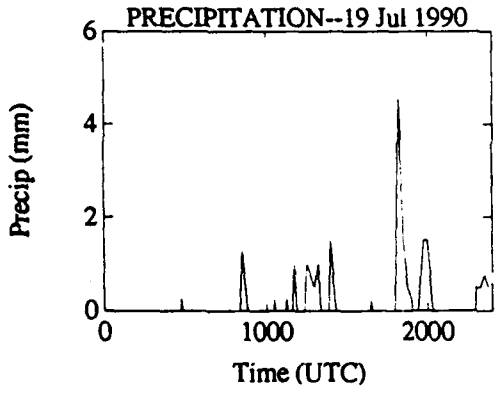
PRECIPITATION--19 Jul 1990
Precip (mm)
Time (UTC)

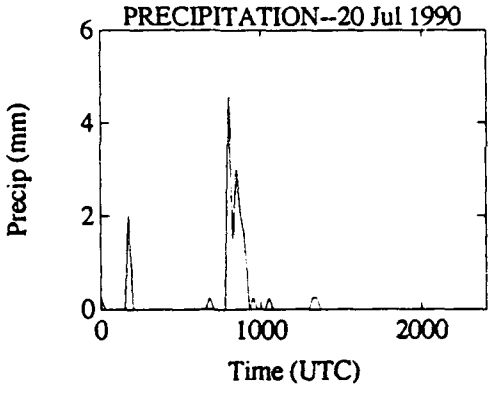
PRECIPITATION--20 Jul 1990
Precip (mm)
Time (UTC)

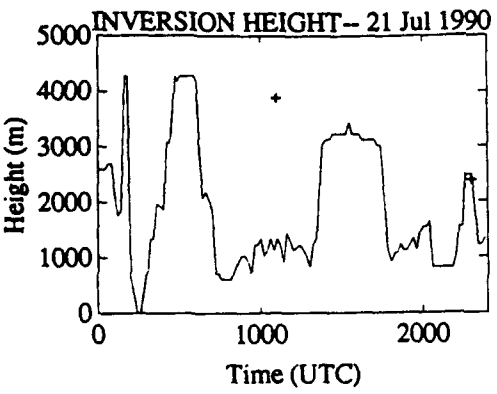
INVERSION HEIGHT-- 21 Jul 1990
Height (m)
Time (UTC)

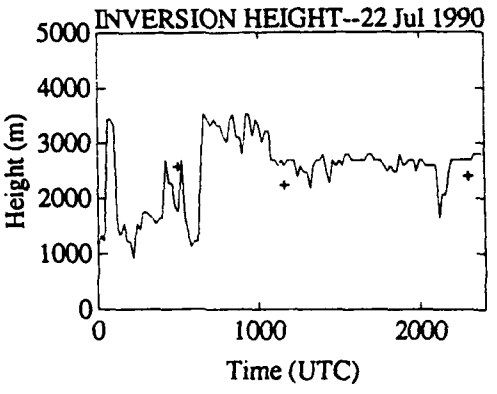
INVERSION HEIGHT--22 Jul 1990
Height (m)
Time (UTC)

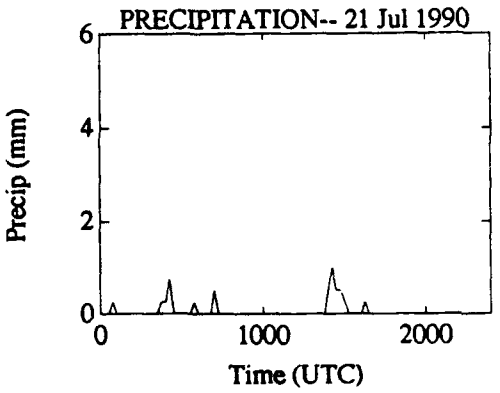
PRECIPITATION-- 21 Jul 1990
Precip (mm)
Time (UTC)

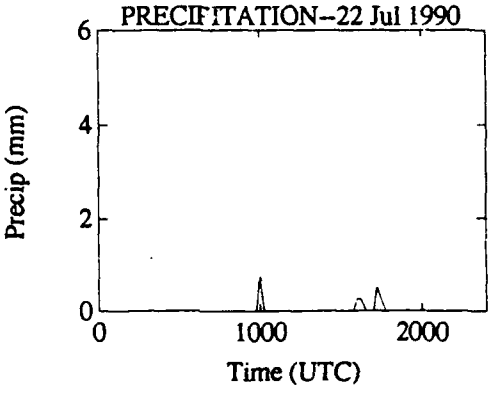
PRECIPITATION--22 Jul 1990
Precip (mm)
Time (UTC)

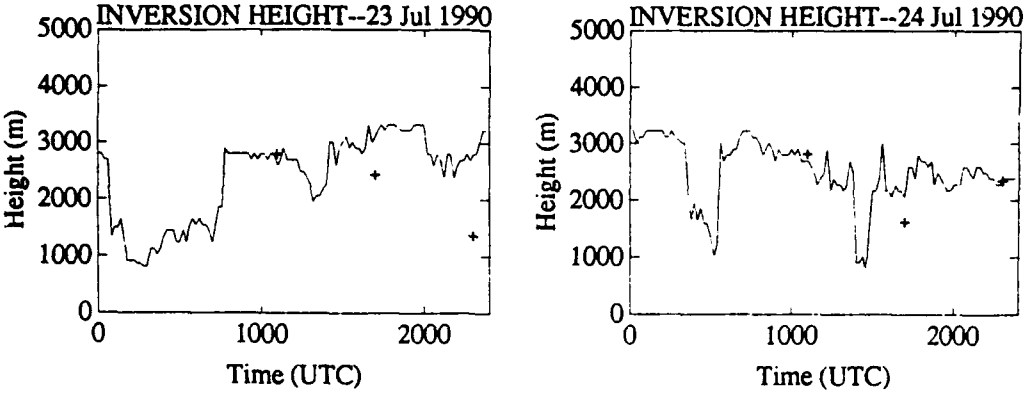
INVERSION HEIGHT--23 Jul 1990
Height (m)
5000
4000
3000
2000
1000
0
0
1000
2000
Time (UTC)

INVERSION HEIGHT--24 Jul 1990
Height (m)
5000
4000
3000
2000
1000
0
0
1000
2000
Time (UTC)

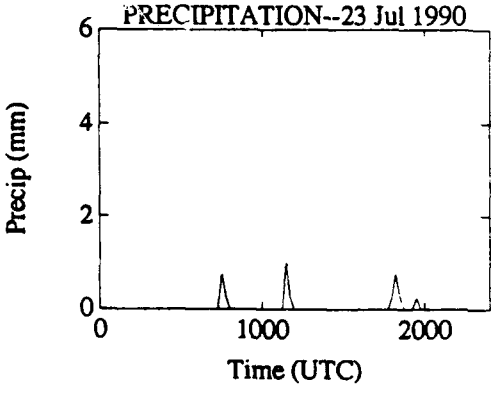
PRECIPITATION--23 Jul 1990
Precip (mm)
6
4
2
0
0
1000
2000
Time (UTC)

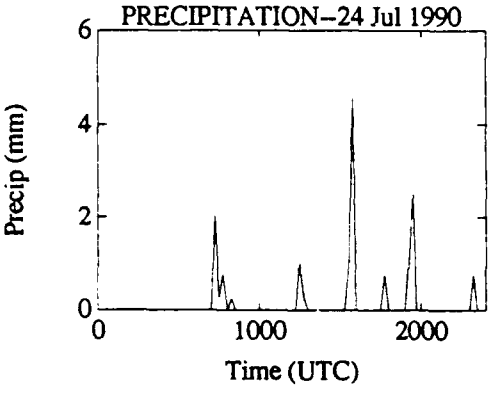
PRECIPITATION--24 Jul 1990
Precip (mm)
6
4
2
0
0
1000
2000
Time (UTC)

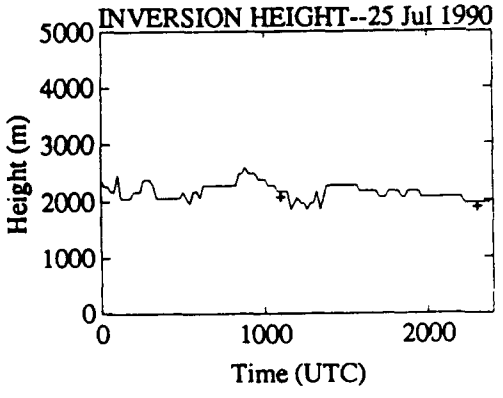
INVERSION HEIGHT--25 Jul 1990
Height (m)
5000
4000
3000
2000
1000
0
0
1000
2000
Time (UTC)

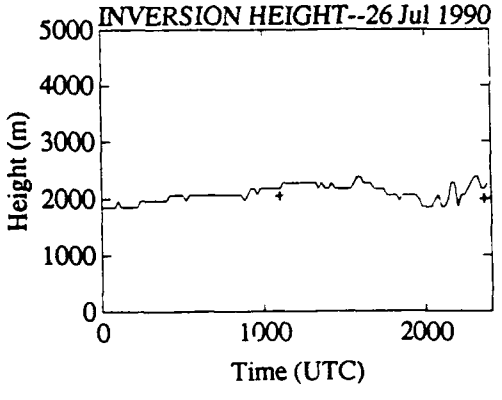
INVERSION HEIGHT--26 Jul 1990
Height (m)
5000
4000
3000
2000
1000
0
0
1000
2000
Time (UTC)

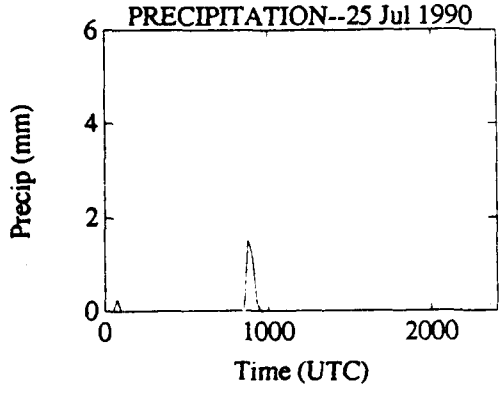
PRECIPITATION--25 Jul 1990
Precip (mm)
6
4
2
0
0
1000
2000
Time (UTC)

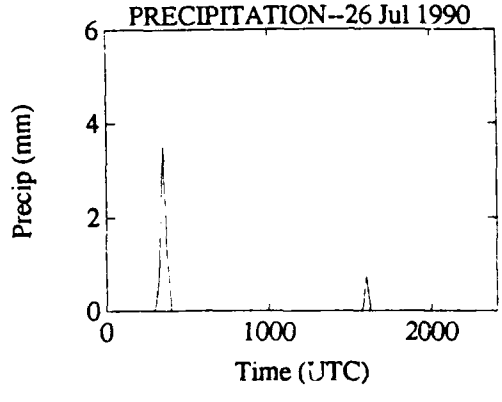
PRECIPITATION--26 Jul 1990
Precip (mm)
6
4
2
0
0
1000
2000
Time (UTC)

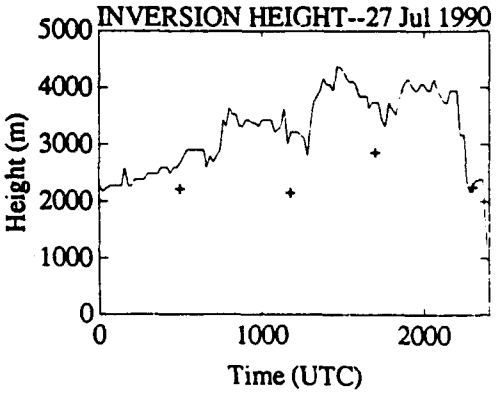
INVERSION HEIGHT--27 Jul 1990
Height (m)
5000
4000
3000
2000
1000
0
0
1000
2000
Time (UTC)

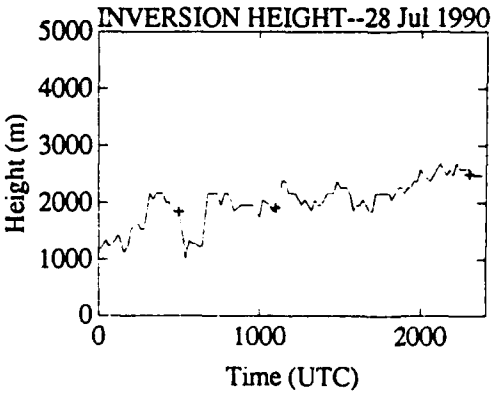
INVERSION HEIGHT--28 Jul 1990
Height (m)
5000
4000
3000
2000
1000
0
0
1000
2000
Time (UTC)

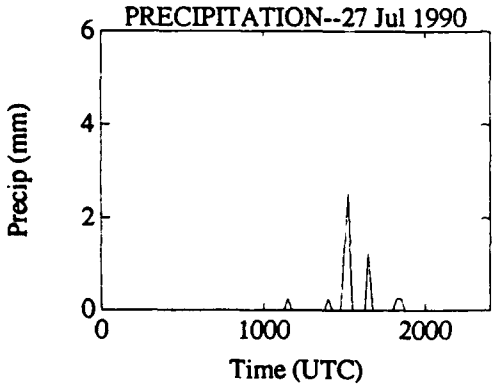
PRECIPITATION--27 Jul 1990
Precip (mm)
6
4
2
0
0
1000
2000
Time (UTC)

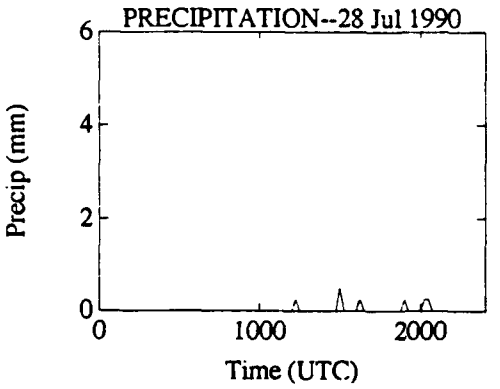
PRECIPITATION--28 Jul 1990
Precip (mm)
6
4
2
0
0
1000
2000
Time (UTC)

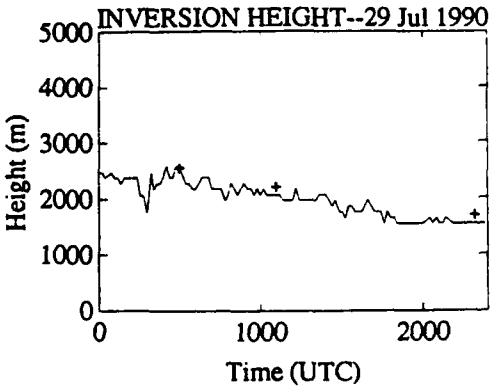
INVERSION HEIGHT--29 Jul 1990
Height (m)
5000
4000
3000
2000
1000
0
0
1000
2000
Time (UTC)

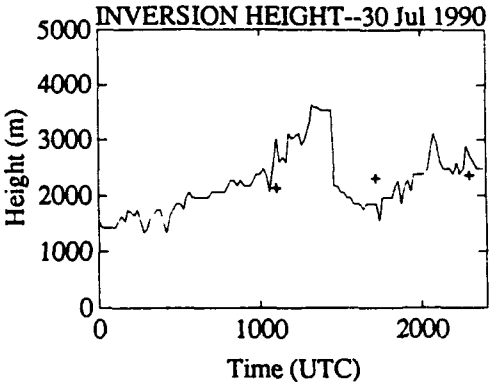
INVERSION HEIGHT--30 Jul 1990
Height (m)
5000
4000
3000
2000
1000
0
0
1000
2000
Time (UTC)

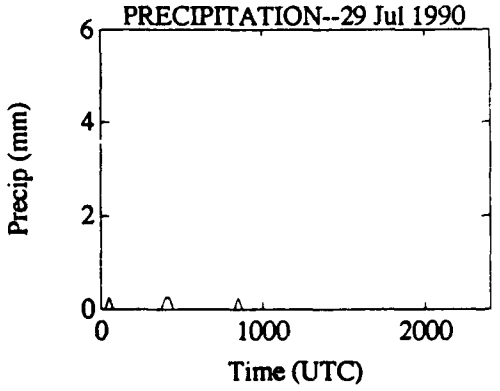
PRECIPITATION--29 Jul 1990
Precip (mm)
6
4
2
0
0
1000
2000
Time (UTC)

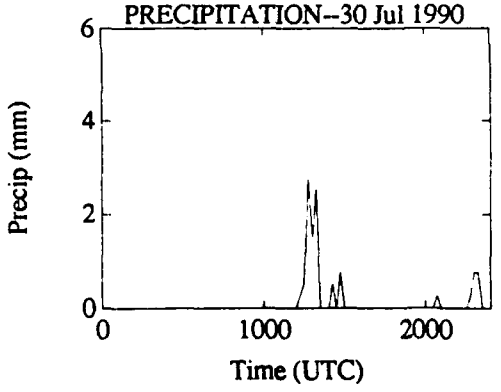
PRECIPITATION--30 Jul 1990
Precip (mm)
6
4
2
0
0
1000
2000
Time (UTC)

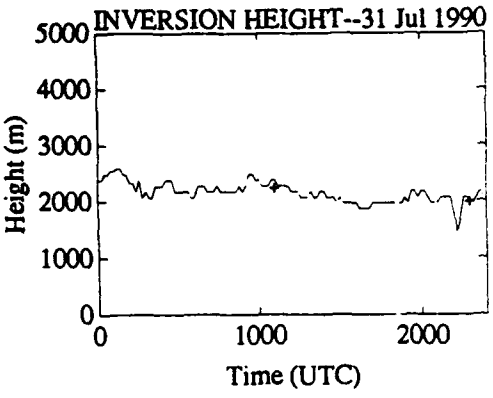
INVERSION HEIGHT--31 Jul 1990
Height (m)
5000
4000
3000
2000
1000
0
0
1000
2000
Time (UTC)

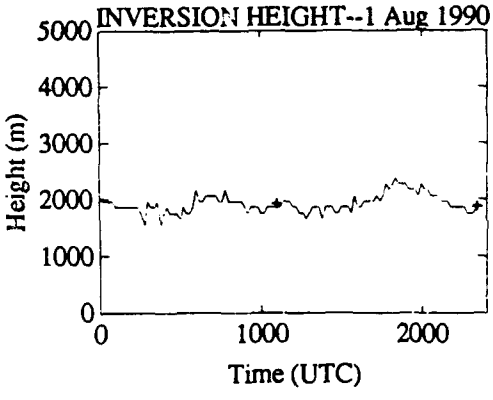
INVERSION HEIGHT--1 Aug 1990
Height (m)
5000
4000
3000
2000
1000
0
0
1000
2000
Time (UTC)

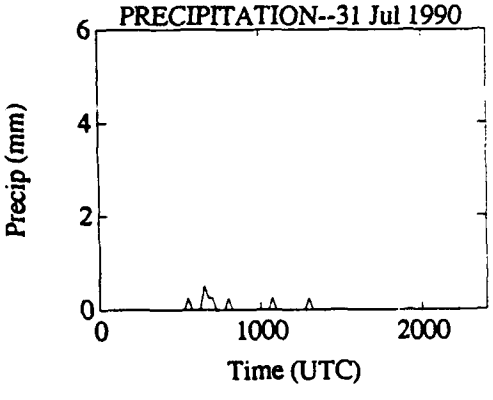
PRECIPITATION--31 Jul 1990
Precip (mm)
6
4
2
0
0
1000
2000
Time (UTC)

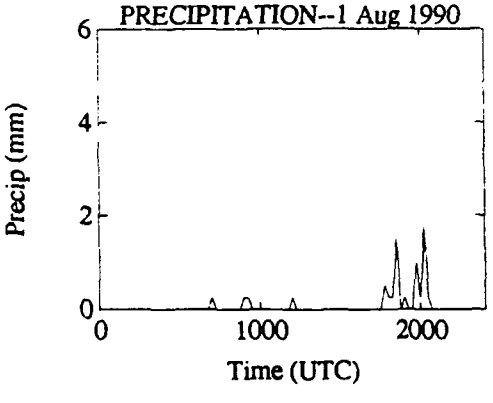
PRECIPITATION--1 Aug 1990
Precip (mm)
6
4
2
0
0
1000
2000
Time (UTC)

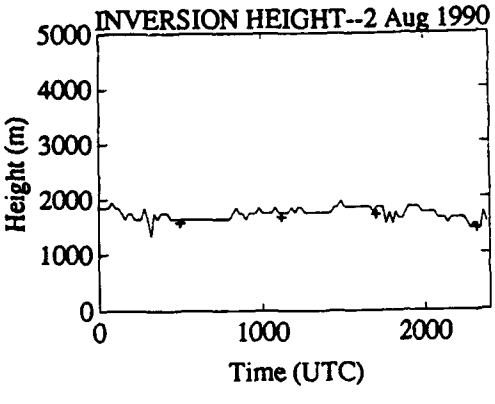
INVERSION HEIGHT--2 Aug 1990
Height (m)
5000
4000
3000
2000
1000
0
0
1000
2000
Time (UTC)

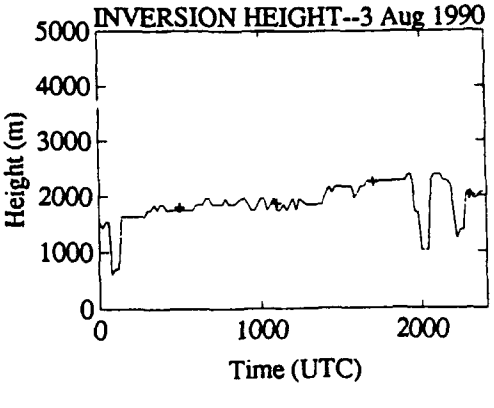
INVERSION HEIGHT--3 Aug 1990
Height (m)
5000
4000
3000
2000
1000
0
0
1000
2000
Time (UTC)

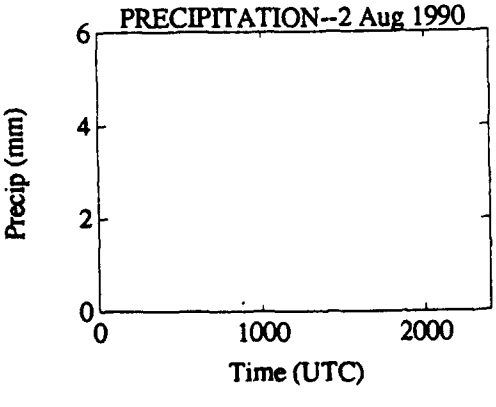
PRECIPITATION--2 Aug 1990
Precip (mm)
6
4
2
0
0
1000
2000
Time (UTC)

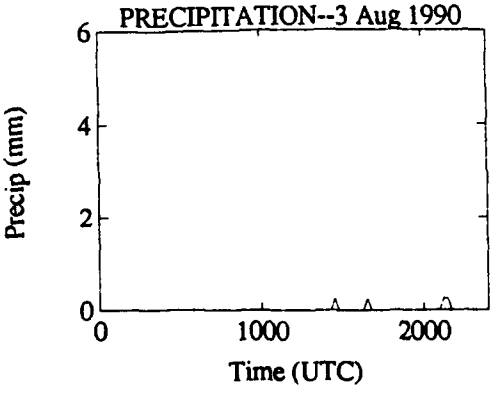
PRECIPITATION--3 Aug 1990
Precip (mm)
6
4
2
0
0
1000
2000
Time (UTC)

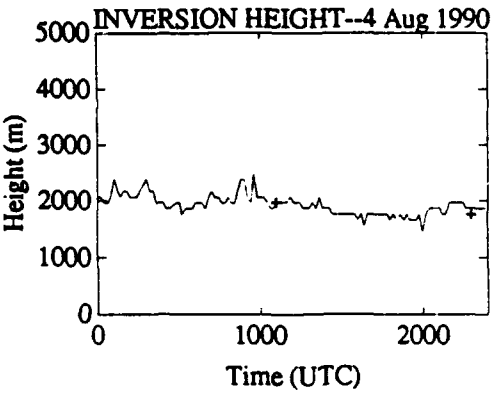
INVERSION HEIGHT--4 Aug 1990
Height (m)
5000
4000
3000
2000
1000
0
0
1000
2000
Time (UTC)

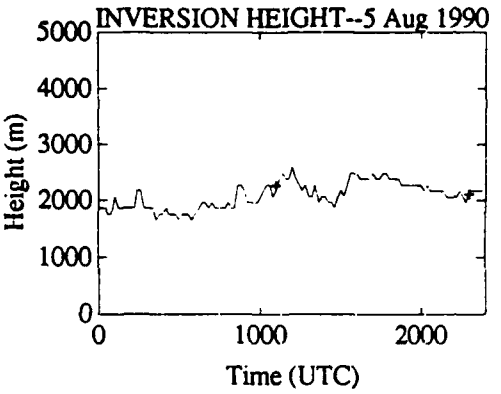
INVERSION HEIGHT--5 Aug 1990
Height (m)
5000
4000
3000
2000
1000
0
0
1000
2000
Time (UTC)

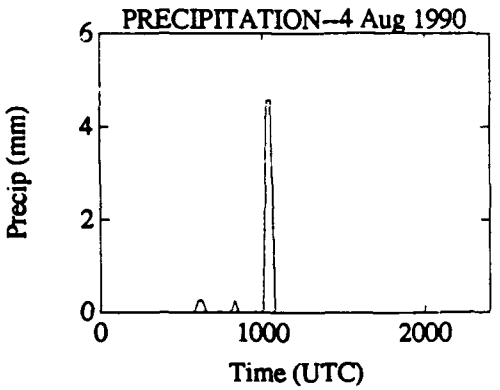
PRECIPITATION--4 Aug 1990
Precip (mm)
6
4
2
0
0
1000
2000
Time (UTC)

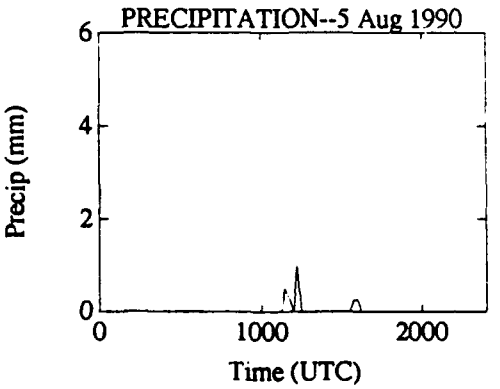
PRECIPITATION--5 Aug 1990
Precip (mm)
6
4
2
0
0
1000
2000
Time (UTC)

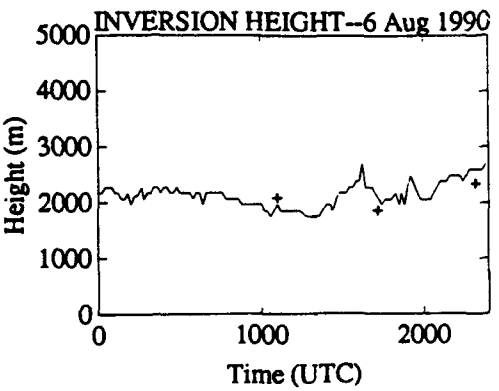
INVERSION HEIGHT--6 Aug 1990
Height (m)
5000
4000
3000
2000
1000
0
0
1000
2000
Time (UTC)

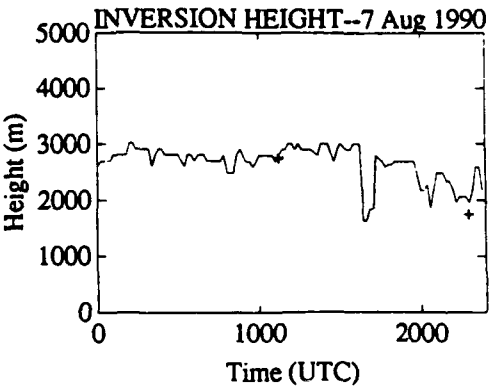
INVERSION HEIGHT--7 Aug 1990
Height (m)
5000
4000
3000
2000
1000
0
0
1000
2000
Time (UTC)

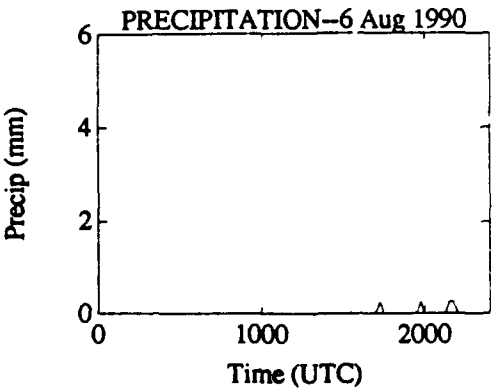
PRECIPITATION--6 Aug 1990
Precip (mm)
6
4
2
0
0
1000
2000
Time (UTC)

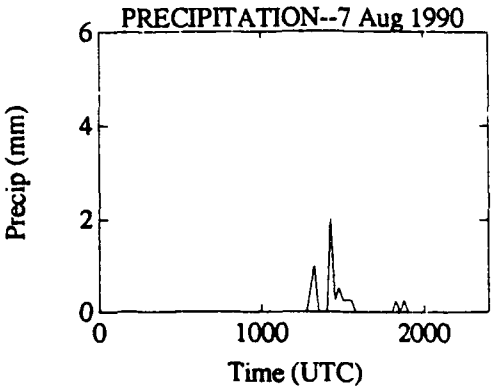
PRECIPITATION--7 Aug 1990
Precip (mm)
6
4
2
0
0
1000
2000
Time (UTC)

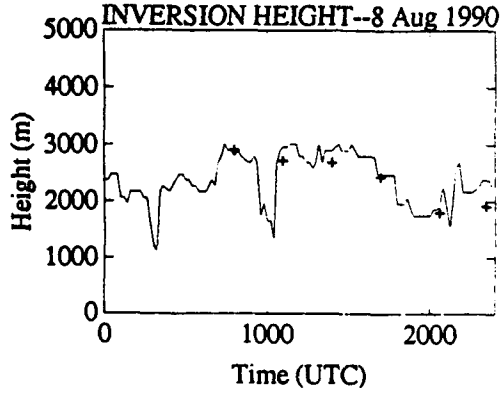
INVERSION HEIGHT--8 Aug 1990
Height (m)
5000
4000
3000
2000
1000
0
0
1000
2000
Time (UTC)

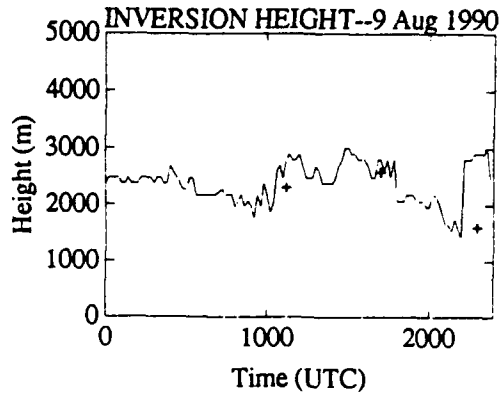
INVERSION HEIGHT--9 Aug 1990
Height (m)
5000
4000
3000
2000
1000
0
0
1000
2000
Time (UTC)

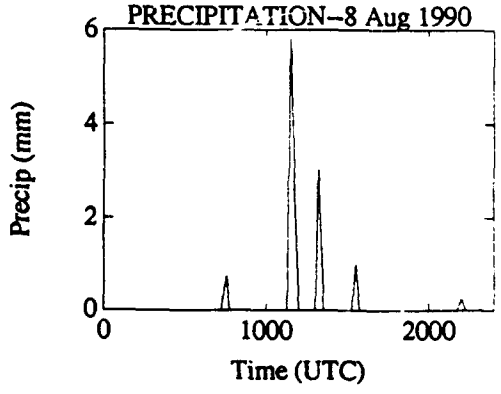
PRECIPITATION--8 Aug 1990
Precip (mm)
6
4
2
0
0
1000
2000
Time (UTC)

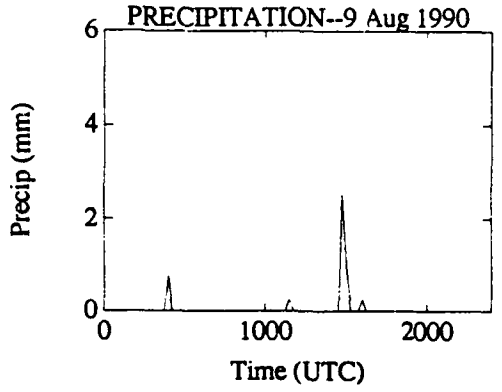
PRECIPITATION--9 Aug 1990
Precip (mm)
6
4
2
0
0
1000
2000
Time (UTC)

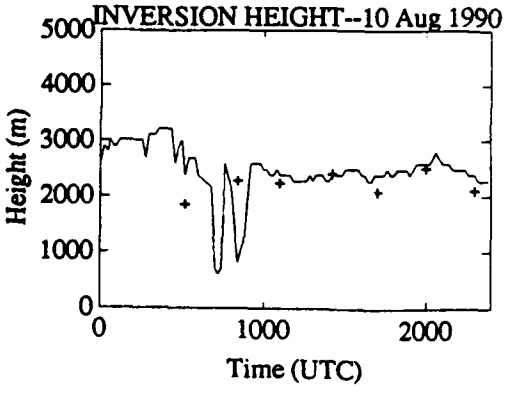
INVERSION HEIGHT--10 Aug 1990
Height (m)
5000
4000
3000
2000
1000
0
0
1000
2000
Time (UTC)

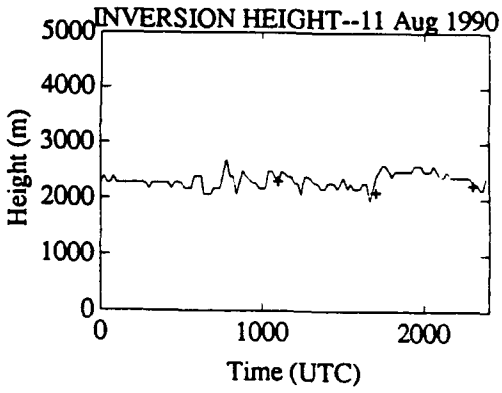
INVERSION HEIGHT--11 Aug 1990
Height (m)
5000
4000
3000
2000
1000
0
0
1000
2000
Time (UTC)

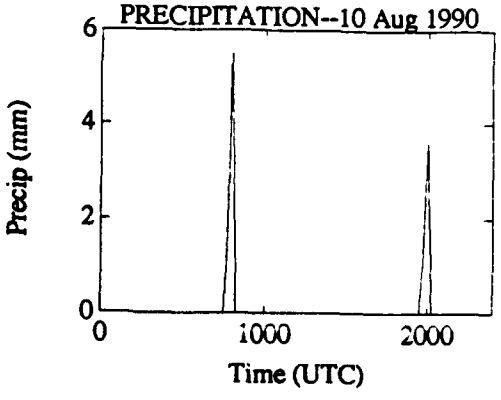
PRECIPITATION--10 Aug 1990
Precip (mm)
6
4
2
0
0
1000
2000
Time (UTC)

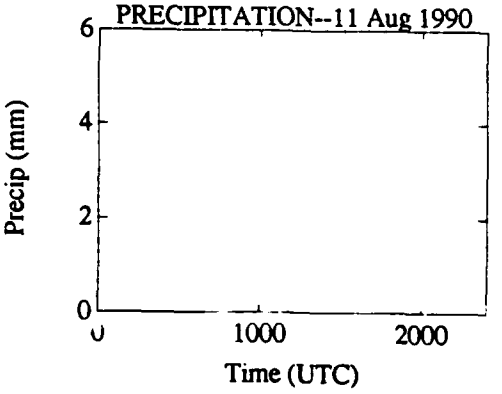
PRECIPITATION--11 Aug 1990
Precip (mm)
6
4
2
0
0
1000
2000
Time (UTC)

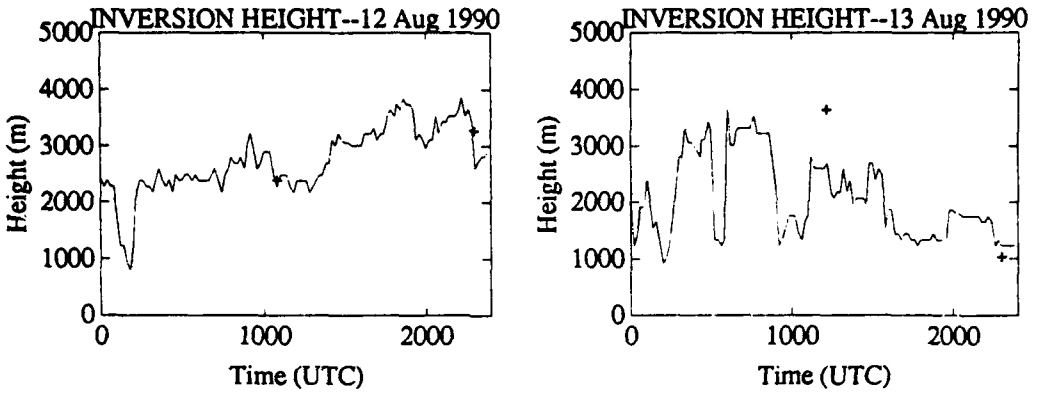
INVERSION HEIGHT--12 Aug 1990
Height (m)
5000
4000
3000
2000
1000
0
0
1000
2000
Time (UTC)

INVERSION HEIGHT--13 Aug 1990
Height (m)
5000
4000
3000
2000
1000
0
0
1000
2000
Time (UTC)

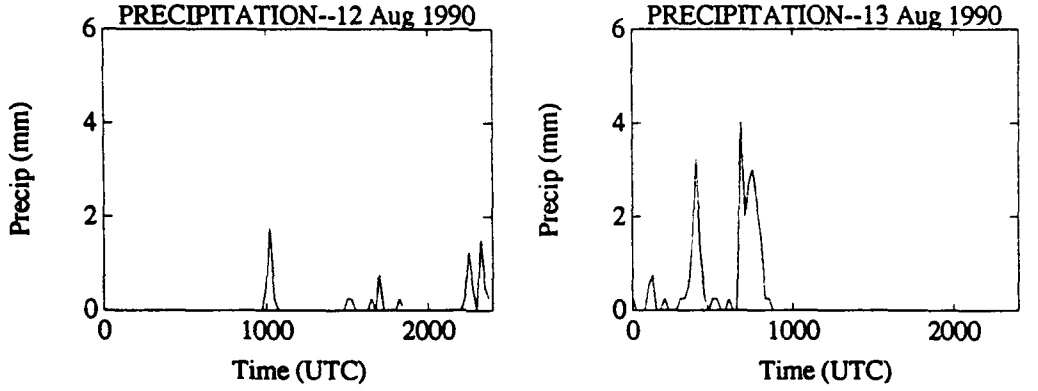
PRECIPITATION--12 Aug 1990
Precip (mm)
6
4
2
0
0
1000
2000
Time (UTC)

PRECIPITATION--13 Aug 1990
Precip (mm)
6
4
2
0
0
1000
2000
Time (UTC)

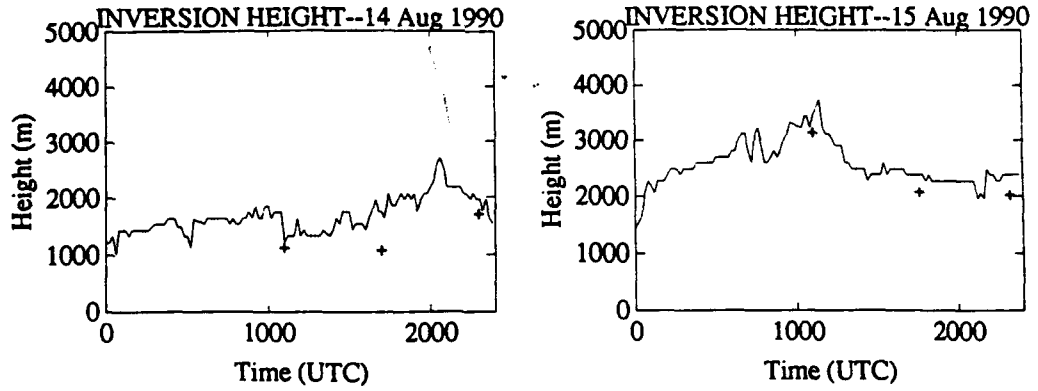
INVERSION HEIGHT--14 Aug 1990
Height (m)
5000
4000
3000
2000
1000
0
0
1000
2000
Time (UTC)

INVERSION HEIGHT--15 Aug 1990
Height (m)
5000
4000
3000
2000
1000
0
0
1000
2000
Time (UTC)

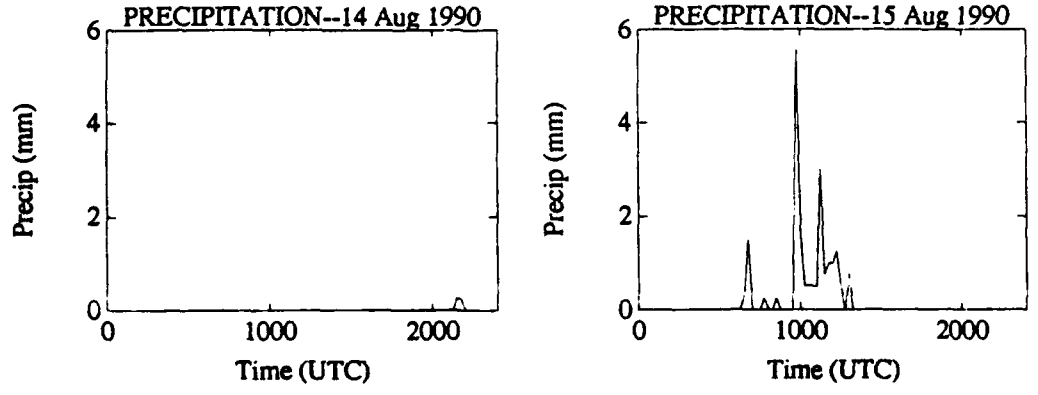
PRECIPITATION--14 Aug 1990
Precip (mm)
6
4
2
0
0
1000
2000
Time (UTC)

PRECIPITATION--15 Aug 1990
Precip (mm)
6
4
2
0
0
1000
2000
Time (UTC)

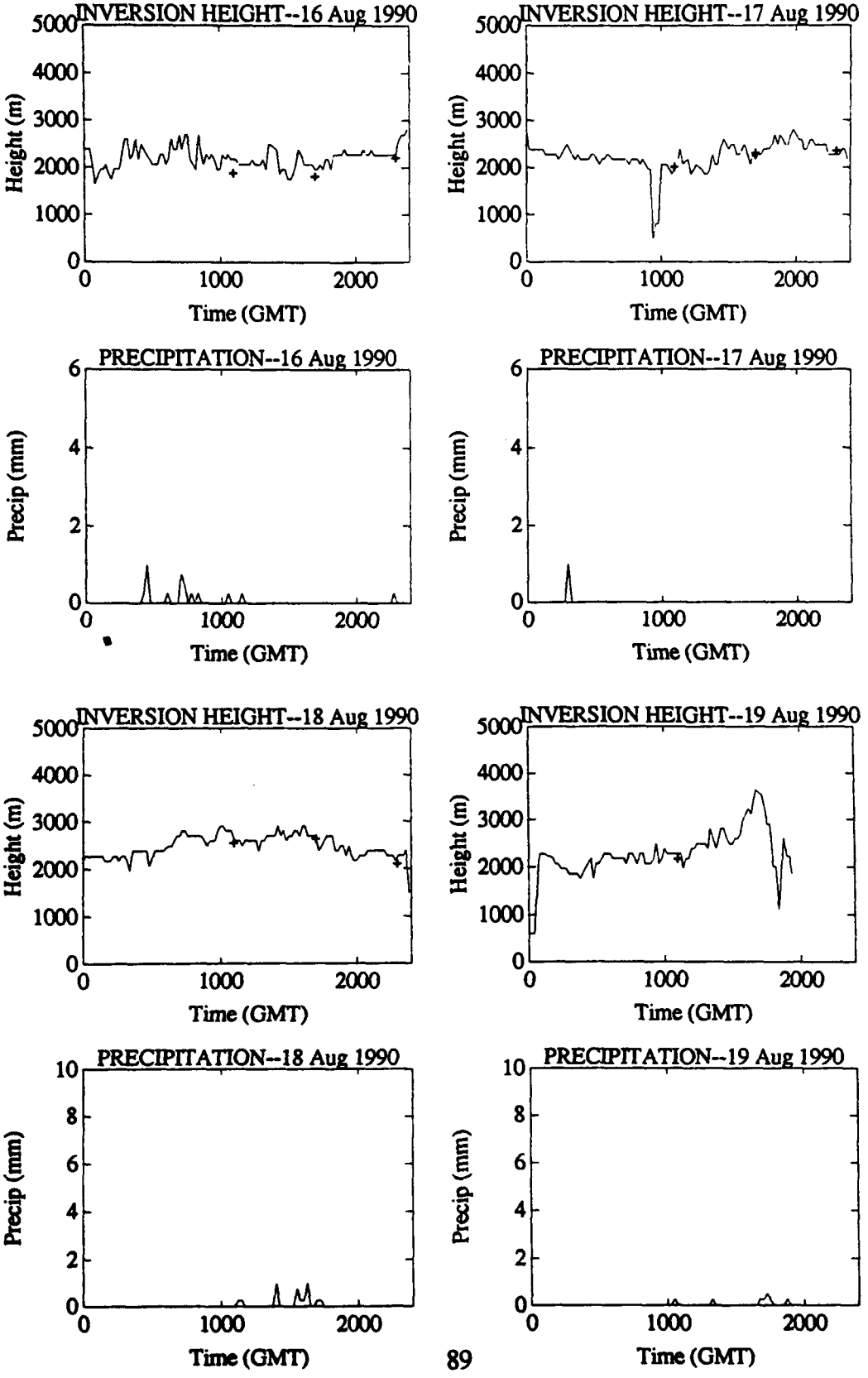
INVERSION HEIGHT--16 Aug 1990
Height (m)
Time (GMT)
INVERSION HEIGHT--17 Aug 1990
Height (m)
Time (GMT)
PRECIPITATION--16 Aug 1990
Precip (mm)
Time (GMT)
PRECIPITATION--17 Aug 1990
Precip (mm)
Time (GMT)
INVERSION HEIGHT--18 Aug 1990
Height (m)
Time (GMT)
INVERSION HEIGHT--19 Aug 1990
Height (m)
Time (GMT)
PRECIPITATION--18 Aug 1990
Precip (mm)
Time (GMT)
PRECIPITATION--19 Aug 1990
Precip (mm)
Time (GMT)

APPENDIX B

REGRESSION ANALYSIS, CORRELATION AND F-TEST

I performed regression analysis, F-test for regression significance, and the correlation between the sounding and profiler following Draper and Smith (1966). The estimated regression equation is:

$$\hat{y}=\bar{y}+b_1(x-\bar{x}) \tag{5.1}$$

$$b_0=\bar{y}-b_1\bar{x} \tag{5.2}$$

$$b_1=\frac{\Sigma(x_i-\bar{x})(y_i-\bar{y})}{\Sigma(x_i-\bar{x})^2} \tag{5.3}$$

where $\bar{y}$ is the mean of the dependent variable (the profiler), and $\bar{x}$ is the mean of the independent variable (the sounding), and b_1 is the slope and b_0 is the y-intercept of the fitted regression line. The correlation (r_{xy}) between x and y is:

$$r_{xy}=\frac{\Sigma(x_i-\bar{x})(y_i-\bar{y})}{[\Sigma(x_i-\bar{x})^2]^{1/2}[\Sigma(y_i-\bar{y})^2]^{1/2}} \tag{5.4}$$

REFERENCES

Ahnert, P. R., 1990: Functional precision of National Weather Service upper air measurements using the VIZ Manufacturing Co. "B-sonde," Test and Evaluation Branch Report, 27 pp, draft.

Albrecht, B. A., 1984: A model study of downstream variations of the thermodynamic structure of the trade winds. *Tellus*, **36A**, 187-202.

Augstein, A., H. Reihl, F. Ostapoff and V. Wagner, 1973: Mass and energy transports in an undisturbed Atlantic trade wind flow. *Mon. Wea. Rev.*, **101**, 101-111.

Bean, B. R. and E. J. Dutton, 1966: *Radio Meteorology*. Dover Publications, Inc., 435 pp.

_____, R. E. McGavin, and B. D. Warner, 1973: A note on the FM-CW radar as a remote probe of the Pacific trade-wind inversion, *Boundary Layer Meteorology*, **4**, 201-209.

Box, G. E. P. and G. M. Jenkens, 1976: *Time Series Analysis: Forecasting and Control (rev.)*, Holden-Day, 575 pp.

Chatfield, C., 1975: *The Analysis of Time Series: Theory and Practice*, Chapman and Hall, 263 pp.

Draper N. R. and H. Smith, 1966: *Applied Regression Analysis*, John Wiley & Sons, Inc., 407 pp.

Ecklund, W. L., D. A. Carter, B. B. Balsley, P. E. Currier, and J. L. Green, 1988: A UHF wind profiler for the Boundary layer: Brief Description and Initial Results, *J. Atmos. Ocean. Tech.*, **5**, 432-441.

_____, 1990: Field tests of a lower tropospheric wind profiler, *Radio Science*, **25**, 899-906.

Fellbaum, S. R., 1984: *The Effects of the Island of Hawaii on the Trade Winds and the Trade Wind Inversion*, M. S. Thesis, University of Hawaii, 86 pp.

Gage, K. S., and B. B. Balsley, 1980: On the scattering and reflection mechanisms contributing to clear air radar echoes from the troposphere, stratosphere, and mesosphere, *Radio Science*, **15**, 243-257.

_____, 1990: Radar Observations of the Free Atmosphere: Structure and Dynamics. *Radar in Meteorology*. D. Atlas, Ed., American Meteorology Society, 806 pp.

Garrett, A. J., 1980: Orographic cloud over the Eastern slopes of Mauna Loa Volcano, Hawaii, related to insolation and wind, *Mon. Wea. Rev.*, **108**, 931-941.

Hawaiian Rainband Project (HaRP) Experimental Design and Operations Plan, 1990: National Center for Atmospheric Research Report, 85 pp.

Hawaiian Rainband Project (HaRP) Scientific Overview, 1989: National Center for Atmospheric Research Report, 39 pp.

Holton, J. R., 1979: *An Introduction to Dynamic Meteorology, 2/ed*, Academic Press, 391 pp.

Larson, R. N., 1978: *Summer Trade Wind Rainfall in the Hawaiian Islands*, M. S. Thesis, University of Hawaii, 85 pp.

Lavoie, R. L., 1967: Air motions over the windward coast of the Island of Hawaii, *Tellus*, **XIX**, 354-358.

_____, 1967: Background data for the warm rain project, *Tellus*, **XIX**, 348-353.

_____, 1974: A numerical model of trade wind weather on Oahu, *Mon. Wea. Rev.*, **102**, 603-637.

Leopold, L. B., 1948: Diurnal weather patterns on Oahu and Lanai, Hawaii, *Pacific Science*, **II**, 81-95.

_____, 1949: The interaction of trade wind and sea breeze, Hawaii. *J. Meteor.*, **6**, 312-320.

Malkus, J. S., 1958: On the structure of the trade wind moist layer, *Papers in Physical Oceanography and Meteorology*, **Vol XIII, No 2**, 1-47.

Nash, A., 1992: *The Diurnal Surface Patterns on the Island of Hawaii*, M. S. Thesis, University of Hawaii, (in progress).

Neiburger, M., 1960: The relation of air mass structure to the field of motion over the Eastern North Pacific Ocean in summer, *Tellus*, **XII**, 31-40.

NOAA, 1990: Local Climatological Data, Monthly Summary, Old General Lyman Field, NOAA, ISSN 0198-1692

Ramage, C. S., and N. E. Oshiro, 1977: *Kauai Wind Power Survey.* Department of Meteorology, University of Hawaii, UHMET 77-05, 33 pp.

_____, 1990: *Forecasters' Guide to Tropical Meteorology.* USAF TR 240 (rev.), 257 pp.

Riehl, H., T. C. Yeh, J. S. Malkus and N. E. La Seur, 1951: The northeast trade of the Pacific Ocean, *Quart. J. Roy. Meteor. Soc.*, 72, 598-626.

_____, 1979: *Climate and Weather in the Tropics.* Academic Press, 611 pp.

Rogers, R. R. , W. L. Ecklund and D. A. Carter, 1991: First results from the HaRP boundary-layer radar, 25th Conference on Radar Meteorology, Paris, June 1991.

Sadler, J. C., 1975: *The Upper Tropospheric Circulation over the Global Tropics.* Department of Meteorology, University of Hawaii, UHMET-75-05, 35 pp.

_____, M. A. Lander, A. M. Hori, and L. K. Oda, 1987: *Tropical Marine Climate Atlas, Vol II, Pacific Ocean.* Department of Meteorology, University of Hawaii, UHMET 87-02, 27 pp.

Schroeder, T. A., B. J. Kilonsky, and B. N. Meisner, 1977: *Diurnal Variation in Rainfall and Cloudiness.* Department of Meteorology, University of Hawaii, UHMET-77-03, 67 pp.

Smolarkiewicz, P. K., R. M. Rasmussen and T. L. Clark, 1988: On the dynamics of Hawaiian cloud bands: island forcing, *J. Atmos. Sci.*, 45, 1872-1905.

Spiegel, M. R., 1991: *Schaum's Outline of Theory and Problems of Statistics, 2/ed,* McGraw-Hill, Inc., 504 pp.

von Ficker, H., 1936: Die Passatinversion, *Veroff. meteor, Inst. Berl. (1)*, 4, 1-33.